The University Of Sheffield.

Department Of Mechanical Engineering

Effect of Cryogenic Treatment on the Abrasive Wear Resistance of Engineering Alloys

Author: Paulo **HERRERA**

Date: January 2020

Supervisors: **Dr. Tom Slatter**

Prof. Roger Lewis

Thesis submitted to The University of Sheffield in partial fulfilment of the requirements for the degree of Doctor of Philosophy

ABSTRACT

Deep cryogenic treatment (DCT) is a heat treatment that utilises low temperatures (below 113 K) and is usually applied in conjunction with conventional heat treatments. Since this heat treatment is relatively new commercially, there are few studies about it in the literature, so a better understanding of its effects in the abrasive wear resistance of engineering alloys can be beneficial for its broader utilisation in industry.

The work presented in this thesis aims to investigate the effect of DCT on the mechanical performance of a selected range of engineering alloys, especially in abrasive wear resistance. To achieve this, alloys with broad application and different characteristics were selected: two types of austenitic stainless steel (AISI 304L and AISI 316L), a type of martensitic stainless steel (AISI 440C), a low alloy pressure vessel steel (SA508 Gr 4N), a titanium alloy (Ti-6Al-4V) and an additively manufactured titanium alloy (Ti-6Al-4V obtained by electron-beam melting). The changes in mechanical performance were assessed through Vickers hardness and microhardness tests, abrasive wear test, and microstructural characterisation. Analyses of the wear scar and its surface were performed using advanced microscopy techniques and by 3D profilometry of the surfaces.

DCT was performed on those alloys and its effects were analysed. Its beneficial effects were found in the increased hardness of AISI 440C and AISI 304L, the former due to the transformation of retained austenite into martensite and the latter due to the nucleation of nano-martensite particles. For the AISI 304L, the DCT also presented a very significant increase in the wear resistance, to the extent of changing the wear morphology of the wear scar. The SA508 Gr 4N specimens showed an increase in their corrosion resistance, an effect not previously reported. All the mechanical effects, wear scar features and microstructure characteristics are presented and thoroughly analysed from a tribological perspective.

ACKNOWLEDGMENTS

I would like to thank God Almighty for giving me the strength, knowledge, ability and opportunity to undertake this research.

I would like to express my sincere gratitude to my supervisors for all the support received during this time. Thank you, Dr. Tom Slatter, Dr. Rob Thornton and Prof. Roger Lewis.

Thanks to my family that were always present, even being more than nine thousand kilometres away. Thank you for guiding me in the right path, cherishing my victories and always helping in the times of need.

A special thanks to my fiancée Christiane for keeping me focused in my task and supporting me in the hard moments. Without your help and friendship this PhD would not be possible. I love you.

Thanks to all the friends that I made in Sheffield, whom made my life here a joy and were always supportive and kind. Sheffield only felt like home because of you.

The author would also like to thank the Brazilian National Council for Scientific and Technological Development (CNPq), that through the Science Without Borders program, supplied the financial support for this PhD.

CONTENTS

LIST OF FIGURES

LIST OF TABLES

NOMENCLATURE

A440	AISI 440C
A440CT	AISI 440C Cryogenically Treated
AISI	American Iron and Steel Institute
ASM	American Society for Metals
ASTM	American Society for Testing and Materials
CAD	Computer-Aided Design
CNC	Computer Numerical Controlled
d	Depth [m]
DCT	Deep Cryogenic Treatment
DSRW	Dry-Sand/Rubber-Wheel
E	Young's Modulus [$N \cdot m^{-2}$]
EBM	Electron Beam Melting
EDM	Electrical Discharge Machining
ETi64	EBM Ti64
ETi64CT	EBM Ti64 Cryogenically Treated
GTA	Graduate Teaching Assistant
H	Material Hardness [$N \cdot mm^{-2}$]
HV	Vickers Hardness [$kg \cdot mm^{-2}$]
K	Kelvin
Kc	Fracture Toughness [N·m]
L	Sliding Distance [m]
N	Newton
RPV	Reactor Pressure Vessel
SA508	Sa508 Gr 4N
SA508CT	SA508 Gr 4N Cryogenically Treated
SAD	Selected Area Diffraction
SCT	Shallow Cryogenic Treatment
SEM	Scanning Electron Microscopy
SS304	AISI 304L
SS304CT	AISI 304L Cryogenically Treated

SS316	AISI 316L
SS316CT	AISI 316L Cryogenically Treated
TEM	Transmission Electron Microscopy
Ti64	Ti-6Al-4V Alloy
Ti64CT	Ti-6Al-4V Alloy Cryogenically Treated
USSR	Union of Soviet Socialist Republics
V	Volume [m^3]
W	Normal Load [N]
XRD	X-Ray Diffraction

1. INTRODUCTION

In this chapter, the research motivation is introduced by presenting a general view of the research field and showing the contextualization of the problems that lead to the development of the research question. The aim and objectives of this research are presented and, lastly, the thesis structure is shown, including a brief explanation of each chapter.

Conventional heat treatment processes, which typically involve submitting material to various heating cycles above the ambient temperature, are largely used in industry to modify the materials properties to best fit its application. The engineering alloys microstructure is formed of grains, that defines and characterise its mechanical properties. When submitting this microstructure to a heat treatment procedure, its properties (composition, size, structure) can be changed, which also causes alterations in the bulky alloy properties. The main parameters that defines the heat treatment procedure are the time, temperature and the cooling rate, which can be fine-tuned to better suit the final mechanical properties needed in each alloy.

Even though the conventional heat treatment can be used to modify the alloy properties, there are some limitations regarding its application and when in the part processing procedure that it can be applied. This type of conventional treatment, for example, can induce the formation of oxides and changes in the surface finish and in the dimensional properties of the heat treat material. Parts that have already been finished would have to undergo the finishing process again, to certify that this part still conforms with the original design. This results in a costly solution, making the conventional heat treatment a process that needs to be precisely defined and applied before any further manufacturing procedures. Another disadvantage occurs when trying to apply the conventional heat treatment to a large part (one that possesses increased size and/or thickness), similar to the ones used in large nuclear pressure vessels. Due to the heat treatment being time and temperature dependant, the bulky proportions of the part makes achieving a homogenous heat treatment very difficult. As a result of the heat affecting the external layer before than the part's core, since the heat is transferred in a gradient that flows from the outside to the inside of the part, the external layer suffers the effect of the heat for an considerable longer period of time than the part's core, which results in a non-homogenously treated part. The examples aforementioned represent some of the limitations encountered when applying the conventional heat treatment, and can limit the usability of this type of heat treatment in some cases.

A less conventional heat treatment is the cryogenic treatment (CT) which instead of using elevated temperature heating cycles, utilises cryogenic temperatures (below 193 K) to change the properties of materials. When compared with the conventional heat treatment, this method presents the advantage of dimensional stability, which makes applying the treatment in the later stages of the part production possible. The effects of this treatment can include an improvement in mechanical properties, like hardness, wear resistance and fatigue life. The most common effect of the cryogenic treatment is the transformation of retained austenite in martensite, that occur when submitting alloys that present a martensitic structure to the cryogenic treatment. As the conventional heat treatment, the cryogenic treatment can also promote other changes in the microstructure, like the precipitation and redistribution of carbides. Due to the research in this field being relatively new and not being as popular as the conventional heat treatment, there is still no full understanding of the mechanisms involved in the CT. This is especially true when related to its application in light alloys, where there is very little literature or published research currently available.

The cryogenic treatment process presents some characteristic factors that limit its implementation and application. While the conventional heat treatment can be achieved (in many cases) just by utilising an oven, the cryogenic treatment involves the utilisation of a medium that is at cryogenic temperature (usually liquid nitrogen), which sourcing and storage can be costly and complex. The deep cryogenic treatment chambers are similar to conventional freezers, that are fed using large liquid nitrogen container, which maintain the temperature during the heat treatment process. Due to the need of this large cryogenic medium reservoirs, the implementation costs are increased. The previously cited factor in combination with the smaller amount of scientific evidence (when comparing to the conventional heat treatment literature) about its effects, makes this type of heat treatment less attractive to commercial heat treating companies.

Stainless steel alloys are a vastly used engineering material, being mostly recognised by its good oxidation resistance. The selection of the stainless steel used in this research was carried keeping in mind the different types of microstructures that each of the select alloys would present and its chemical composition. The stainless steel type 304 is an austenitic stainless steel that presents good mechanical strength and corrosion resistance, being also recognised by its machining capabilities. The austenitic stainless steel type 316 presents a high corrosion resistance and can be utilised in elevated temperatures applications, presenting a resistance to oxidation until 1148 K. Type 304 is the most used alloy among the austenitic

stainless steel range, closely followed by the type 316, largely employed in applications that need a good corrosion resistance, like food industry, pharmaceutical and naval applications.

The last of the stainless steel alloys studied in this research is the high carbon martensitic stainless steel type 440, which offers good mechanical properties, wear resistance and corrosion resistance. This alloy can present the highest hardness and strength among the stainless steel when submitted to specific heat treatment, which makes it an excellent candidate for applications that need good mechanical resistance, such as cutlery, ball bearings, moulds and dies. Another steel studied is the low alloy steel SA508 Gr 4N, that is used in the nuclear reactor pressure vessel (RPV) application. In comparison to other RPV, this alloy presents a higher strength and toughness due to its tempered martensite structure.

Light alloys are largely used in applications in which the density of the material plays an essential role in material selection. Titanium alloys are classified as light alloys and present good corrosion resistance, high strength and relatively low density. These properties can vary according to the other chemical elements that are present in the alloy grade and the type of heat treatment it has been submitted to. The most widely used titanium alloy is Ti-6Al-4V (Ti64), which is an alpha-beta alloy containing aluminium (≈ 6% wt.) and vanadium (≈ 4% wt.) as the main alloying elements. Ti64's broad applicability comes from its excellent corrosion resistance, good machinability and biocompatibility, which allows the implementation of this alloy in many types of applications, such as automotive, aerospace and biomechanical. The typical limiting factors for the Ti64 application are the poor wear resistance (particularly in sliding), high cost of the alloy itself and increased costs related to the processing of the parts (when compared to more conventional alloys, like steel and aluminium).

Recently, Ti64 has been used in the additive manufacturing (3D printing) field, such as the EBM (electron beam melting) technology. This process produces parts, layer by layer, directly from a CAD (computer-aided design) model. The alloy powder is layered in a vacuum environment, and each layer is melted, according to the design, using a powerful electron beam, producing a dense solid part. Any unmelted alloy powder is later removed and can be re-utilised. This new technology makes possible the manufacturing of solid parts with complex shapes and good tolerances, which are characteristics presented in high-performance engineering components and also medical implants.

An important part of an engineering project is the material selection, since the selected alloy must present the necessary characteristics to fulfil the initial project considerations. Even

though the materials presented here are vastly used in engineering projects due to their specific characteristics, all of them are susceptible to wear during life as a component. Wear resistance is a desirable property and, in most cases, the limiting condition when related to the component lifecycle (durability). Wear can occur in different forms (as explained in Section 2.3), but the main wear mechanism, responsible for more than half of all wear occurring in engineering applications, is known as abrasive wear. It is important to assess the effects of the cryogenic treatment on the abrasive wear resistance of the selected alloys, which is the aim of this research, once the better understanding of the changes due to this treatment can be economically beneficial to the industry.

1.1. AIM AND OBJECTIVES

This work aims to provide a better understanding of the cryogenic treatment effects on the abrasive wear resistance of a broad range of industrially relevant materials. To be able to do so, stainless steel alloys (austenitic and martensitic), a steel grade used for nuclear pressure vessels and titanium alloys (cast and EBM obtained) were studied. To accomplish this aim, the following objectives for this research were set.

1. Based on the current state-of-the-art, select engineering alloys which the deep cryogenic treatment is likely to be beneficial in improving their abrasive wear resistance;
2. Design a custom ASTM G65 test rig and associated test methodology to be capable of discerning between the likely wear resistance levels of the selected alloys in their conventionally heat treated and cryogenically treated states.;
3. Perform experimental tests to assess the abrasive wear resistance of the selected alloys in their conventionally heat treated and cryogenically treated states;
4. Analyse the wear scar and microstructure, comparing the results for the conventionally heat treated and cryogenically treated samples;
5. Pinpoint which alloy(s) benefit from the cryogenic treatment the most, which need more investigation, and which have no prospect of useful improvement.

Also, these activities seek to fill the gaps found in literature pertaining to the testing of the effects of the cryogenic treatment in the abrasive wear resistance of the chosen alloys, especially when related to novelty alloys like the EBM obtained titanium, which does not have enough studies related to the deep cryogenic treatment.

It is anticipated that the novelty of this work is primarily to provide insight into the efficacy of cryogenic treatment on common engineering alloys outside of the well-researched area of tool steels. It is also anticipated that the work will provide a robust test and analysis methodology for further work in this area of characterising the influence of cryogenic treatment, allowing researchers the best chance of establishing which alloys are worthwhile treating on a commercial basis.

1.2. THESIS STRUCTURE

Firstly, the background knowledge and published research work in the related field are presented, followed by the research methodology, test rig development, material selection and characterisation methods. The results are presented and analysed for each group of materials, being the key points for all the found results linked to the literature and discussed later. Lastly, the conclusions are highlighted based on the found results and literature, followed by the relevance and contribution of the work and the possible future work to be developed based in this research. Table 1 summarises the content presented in each chapter of this thesis.

Table 1 - Chapter content outline.

Chapter	Chapter Content Outline
1	Introduction to the cryogenic treatment and abrasive wear, with the definition of the work aim and objectives, followed by the outline of following chapters.
2	Background knowledge on conventional heat treatment, cryogenic heat treatment, tribology and wear testing. Summary of the state of the art publications in the cryogenic treatment research field.
3	Development of the test methodology, including the design, building and fine-tuning of the custom ASTM G65 test rig. Detailed material selection, sample preparation and heat treatment parameters. Description, methods and parameters for the mechanical and microstructural analysis.
4	AISI 440C and SA508 Gr 4N results for the hardness, microhardness and wear volume. Abrasive wear tests results, advanced analysis of the wear scar and microstructural characterisation. Comparison of the conventionally heat treated and cryogenically treated samples of each alloy, followed by discussion of the found results and properties.
5	Cast Ti64 and EBM Ti64 results for the hardness, microhardness and wear volume. Abrasive wear tests results, advanced analysis of the wear scar and microstructural characterisation. Comparison of the wear performance of the cast and EBM samples, followed by the comparison of the untreated and cryogenically treated samples of each alloy. Discussion of the found results and properties.

6	AISI 304L and AISI 316L results for the hardness, microhardness and wear volume. Abrasive wear tests results, advanced analysis of the wear scar and microstructural characterisation. Advanced analysis using XRD and TEM. Comparison of the conventionally heat treated and cryogenically treated samples of each alloy, followed by discussion of the found results and properties.
7	Discussion linking the results and mechanisms found in the previous chapters and the literature. General discussion of the cryogenic treatment effect in the engineering alloys.
8	Conclusions resulting from the analysis and discussion based in the tests' results for all the studied alloys; research contribution based on conclusions; possible future work based in this work findings.
9	References to all sources cited in this work.

2. LITERATURE REVIEW

This chapter contains the background information about the main subjects that are discussed during the development of this research, focusing on establishing a base knowledge on the most important topics and presenting the state of the art literature related to the research aim. Conventional and cryogenic heat treatments are presented, followed by a tribology overview and concluding with a focus in the wear testing topic, specially the Dry-sand/Rubber-wheel abrasive wear test.

2.1. CONVENTIONAL HEAT TREATMENT

Engineering alloys are used for a range of applications with specific requirements, which leads to the need of tailoring the properties of these alloys to better suit its engineering application. The most commercially usual way of achieving the desired properties (to a certain extent) on a suitable type of alloy is submitting this alloy to a heat treatment process. Heat treatment is the process of submitting an alloy to a controlled temperature for a defined period of time and also controlling the heating and cooling rates of this process [1,2]. The two broader categories of heat treatment are the cold heat treatments (in which the treated alloy is submitted to a temperature below 273 K) and the conventional heat treatments (which involves heating the treated alloy to temperatures above 273 K).

During the heat treatment process, the alloy being treated can be subjected to a sequence of heating, holding/soaking and cooling procedures, depending on the changes that are needed to achieve the desired alloy properties. The heat treatment process shown in Figure 1 is an example of a combination of conventional heat treatment and cryogenic heat treatment, once the treated part is submitted higher temperatures and later to cryogenic temperatures. More complex heat treatments are not necessarily a combination of a conventional and a cryogenic treatment, since the overall treatment process can present several different stages of specific heat treatments.

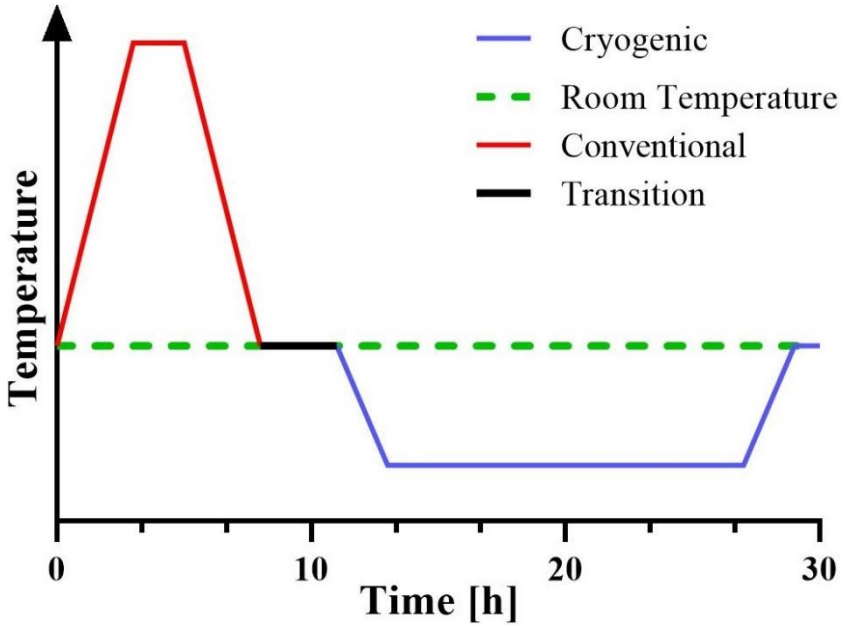

Figure 1 - Example of heat treatment with a combination of conventional and cryogenic heat treatment.

Heat treatment processes work by altering the microstructure of the treated alloy, which modifies the alloys' physical properties and makes achieving the needed characteristics possible. The chemical composition and the microstructure of the engineering alloy determines its physical properties. Each alloy has several properties, which can be divided in two groups [3]:

- Dependent of the microstructure: hardness, wear resistance, electrical conductivity, fracture toughness, ductility, thermal conductivity, fatigue strength, creep strength, tensile strength, yield strength and corrosion resistance.
- Independent of the microstructure: elastic moduli, density, thermal expansion coefficient, Poisson's ratio and specific heat.

The properties that are independent of the microstructure are not affected by the heat treatment. Understanding the phases that are present in the alloy, based in the alloys' composition, is an important part of selecting the right alloy and also planning the right type of heat treatment for the engineering application. The phases present in an alloy can be identified using an appropriate phase diagram, which indicates the phases present at a given temperature (in the Y axis) and composition (in the X axis), under isothermal conditions. Figure 2 presents the iron-carbon phase diagram, which is a binary system due to it only correlating to a system formed by two components, in this case iron and carbon [3].

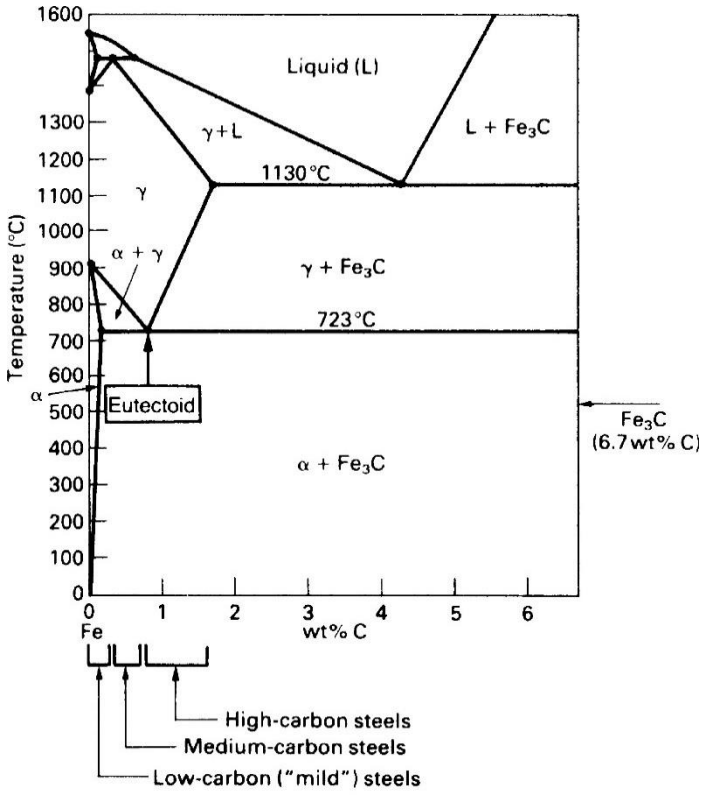

Figure 2 - Fe-C phase diagram: γ - Austenite; α – Ferrite; Fe_3C – Cementite. (Modified from [3])

The phases that are present in the alloy during the heat treatment process will determine its microstructure, this way using the phase diagram to choose the right alloys composition will help predict which type of microstructure an alloy is likely to achieve. Changing the properties that are dependent on the microstructure is the aim when choosing the heat treatment parameters and, to do so, a time temperature transformation (TTT) diagram can be used. Figure 3 presents an example of a TTT diagram for the 0.8% wt. carbon steel [3].

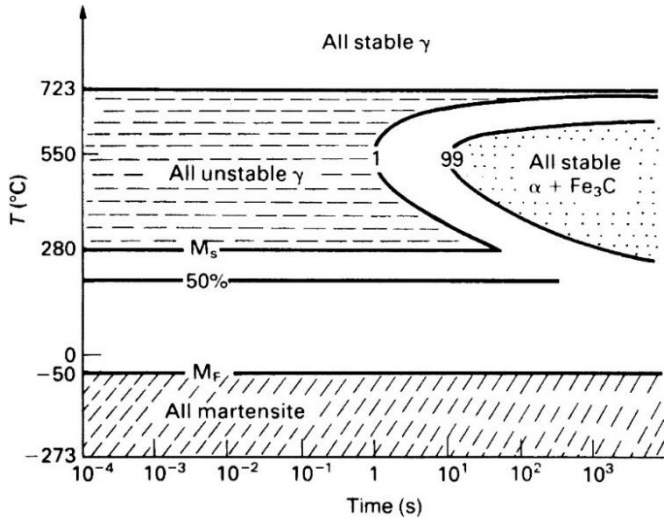

Figure 3 - Time Temperature Transformation (TTT) diagram for a 0.8% carbon (eutectoid) steel (from [3]).

The time temperature transformation correlates the temperature (in the Y axis) with the time (in the X axis), this way giving a clear guideline to choosing the right parameters (time and temperature) to achieve the desired type of microstructure. As an example: for the 0.8% carbon steel (Figure 3), if the alloy is heated to 550 °C (823 K), held at this temperature for a period bigger than 10^2 and then cooled to room temperature, this alloy would present a stable pearlite (eutectoid $\alpha + Fe_3C$) microstructure at room temperature. For this same alloy, a fast cooling (at a constant rate and in a period close to one second total time) from the same temperature of 550 °C (823 K) is needed to achieve a structure that would present a combination of martensite and retained austenite (γ) at room temperature. The M_s indicates the start of the austenite to martensite transformation and the M_f indicates the end of this transformation, which means that below M_f all the austenite would be transformed to martensite. This way, for this alloy to present a complete martensitic microstructure, a cold treatment that achieves temperatures below -50 °C (223 K) in less than around 10 s is needed.

The commonly used heat treatments (e.g., annealing, normalizing, tempering, quenching and cold treatments) aim to affect the microstructure of the treated alloy to achieve the desired effect in the microstructure dependent properties, and are the heat treatment parameters defined according to each alloy's TTT diagram.

2.2. CRYOGENIC TREATMENT

Cryogenic treatment, also referred as cryotreatment or cryogenic processing is a type of heat treatment that, instead of using the elevated temperatures used in the conventional heat treatments, benefits from cooling the material to temperatures below zero degrees Celsius (also known as sub-zero), usually being utilised along with conventional heat treatments [4]. The treatments that occur at temperatures below 273 K can be classified in two different categories; 'cold treatment' which includes those that utilise temperatures from 273 K down to 193 K, and 'cryogenic treatment' for those that utilise temperatures below 193 K. The latter classification is also divided in to two different types of cryogenic treatment [5], 'shallow' and 'deep' as presented in Section 2.2.1.

Being a relatively recent commercial development when compared to conventional heat treatment, the initial documented utilisation of cryogenic treatment dates from the first half of the 20^{th} century when this type of treatment was studied and applied in the USSR [4]. Zhmud [6] and Popandopulo and Zhukova [7] describe how A.P. Gulayev was one of the pioneers on the research of the effect of cold treatments in the mechanical properties of alloys.

In the research published in 1946 by A.P. Gulayev on the cold treatment of steel (translated to English in 1998 [8]), it is also shown that sub-zero treatments had been studied for more than 30 years (i.e. since the First World War) and points towards important discoveries published by other Soviet and American researchers, like the transformation of austenite into martensite in a range of engineering steels. Some of the most important positive results in the early research in the field of the deep cryogenic treatment were conducted in 1982 by R.F. Barron [9], who presented an extensive study about the effect of cryogenic treatment on the performance of nineteen steel alloys (between tool steels, stainless steels and other steel alloys). In this work, Barron presented the effect of the shallow cryogenic treatment (SCT) and deep cryogenic treatment (DCT) in the wear resistance of a wide range of iron alloys, which showed that (for the majority of the tested steels) a positive effect in the wear resistance was found, in some cases (D-2) the DCT increased the wear resistance of the alloy by 700%.

Cryogenic treatment is mostly known for its use as a complementary treatment, being responsible for the further transformation of the retained austenite into martensite after a traditional processing route. It is also applied in situations where there is a need to increase the mechanical properties of alloys, usually the hardness and wear resistance, without the need for more procedure. Other effects that have also been reported are the better mechanical resistance, better dimensional stability and a good ratio between properties like hardness and toughness [4,10,11]. The results for this type of treatment will be better shown in Section 2.2.3.

2.2.1. Types of Sub-zero Treatments

Sub-zero treatments can be divided into different categories according to the methods and temperatures employed during the procedure [5,10,11]:

Cold Treatment: The minimum temperature at this treatment is 193 K, being usually achieved by placing the sample in a low temperature freezer (which has a closed cooling system, without the need of putting the boiling gas in contact with the sample to remove further heat).

Shallow Cryogenic Treatment (SCT): The temperature range goes extends just below 193 K to around 113 K, usually achieved by using a container with dry ice or by boiling a low temperature fluid in a chamber. Even though this is a much simpler type of cryogenic treatment, the procedure is often not controlled very accurately. The typical procedure is to introduce the material in a chamber for a period and later bring it to room temperature, without any specific cooling or heating control.

Deep Cryogenic Treatment (DCT): The material is submitted to a controlled cooling rate until temperatures below 113 K are achieved, held at this temperature for a period and then heated to room temperature at a fixed heating rate. This type of treatment is usually performed in a chamber with nitrogen, which has the temperature around the nitrogen boiling point (77 K). Since this is a much more refined and repeatable cryogenic treatment, all the temperatures, holding periods, cooling and heating rates are monitored and automated. This procedure is presented in more detail in Section 2.2.2.

Figure 4 presents a simple scale with the different types of cryogenic treatment.

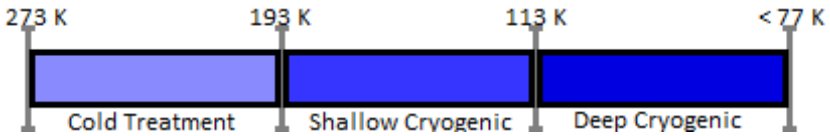

Figure 4 - Scale of temperature for the Sub-zero treatments.

It is important to note that even though the disciplines of cryonics and cryogenic machining also employ cryogenic temperatures to achieve a desired result, they are not directly linked to cryogenic treatment in the context of the work presented here.

2.2.2. Deep Cryogenic Treatment Procedure

The deep cryogenic treatment consists of the gradual cooling of the material being submitted to the treatment at a constant rate, holding it at the desired temperature and finally bringing it back to room temperature also at a steady heating rate.

The deep cryogenic treatment process most commonly used in industry, and also to be used in this research, is pictured in Figure 5 in which the samples are kept inside an insulated treatment chamber with a nitrogen atmosphere (that keeps the parts dry).

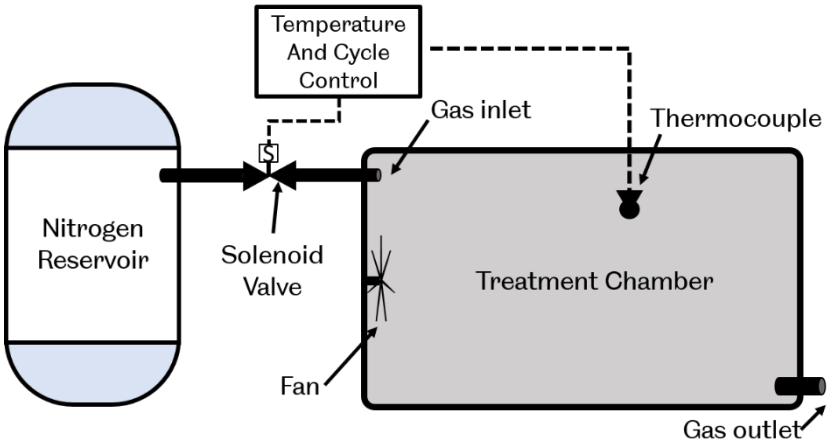

Figure 5 - Schematic of the treatment chamber and system for cryogenic treatment.

The treatment cycle can be divided in three stages:

Cooling: The first stage consists of the controlled cooling of the sample. The cooling rate is usually not greater than 2 K/min, that way preventing undesired thermal shock.

Soaking (holding phase): This is the longest of the stages, in which the controller maintains the constant temperature through the whole soaking time.

Heating: The last stage of the treatment, which consists of heating the sample at a controlled rate to the room temperature, usually similar to the cooling rate.

The process of cooling can be achieved through different methods, but to achieve a controlled cooling and heating rate, a cycle and temperature control feedback setup is necessary.

In the simplest setups, the cooling can be achieved by submerging the samples in a liquid nitrogen bath, which can lead to thermal shock and, subsequently, crack growth [12–14]. To prevent thermal shock, it is important to be able to control the cooling rate by controlling the nitrogen flow to gradually decrease the temperature inside the chamber where the samples are being treated and there are two methods of achieving this. In one the methods the nitrogen flows in a closed system and is only used to cool the air inside the treatment chamber, but this can lead to undesired condensation of water on the surface of the samples. Another method is to vaporize the nitrogen directly inside the chamber, creating a nitrogen atmosphere and cooling the parts submitted to the process.

Practically and as typically used in commercial cryogenic treatment systems such as the setup presented here, the temperature control system is composed by a nitrogen reservoir connected to the treatment chamber through a solenoid controlled valve, thermocouples inside the chamber and a programmable temperature and cycle controller. This system is responsible for the cooling and heating rate (as per the programmed treatment cycle) through controlling the volume of gaseous nitrogen flowing to the treatment chamber.

Figure 6 shows the typical graph of the DCT cycle, which presents the three stages. The dashed line shows the maximum temperature that can be used during a DCT (113 K) and the bottom continuous line is at the minimum temperature of a DCT using nitrogen (77 K). In special cases, lower temperatures can be achieved using helium to a minimum temperature of 5 K [4].

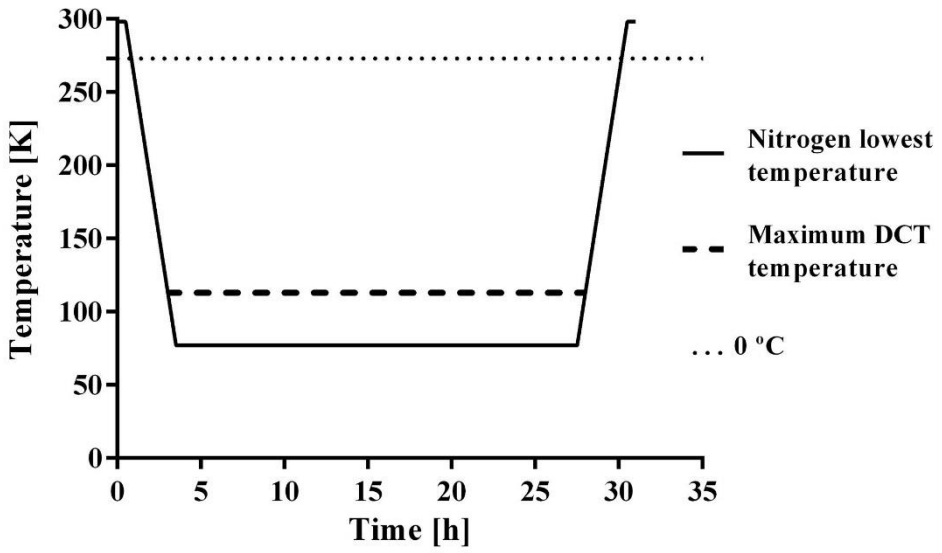

Figure 6 - Typical deep cryogenic treatment cycle.

In a study conducted by Darwin *et al.* [13], the influence of the cryogenic treatment parameters (e.g. cooling rate, soaking time and the holding temperature) on the wear resistance of a 18% Cr martensitic stainless steel was analysed. Utilising the Taguchi's design of experiment technique, it was reported that the most influential parameter on the success of a treatment process was the soaking temperature, therefore presented by the author as the dominant parameter on the treatment. According to this research, the soaking temperature has a contribution of 72% (when compared to the other parameters) to the improvement of the wear resistance and the optimal soaking temperature for this specific material is 89 K. The second most important factor was the time that the sample was hold at this temperature (36 hours), this one contributing 24% to the improvement. The cooling rate was classified as the third important factor and had a contribution of 10%. In the optimum condition, the samples had an increase in the wear resistance performance of 43%.

2.2.3. Mechanical Properties and Mechanisms

The outcomes of the cryotreatment are highly dependent on the composition of the alloy and the type of heat treatment it was submitted to, and in some cases these effects are only observable for some properties or not present at all. Table 2 presents a summary of research works that characterised the effects of the cryogenic treatment in different alloys, focusing on studies that reported changes in hardness and/or wear resistance.

Table 2 - Results found on the bibliography for the cryogenic treatment.

Reference*	Alloy	Property	Results**	
			SCT	**DCT**
Barron [9]	S-7 tool steel		+141.7%	+403.1%
	P-20 mould steel		+23.1%	-2.8%
	O-1 die steel		+121.6%	+172.1%
	A-2 die steel		-1.8%	+11.6%
	A-10 tool steel		+130.5%	+164.5%
	D-2 die steel		+216.4%	+717.7%
	H-13 die steel		+64.6%	+109.4%
	T-1 tool steel		+41.8%	+76.3%
	M-1 tool steel	Wear resistance	+45.5%	+125.3%
	M-2 tool steel		+12.5%	+20.4%
	303 Austenitic SS		+5.3%	+10.8%
	430 Ferritic SS		+16.2%	+19.9%
	440 Martensitic SS		+28%	+21.8%
	AQS Meehanite		-3.4%	-3.6%
	CPM-10V alloy steel		-6.1%	+31.3%
	8620 NiCrMo alloy		+3.7%	+11.6%
	C1020 plain carbon		-1.8%	-2.8%
Meng *et al.* [15]	Fe-12Cr-Mo-V-1.4C	Wear resistance	+110% to +600%	
Yun *et al.* [16]	W18Cr4V (T1)	Hardness	+2.8%	
	high speed steel	Bending strength	+24.8%	
		Impact toughness	+57.7%	
	W6No5Cr4V2 (M2)	Hardness	+2.7%	
	high speed steel	Bending strength	+19.9%	
		Impact toughness	+42.8%	
Molinari *et al.* [17]	AISI M2 tool steel	Hardness	+8.26%	
		Wear resistance	+51.35%	
	AISI H13 tool steel	Hardness	+6.9%	
		Impact energy	+1.1%	
		Fracture toughness	+14.7%	
Singh *et al.* [18]	AISI 304L	Hardness	~0	
	stainless steel	Micro-Hardness	+18.8%	
	welded joint	Tensile strength	+1.2%	
		Elongation	-5.6%	
Bensely *et al.* [11]	EN 353		**SCT**	**DCT**
	carburized steel	Hardness	+3.5%	+3.5%
		Wear resistance	+124%	+867%
Darwin *et al.* [13]	SR34 - 18% Cr	Wear resistance	+43.8%	
Das *et al*. [19,20]	AISI D2 tool steel	Hardness	+4.3%	+11.4%
		Wear resistance	+50%	+257%
Senthilkumar *et al.* [21]	4140 steel	Hardness	+6.7%	+10%
Koneshlou *et al.* [22]	AISI H13 tool steel	Tensile strength	+3.8%	+7.3%
		Hardness	+4.1%	+12.2%
		Impact energy	+4.5%	+12.3%
Thornton *et al*. [23]	Grey cast iron	Hardness	+2%	
	(SAE J431 G10)	Wear resistance	+81%	
Slatter *et al*. [24]	EN-GJL-250 grey	Wear resistance	+200%	
	EN-1A mild steel	Wear resistance	+400%	
Gu *et al.* [25]	Ti–6Al–4V	Hardness	0%	
		Plasticity	+22.7%	

Thornton *et al*. [26]	EN10083 C50R	Hardness	+28%
		Wear resistance	+23%
	AISI A2 tool steel	Hardness	0%
		Wear resistance	+26%
	AISI D6 tool steel	Hardness	+4%
		Wear resistance	+30%
	AISI M2 tool steel	Hardness	+2%
		Wear resistance	+31%
Prieto *et al.* [27]	AISI 420	Hardness	+5%
	stainless steel	Impact energy	+10%
Pérez *et al.* [28]	H13	Hardness	-1.1%
	tool steel	Fracture toughness	+24%
Yumak *et al.* [29]	Ti−6Al−4V	Hardness	+2.2%
		Tensile strength	-0.3%
Li *et al.* [30]	AISI M2	Hardness	+6.4%
	tool steel	Wear resistance	+54%
Pillai *et al.* [31]	VIKING tool steel	Hardness	+14.8%
	(AISI A8)	Wear resistance	+16.5%
Hariharan *et al.* [32]	D7 tool steel	Hardness	+4.6%
Weng *et al.* [33]	30CrMnSi alloy	Hardness	+8%
	structural steel	Impact toughness	+5%
		Tensile strength	+6%
Liu *et al.* [34]	25# valves alloy	Hardness	+28.9%
	steel	Tensile strength	+215%
		Yield strength	+511%

*Organized in chronologic order; **These refer to the biggest change reported in the research.

One of the important works in the cryogenic treatment effects in various alloys is the research done by Barron [9], in which the effects of the cryogenic treatment (dry ice at 189 K) and deep cryogenic treatment (liquid nitrogen at 77 K) in the abrasive wear resistance of ferrous alloys was assessed. The abrasive test consisted of grinding a cylinder made of the alloy to be tested against a coarse-grit alumina wheel, with a normal load of 430N. The researched materials consisted of 19 ferrous alloys, that were divided into tool steels, stainless steels and other metals.

According to Barron, the deep cryogenic treatment presented the most beneficial effect when applied to the tool steels, as it was found that this treatment increased the wear resistance of some of these alloys by up to 700%. The author attributes this beneficial effect to a more complete transformation of the retained austenite into martensite. The stainless steel studied also presented an increase in wear resistance due to the cryogenic treatment, showing very similar (less than 10% difference) results for the shallow (189 K) and deep cryogenic treatment (77 K). The highest measured increase in wear resistance for the stainless steels was of 10.8% for the austenitic (DCT), 19.9% for the ferritic (DCT) and 28% for the martensitic (SCT). The alloy group that present little or no cryogenic treatment effect was the carbon steels, which

Barron attributes to the structure already being all martensitic before the cryogenic treatment. The detailed results for each of the alloys is shown in Table 2.

The work presented by Barron is important due to the large selection of alloys that were tested, but it lacks in explanation and more details about the effect of the cryogenic treatment in the microstructure of the alloys, focusing more in the mechanical properties (hardness and wear resistance). The very noticeable effect of the cryogenic treatment in the mechanical properties of the tool steels was of great importance for the industry, once a higher wear resistance means less tool wear, which led to more researches focusing on this specific range of alloys.

The research done by Meng *et al.* in the effect of the cryogenic treatment in the wear resistance of Fe-12Cr-Mo-V-1.4C tool steel [15] showed an increase of 600% in the wear resistance. This drastic increase in the wear resistance was attributed to the precipitation of fine η-carbides, that affects the martensitic matrix enhancing its toughness and strength. These fine carbides form due to the expansion and contraction of the iron atoms, that slightly shifts the carbon atoms. According to this work, this carbide precipitation has a bigger influence in the wear resistance than the retained austenite removal. In the work done by Yun *et al.* on the deep cryogenic treatment of hight speed steels [16], a similar phenomenon is found. In conjunction with the transformation of retained austinite in martensite, the diffuse precipitation of ultra-fine carbides is considered a key factor in the increase of the mechanical properties.

As seen in the previous cited publications, the precipitation and refinement of carbides is a well-accepted effect of the cryogenic treatment and was also explored in detail in the work done by Das *et al.* [19,35] on the effect of the cryogenic treatment in the D2 tool steel. In these works, it is affirmed that the cryogenic treatment increases the amount and the population density of the secondary carbides, which makes the distribution of the carbide particles more uniform, without changing its chemical nature. Figure 7 from the research done by Das *et al.* [19] presents the effect of the heat treatment applied to the D2 tool steel in the phases present. They also note that the deep cryogenic treatment effect in these aforementioned properties is significantly higher than the cold or shallow cryogenic treatment. This way, it is well established that the cryogenic treatment when applied to tool steels affect the precipitation, size and distribution of fine carbides, which is also cited and agreed by other published researches [26,28,30–32].

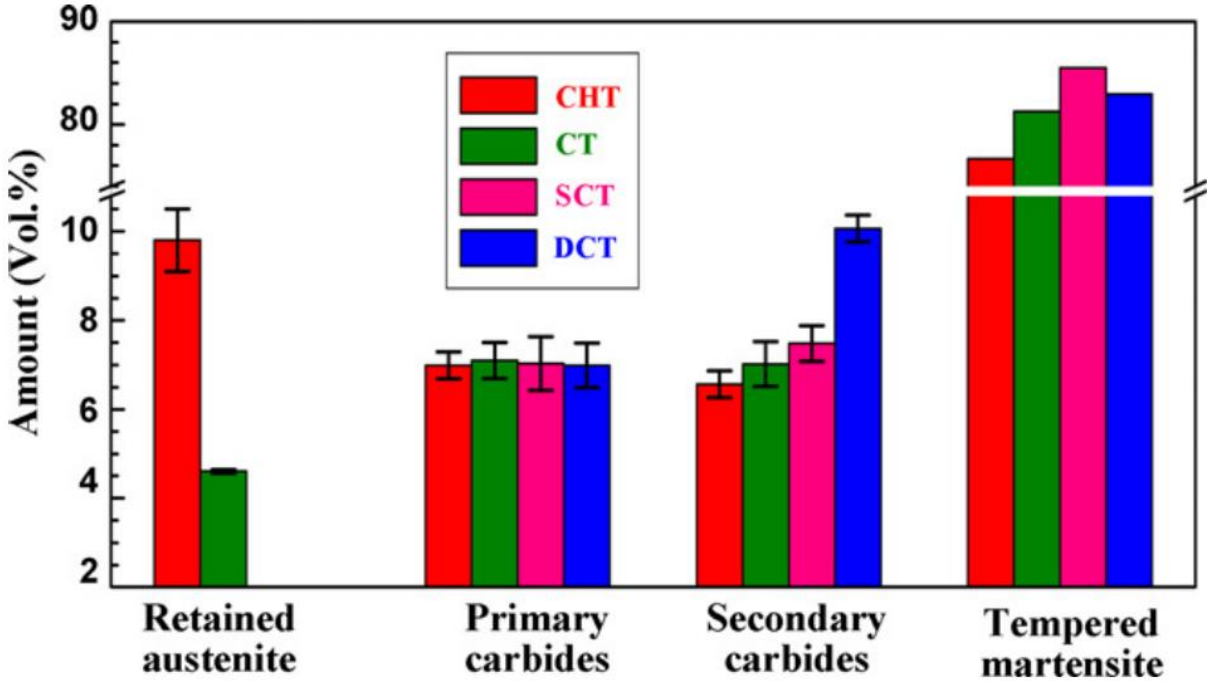

Figure 7 – Effect of the heat treatments in the amount (volume %) of each phase.
CHT: conventionally heat treated; CT: cold treated; SCT: shallow cryogenically treated;
DCT: deep cryogenically treated.
From: Das *et al*., Sub-zero treatments of AISI D2 steel: Part I. Microstructure and hardness [19].

The mechanism that enables the improvement of the mechanical properties in the austenitic stainless steels are different from the ones cited so far, once the microstructure of these alloys is composed mainly of austenite. In the work done by Singh *et al.* [36] on the effect of the cryogenic treatment on the fatigue life of weldment joints in the AISI 304L, it was found that the cryogenic treatment presented improvements to the fatigue properties. A similar result was presented by the same author in the work in which the fatigue life extension of notches in weldments on the same alloy is researched [18]. In these works, it is stated that the improvements are owed to the presence of strain induced martensite that are formed during the cryogenic treatment, due the compressive stresses in the weld material.

The formation of martensite in the austenitic stainless steels is also explored in the research by Myeong *et al.* [37], which analysed the extension life method for high cycle fatigue by using the micro-martensite transformation. In this study, the fatigue life in a low stress amplitude, due to the cryogenic treatment, was increased by more than 60 times. This positive effect is a result of the nucleation of nano-sized martensitic particles, that locks the dislocations and supresses the motion at low stress amplitudes. In the research of Shimojo *et al.* [38], who is also a co-author of the previous paper, it was stated that by controlling the temperature and the dislocation density, a controlled nucleation of the nano-martensite particles could be achieved, agreeing with the results presented by the previous work.

Based on the literature, the main mechanisms responsible for the beneficial effects of the cryogenic treatment found in the mechanical properties of steel alloys are: the transformation of the retained austenite in martensite [9]; precipitation and distribution of nano-carbides in the microstructure of the material [35]; increase in dislocations and twins occasioned by the thermal contractions in the microstructure of the alloy [39]; locking of the dislocations due the nucleation of nano-martensite in the intersection of dislocations .

There is little research about the effect of the cryogenic treatment on light alloys such as titanium alloys. In the few papers researching Ti64 [25,40], the improvement of the wear resistance is attributed to the refinement of the grain size and the reduction and transformation of the β phases in stable β phase and α phase, although this does not present a change in hardness. Also, the cryogenic treatment form high dislocation density and the appearance of twins, which can resist the formation of crack by dissipating energy, that way improving the wear resistance. These both mechanisms are also beneficial to the improvement of the plasticity of this alloy.

2.3. TRIBOLOGY

Tribology is considered a relatively new field of research science, being defined by a committee of the Organization for Economic Cooperation and Development in 1967, as the study of the interaction between surface and relative motion, friction, wear and lubrication [41]. Wear is characterised as the gradual removal of material from a surface, by mechanical separation, due to its interaction with another surface in relative motion [42]. A better understanding of the wear mechanism in different alloys, and the means to improve their wear resistance, can facilitate the design of more efficient machines, as the wear of machine parts can greatly impact their efficiency and life [41,42]. As a tribology study is core to this research, the typical wear mechanisms are presented in the next section, with a particular focus on abrasive wear due to it being responsible for as much as 50% of all wear in industrial applications.

2.3.1. Wear Types

Wear is characterised as the phenomenon of mechanical material removal due to the interaction between two surfaces, being this removal a result of chemical dissolution, microfracture or melting in the wear region [42]. It is not a simple phenomenon, as it can be heavily influenced by different material and environmental characteristics, and it can also present several combinations of the basic mechanisms [9,42].

The basic wear mechanisms can be defined as: corrosive, adhesive, abrasive and fatigue. The wear that occurs on real applications can present a combination of these mechanisms or also some specific case of the basic mechanisms, like: scuffing, galling or oxidative wear. It is also important to note that the wear mechanisms can change during the contact life, once the material properties and the environment can influence the type of wear occurring.

The four basic wear mechanisms, that are considered the representative wear modes, are presented in Figure 8 and detailed in the following sections, as described by previous authors [9,41–44]. To better illustrate the effect of the cryogenic treatment in the wear resistance of alloys under different types of wear environment, a small literature review will be presented, when possible, at the end of each section.

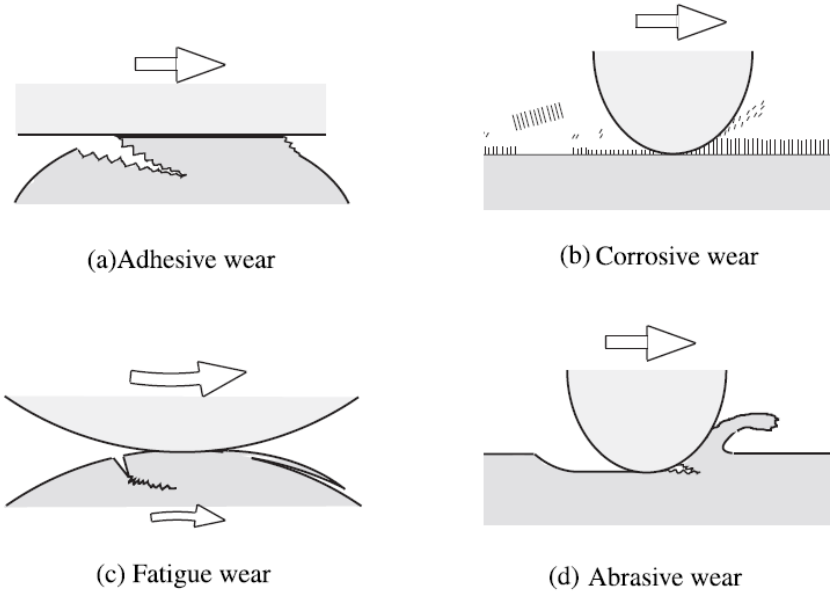

Figure 8 - Schematic of the basic wear mechanisms. [Edited [42]]

2.3.2. Adhesive Wear

Adhesive wear is mainly characterised by the transfer and bonding of material from one contact surface to another. The relative movement of the surfaces and the pressure present in this region generates plastic deformation, which leads to the formation and propagation of cracks. Once these cracks reach the surface and enough adhesive bonding strength is present on the contact patch, due to the contact load (plastic), junctions are formed and subsequently wear particles are bonded to the other surface. This results in one surface presenting lumps from the other material.

Scuffing, also known as scoring, is a form of adhesive wear which presents hardened protrusions originated from local cold-welded junctions due to a poor lubricated contact region. The surface affected by scuffing presents torn or furrowed markings in the sliding direction. The more severe form of this phenomenon is denominated galling, presenting gross damage to one or both surfaces, localized macroscopic material transfer (stuck or friction welded) and, subsequently, the surface failure. This process usually occurs in high loads and poor lubrication conditions. Ductile materials, that asperities tend to plastic deform, are more prone to galling than materials with a harder surface, which the surface asperities tend to fracture under high loads. Since these are complex phenomena, other material characteristics, such as the stacking-fault energies, can also affect the way the surfaces in the contact region interact. Therefore, previous analyses of the materials and conditions are recommended when investigating this type of wear.

The material microstructure can also affect its wear performance when related to adhesive wear. A research conducted by Podgornik *et al.* [45] investigated the effect of the DCT and plasma nitriding on the wear performance of a powder-metallurgy high speed steel. According to this study, the DCT produced fine needle-like martensitic structures, which improved surface hardness, material friction and galling resistance (when against AISI 304). It is also reported that when combining the DCT with plasma nitriding the galling resistance is reduced.

2.3.3. Corrosive Wear

This type of mechanism works as a modifier of the other types of wear, and is generally known as corrosive wear when resultant from a chemical process, or oxidative wear when specifically, due to the interaction of the body and the atmospheric air. The medium in which the wear occurs and the temperature at which it takes place, have a great impact in the wear rate. The removal of the reaction layer, present on the surface of the material and resultant from the previous explained reactions, by the other wear mechanisms characterise the corrosive wear. A reduced coefficient of friction and accelerated wear rate are usual characteristics of the corrosive wear.

Since corrosion can greatly increase the wear rate, heat treatments and protective films are used to increase the corrosion resistance of alloys. The effect of the cryogenic treatment when related to corrosion is not yet defined for many materials. Work conducted by Akhbarizadeh *et al.* [46] on 1.2080 tool steel found that samples submitted to the DCT

presented an increase in carbide content and also a more uniform distribution of these carbides. Due to these effects, the alloy had an increase in the corrosion and wear resistance.

Conversely, however, on the research carried by Gao *et al.* [47], the cryogenic treatment slightly decreased the corrosion resistance of the WCFeNi cemented carbides. Due to the cryogenic treatment, martensitic phase transformation took place and increased the amount of α-(Fe,Ni) phase content in the binder, which presents a lower corrosion resistance than the previous γ-(Fe,Ni) phase. The α phase content increased with the cryotreatment soaking time and, after 24 hours of cryotreatment, the binder content of α-(Fe,Ni) was of 86.8 wt.% (γ 13.2 wt.%). Since the main content of the binder phase had a lower corrosion resistance, the material also presented a lower corrosion resistance after the cryogenic treatment, as expected.

2.3.4. Fatigue Wear

Fatigue wear is usually present in bodies which contacts presents cyclic loads due to relative movement (sliding, rolling or oscillating), high local stresses and which the particles do not adhere to one of the surfaces. The contact region, due to fatigue, is susceptible to the formation and propagation of small cracks close to the surface. This type of wear can also be present in well-lubricated environments, which present high surface contact and enough cycles. The number of cycles that are necessary for the formation of the wear particles is dependent on the material and contact characteristics, and it is possible to find low and high cycle fatigue wear. The presence of high levels of plastic strain and modification of the material microstructure on the contact region are a common characteristic of the fatigue worn surface.

Previous published work showed that the cryogenic treatment can improve the fatigue life on steel alloys. Benseley *et al.* [48] found that submitting EN 353 steel to shallow cryogenic treatment (SCT) increased the fatigue life by 71.42% (when compared to conventional heat treatment) while samples that had undergone DCT had an improvement of 26%. This work also found that the presence of low retained austenite is less beneficial than higher retained austenite when combined with fine carbides. Manoj *et al.* [49] reported that, in a rolling contact fatigue experiment, DCT applied in a case carburized EN 353 alloy improved the surface fatigue strength by 10.16% when compared to the rollers without DCT. In addition, the DCT improved the hardness of the samples by 10.19% and the bending strength by 38%.

The DCT will have an increasing effect on the hardness due to its capabilities of transforming retained austenite into martensite, which may increase the rolling contact fatigue. When related to the low strain fatigue life, the retained austenite can absorb the crack tip energy

and reduce its propagation, hence why the SCT has increased the fatigue life more than the DCT. One important aspect when improving fatigue life is to improve the alloy capability to resist the crack initiation and propagation, which, in this case, can be increased in the presence of fine carbides and an optimum level of retained austenite [48,50]. In applications which the presence of austenite may be beneficial, the increased temperature cryogenic treatment (SCT) can be more beneficial than a DCT.

2.3.5. Abrasive Wear

Abrasive wear is the most common form of wear mechanism, being responsible for as much as 50% of all wear in industrial applications [51]. This type of wear mechanism occurs when particles of one material slide against another material, with equal or lower hardness, promoting material removal (ploughing) during this relative movement process. Although soft materials are more prone to plastic deformation, it can also cause abrasion once its surface is subjected to work hardening and/or phase transitions and present hard particles, even when the bulk hardness of the material is considered soft. The ploughing promoted by abrasive wear, in most cases, is the result of several mechanisms working in conjunction, which can make the analyses of the process difficult. The next sections will present in more detail how types of abrasive, surface and load affect the wear and its mechanisms.

Brittle Fracture

This mechanism is the result of the contact between a brittle surface and a sharp particle under heavy load. The movement of sharp grits on the surface of the brittle material generates cracks during the ploughing, which propagate on the substrate promoting the material removal due to fracture. Since this mechanism is dependent on the shape of the particles, materials that have a hard surface and are resistant to more rounded particles may not be as resistant to the sharp particles, once a brittle surface can facilitate the crack propagation. In this case, the fracture toughness of the material plays an important role on its wear rate. Figure 9 presents the schematic of the brittle facture that occurs during abrasive wear ploughing in a brittle material.

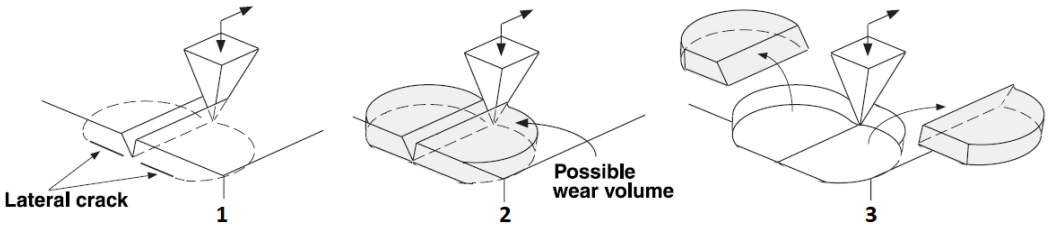

Figure 9 – Three stages of the abrasive wear brittle fracture. (modified [42])

One mathematical model utilised to estimate the wear behaviour of brittle materials was developed by Evans and Marshall in 1981 on their work "*Wear mechanism in ceramics*" [52], and is presented on Equation 1:

$$V = \alpha \frac{W^{9/8}}{K_c^{1/2} + H^{5/8}} \left(\frac{E}{H}\right)^{4/5} L \qquad 1$$

From this equation, it is possible to see the high dependency of the wear volume V to the material hardness H and fracture toughness K_c. To be able to calculate the wear volume, it is also necessary to input the normal load W, sliding distance L, Young's modulus E and the constant α related to fracture properties, which is material dependant and determined based on a well-characterised material. This equation is backed by experimental data [42].

Ductile Wear

The phenomenon of abrasive wear can be easily seen when a third body composed from hard particles is present. However, this type of wear can also happen when two bodies composed of ductile material are in contact and have relative motion. In the case aforementioned, wear can be divided in three modes: cutting, wedge forming and ploughing [53]. These modes can appear combined in a real wear situation and the occurrence of these wear modes is linked with the hardness and shape of the abrasive, the load applied on the contact and also the shear strength of the contact surface [53,54]. Figure 10 presents a schematic of each of these models.

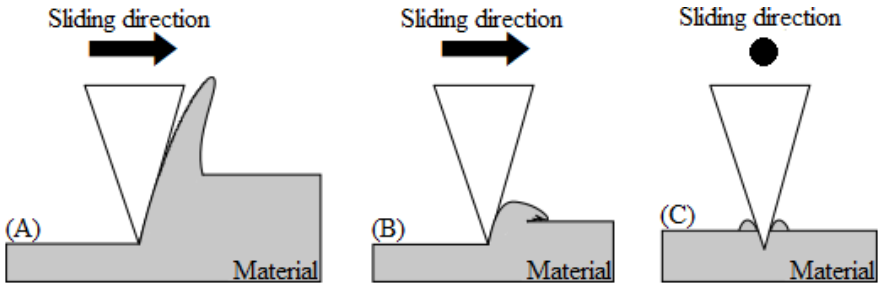

Figure 10 - Wear modes: (A) Cutting; (B) Wedge Forming; (C) Ploughing.

The wear scar and the wear particles formed from this phenomenon will exhibit different characteristics according to the mode of wear that occurred. Cutting is the most efficient mechanism of wear, being able to remove more material than the other two. It is similar to a tool cutting, which the model presents a cone that does a deep cut at each pass, removing an amount of material that can be measured by the volume of the groove left on the wear scar. The wear debris occasioned by cutting resemble curled ribbon-like chips, also similar to the ones formed by a cutting tool [55]. Even though the amount of material removed

can be measured, the total wear is just an approximation of this volume, since there is also a small amount of ploughing occurring on the edges of this groove, which represents material removed from the contact region that is plastic deformed but not totally removed from the body. Equation 2 presents the material removal volume (V) due to this type of wear, that can be calculated by approximating the wear groove formed to a cutting done by a sharp cone, which presents a depth d, a conical angle θ and a sliding distance L.

$$V = d^2 * \tan\theta * L \quad (2)$$

Wedge forming is a mechanism similar to cutting, but there is a minimum formation of debris, once during the groove formation the material accumulates at the tip of the grooving asperity. During this mechanism, a wedge is formed at the tip of the wearing grit particle and then grows with the sliding distance due to the adhesive transfer of the removed layer on the worn surface, as presented on Figure 10(B). The groove formed during this wear presents a small ridge on the sides (due to small scale ploughing) and the wedge formed on the tip stays on groove helping its formation. Once the wedge is formed gross sliding occurs at its base and no further wear debris are formed, being the initial wedge the only wear particle resultant of this wear mode [55].

The two modes previously explained share a characteristic that can occur on its own and is known as ploughing. In this mode, the wear groove formed is shallow and, on a single sliding pass, there is no wear particles formation. After repeated cycles wear, debris can be formed due to the accumulated deformation, this way releasing the ridges from the surface. Since the side wedges formed can stay on the worn material, having been displaced from the contact but not lost from the mass as shown in Figure 10(C), a more refined method should be used to enable the precise measurement of the wear volume. This is because simply using the mass loss and the density of the material to approximate the volume of the wear scar region will not be accurate.

Two and Three Body Abrasion

This classification of wear relies on the type of movement that occurs when the abrading grits pass over the surface being worn, which are denominated as two-body or three-body abrasion. Figure 11 presents the two-body abrasion (A, B) and the three-body abrasion (C).

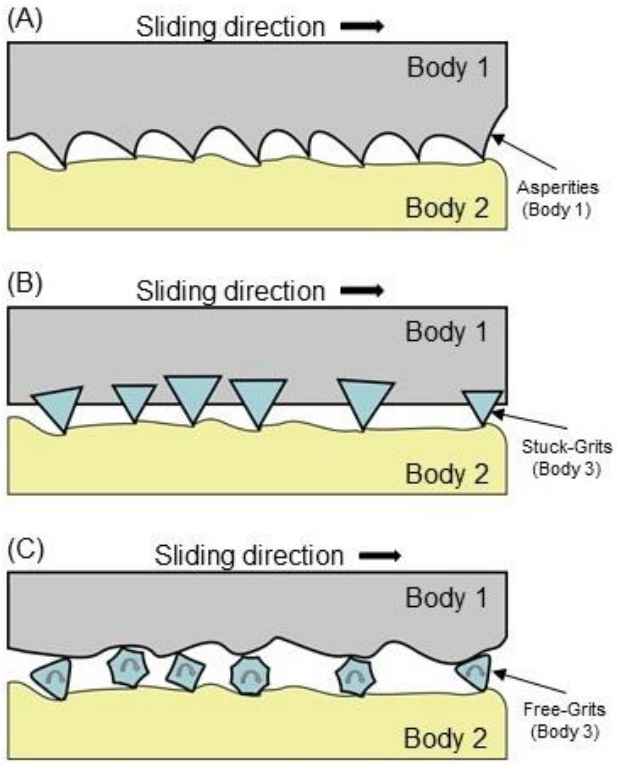

Figure 11 - (A, B) Two-body abrasion; (C) Three-body abrasion.

The two-body abrasion occurs when the grit is stuck to one of the bodies, which act more like a cutting tool and originates a groove on the other body in relative motion. In this case, the grit particles do not need to be from another material, since the asperities on one of the bodies can act as the cause of the wear scar on the other body, as shown on Figure 11(A).

When there is a presence of a third body in the middle of the surface in motion, the wear is caused by a three-body abrasion. The rolling grits can be formed by the shattering of the asperities on the bodies or by the introduction of another material in the interface of these bodies. This type of wear may not present grooves, instead a random topography is presented, which suggests that the material is gradually removed during each pass of the rolling grit. The three-body abrasion is found to be a slow wear method, being 10 times slower than two-body abrasion [41].

2.4. WEAR TESTING

Testing a material application under real work situations can be difficult and costly in terms of time and resources. Attempts to overcome this have resulted in many different test rigs being developed by researchers to simulate and quantify the diverse types of wear that may occur during the material life in its real operation.

Wear and friction are complex material parameters that result from a sum of factors and are not only dependant on the material properties [42]. This way, it is necessary to select the test that best represent the material application, e.g., applied load, duration, contact type and environment characteristics.

Through the years that wear research has been developed, many types of wear tests were proposed and some became well established tests with technical standards for better reproducibility. The ASTM G190 standard [56] presents a list of the available ASTM standards for wear tests as well as a guidance for the test selection and development.

2.4.1. Abrasive Wear Testing

In engineering applications, abrasive wear is presented as the most common cause of mechanical failure, being responsible for as much as 50% of all wear problems presented in industry [51,57]. This type of wear is present in many different forms (loads, abrasive particles) and, for this reason, different rigs can be utilised to quantify a material's abrasive wear resistance. There are many popular abrasive wear tests, for instance: pin-on-disk, rubber-wheel/dry-sand, Taber abrasive wheel tester, and many others.

Laboratory wear tests are not limited to the measurement of a single specific wear parameter, and some wear rigs present a more realistic test method, which may include the utilisation of parts and mechanisms used in the actual engineering application. It is possible to quantify the wear resistance of the material pair by simulating the real situation in a controlled environment, for example, assembling a reciprocating driven piston on an engine block.

In this research, the dry-sand/rubber-wheel test was selected due to its broad application in industry, the simple setup and specimen preparation, and the straight forward wear resistance quantification. Depending on the real application the abrasive wear test can present different forms, being also utilised with higher loads (jaw crusher abrasive wear test) or in the presence of a slurry instead of dry sand. These test methods and parameters must be selected according to the best fit for the desirable results.

2.4.2. Dry-sand/Rubber-wheel Abrasive Test

The Dry-Sand/Rubber-Wheel (DSRW) is an abrasive wear test that is used to quantify the abrasive wear resistance of a material in a direct and simple way, being standardised by the ASTM G65, which was developed by ASTM Subcommittee G02.30 [58]. Its ease of use and vast applicability have led to it being widely used in industry. This type of test presents the

situation where the abrasive wear is defined by a low-stress and three-body abrasion mode, once the particles are introduced as a third abrading body [59]. Since the creation of the ASTM G65 standard [58], this became the most popular abrasive wear test, being employed in many companies to characterise and compare the materials, since it presents a simple mechanism and qualitative comparable results (volume of wear material) [59–61]. The DSRW presents results that could be correlated to the ones found in the real application, once the field presents the same mechanisms as this test, meaning that it could be used as guideline for the selection of the best applicable material for the situation [59]. Figure 12 presents basic mechanism design of a DSRW rig.

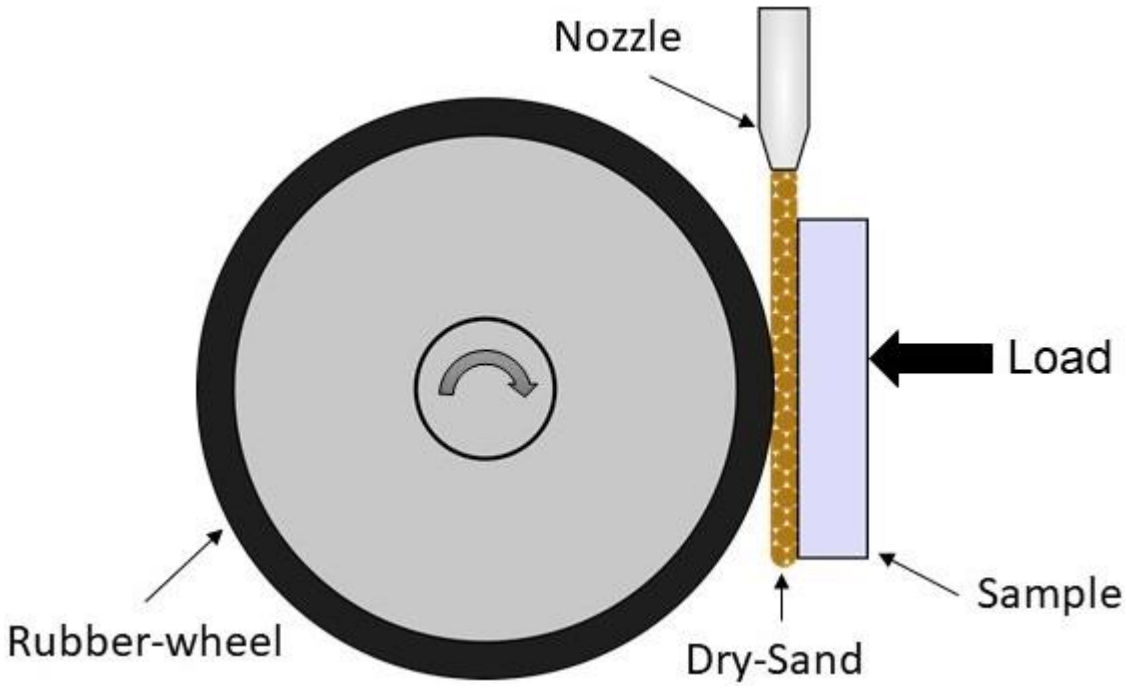

Figure 12 – Basic mechanism of the standard DSRW rig.

The test rig presents simple mechanisms; it is composed of a wheel clad in rubber, a load mechanism and a flow of abrasive. The ASTM G65 presents the parameters that are necessary for the construction of a standard test rig, which will have standard dimensions, rubber composition, applied load and abrasive. According to the standard, the material wear should be reported in material volume loss when submitted to a specific load and slide distance, which makes comparison between materials simpler for the ones that are not from the field. The only other equipment necessary to measure the volume loss is a precision scale, because the material density is known. This type of apparatus is utilised in this study and is presented in more detail in Section 3.2.

2.5. LITERATURE REVIEW SUMMARY

Based on the background information and the state of the art publications found in this chapter, the following points are of importance:

- Heat treatments are processes used to alter the alloys microstructure and, consequently, some of its mechanical properties.
- Conventional heat treatments are treatments that use temperatures above 273 K.
- Cryogenic heat treatments are treatment that use temperatures below 273 K, being divided in: Cold treatment (273 K > T > 193 K), shallow cryogenic treatment (193 K > T > 113 K) and deep cryogenic treatment (113 K > T).
- Wear is a gradual removal of material from a surface, being the type of wear that's the focus of this study the three-body abrasive wear.
- There are several test rigs to test a material's wear resistance. In this work, the chosen test is the ASTM G65 Dry-sand/Rubber-wheel test.
- Due to the cryogenic treatment being relatively new, there are still lack of published work that deeply analyses its mechanisms.
- There are few published works about the deep cryogenic treatment effect in the Ti64.

3. METHODOLOGY

The methodology of the experiments and analysis used in this research to achieve its defined aims and objectives are presented in this chapter. Firstly, the methodology structure is presented, followed by the detailed design and development of the test rig that was built and used during this research. The materials selection, sample preparation and the development of the experimental test are described. Finally, the analysis methods used to obtain the results (presented later) are explained and the used parameters listed.

3.1. DESIGN OF METHODOLOGY

The materials chosen for this study (Section 3.3) were submitted to conventional heat treatment, as per their specification, regardless of their state as-received. A quantity of each material was also submitted to the deep cryogenic treatment (DCT). After treatment (explained in detail in Section 3.4.2), the samples were sectioned according to the specification of each of the analysis methods carried out during the characterisation, as described in Section 3.3. Figure 13 presents a flowchart of the general methodology used in this analysis.

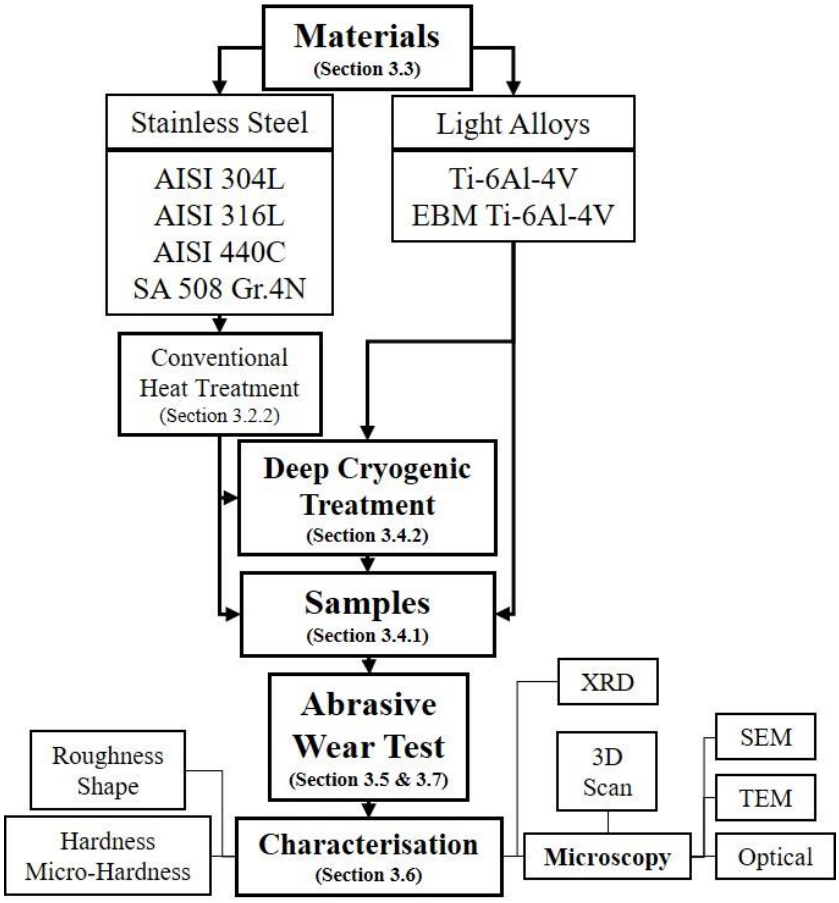

Figure 13 - General methodology flowchart.

The experimental work performed during this research was split into two main stages. The first stage used more commercially common stainless-steel alloys and a more specialist stainless steel alloy typically used in pressure vessels, and in the second stage a light alloy and a printed alloy.

3.2. DESIGN OF TEST RIG

The test rig used during this research was designed based on the ASTM G65 standard. The development process, the new features and the building and refining of this rig are described in detail during this chapter.

3.2.1. Initial Concept

As part of this work, a new abrasive wear test rig that uses the rubber wheel with dry sand wear principle, based on ASTM G65 - 16e1 (Standard Test Method for Measuring Abrasion Using the Dry Sand/Rubber Wheel Apparatus), was developed. The main difference compared to the standard design concerns to the wheel rubber material responsible for movement of the sand particles on the surface of the sample to be abraded. ASTM G65 defines that a chlorobutyl rubber supplied from a single global supplier, but this is now unavailable in the market. This chlorobutyl coating material was substituted by a neoprene rubber layer, which presents the same hardness and nominally similar behaviour and has also been used by commercial vendors for the same application. Otherwise, the wheels used in the new test rig are the same physical dimensions as the one presented in the standard.

None of the other features of the new rig directly related to the test itself (wheel geometry, location of the wear contact patch, wheel rotational speed, motor power and applied contact force) were altered. The sand used in the test was not the same sand as used in the standard tests and is described and analysed in Section 3.5.2.

3.2.2. Initial Design

Figure 14 shows a simplified schematic of the main parts of the wear test rig designed during this research. The load arm has an eye bolt which is used to secure and locate the mass responsible for applying the load on the sample placed in the sample holder. The sample holder was designed to securely hold samples sized as per the standard (Section 3.4.1). The lever is used to lift the load arm and make/break the contact between the sample and the rubber wheel, which also makes this procedure smoother and lighter to handle. The constant sand flow comes

from the nozzle, which is positioned just above the region where the contact between the wheel and the sample occurs. This nozzle is designed to offer a good and thick curtain flow with no turbulence, being that the original dimensions are determined in the standard.

The rig mainframe (Figure 14) was manufactured from 6082 aluminium alloy of two thicknesses: 5/8" (back-plate) and ½" (top, bottom and side plates). Since the load arm (Figure 15) is responsible for transmitting the load to the sample being tested it is important that it does not deform during the loading procedure and, for that reason, the load arm was designed by CAD, underwent the working load simulation and was later CNC machined from a high grade 6082 T651 aluminium plate, ensuring its rigidity during the tests.

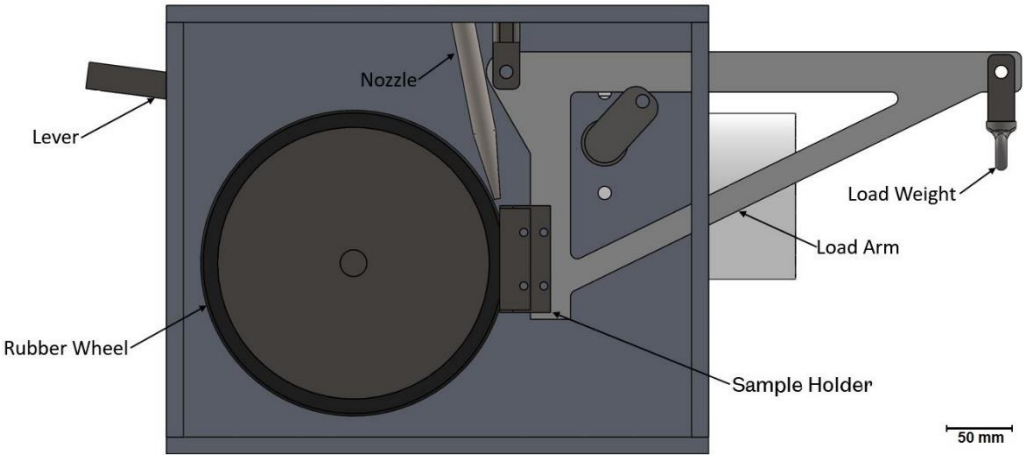

Figure 14 - Simplified schematic of the rubber wheel and sand abrasive test rig.

The test rig also features two different designs of sample holder, allowing both standard ASTM G65 samples and the 440C circular samples used. Both of the sample holders present the contact of the sample in the same region of the wheel and also present the same balance point in the load arm. Small grub screws were added to ensure no sample movement during the tests. Figure 16 illustrates the differences between the sample holders.

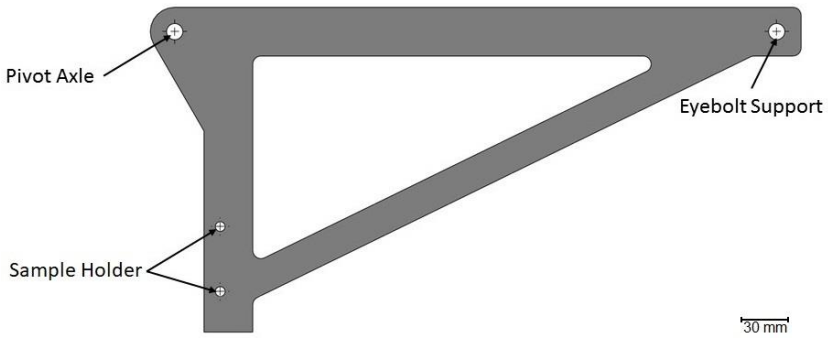

Figure 15 - Load Arm schematic drawing.

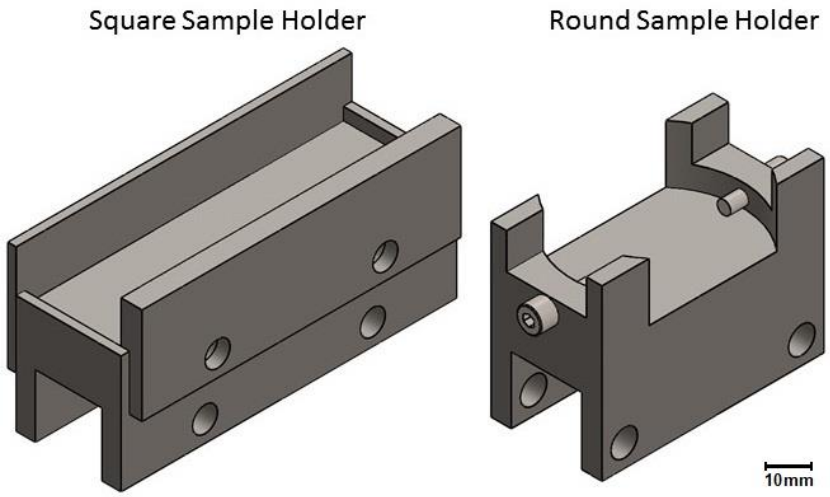

Figure 16 - Sample holders schematic drawing.

The design of the new rig took into account that different types of users would operate it. The lever was designed to facilitate the unloading of the sample by ensuring that the force necessary to unload it using the lever is significantly less than the weight of the load applied to the end of the load arm. Another aspect that guided the design of the rig was the form factor, which kept the rig to a smaller size when compared to similar test rigs. An acrylic window, in front of the rig mainframe shown in the Figure 14, ensures the user is protected from the moving parts and any debris that may result from a test. Figure 17 presents the initial assembly of the real DSRW rig.

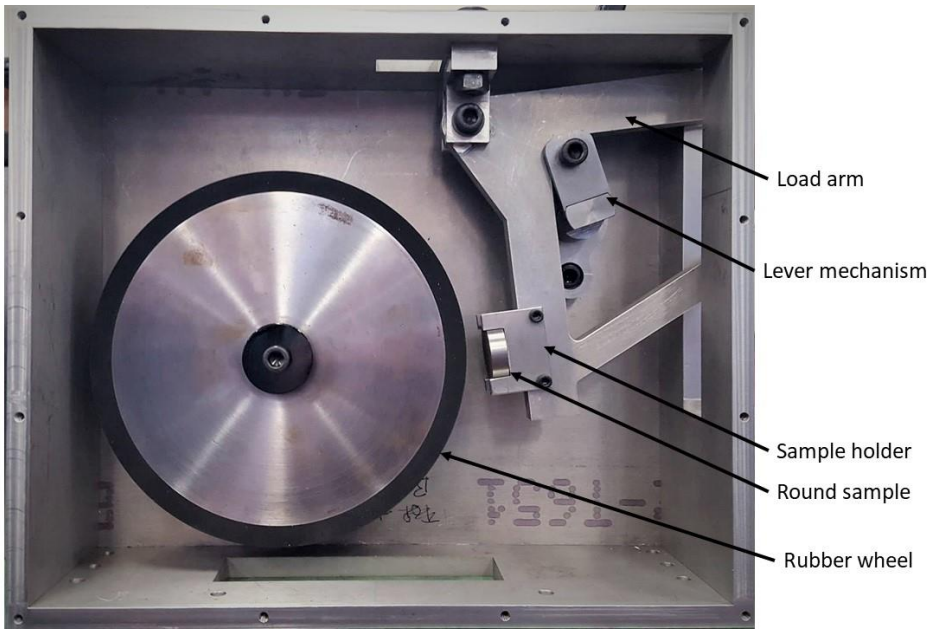

Figure 17 - Initial assembly of the DSRW Rig.

Since this is a comparative test, the results will be only compared with results of tests performed on the same equipment. It is expected that the differences compared to ASTM G65 do not alter the repeatability of the results. If strictly needed, the materials that are not in accordance with the standard (round sample holder and sand) can be easily replaced to those that meet the standard without any modification to the equipment design.

3.2.3. Final Version of the Abrasive Wear Test Rig

Figure 18 shows the final rig assembly that was used during all the testing performed in this research. Once the rig was assembled, some final minor refinements were needed to guarantee the best and most efficient usage of it. As it is shown on Figure 18 (Detail A), the mainframe of the test rig had a column added in the middle, which added to the stiffness of the rig and made possible to add two transparent windows, being one fixed (left side) and one with a latch (right side) to facilitate the loading and unloading of the sample holder. Inside of the area in which the test takes place, a rubber catch was made to make it easier for the sand to flow to the bottom sand container, this way making sure that sand would not accumulate in the corners of the mainframe and reducing the time needed for the preparation between tests. In front of the transparent door an aluminium sand catch was added to minimize the sand spillage when opening the access door.

The sand hopper was originally fitted with a plastic globe valve that was used for the initial tests, needing replacement due to constant blockages. The internal mechanism of the plastic globe valve was removed and an alloy valve was designed and fitted, presented on Figure 18 (Detail B). The bottom sand container chosen is made of metal, since polymer containers would increase the static charge generated by the sand. The rig is fitted with a control box on the left side, which presents the start/stop button and the emergency stop button. An Arduino microcontroller was used in conjunction with a hall sensor to monitor the speed and count the revolutions of the wheel.

The final step of the rig commissioning was the calibration of the sand flow and the wheel speed. According to the ASTM G65 standard, the wheel speed should be near to 200 rpm and the sand flow should be 300 to 400 g/min. The sand flow was measured using a timer and a scale and the nozzle was calibrated accordingly, also certifying that the sand flow would not be turbulent. Once the gearbox and pulleys were selected and installed, the wheel speed was measured using a tachometer. All these parameters can be easily adjusted and calibrated if

ever needed. Details C and D of Figure 18 present the details of the nozzle, sand flow and sample holder.

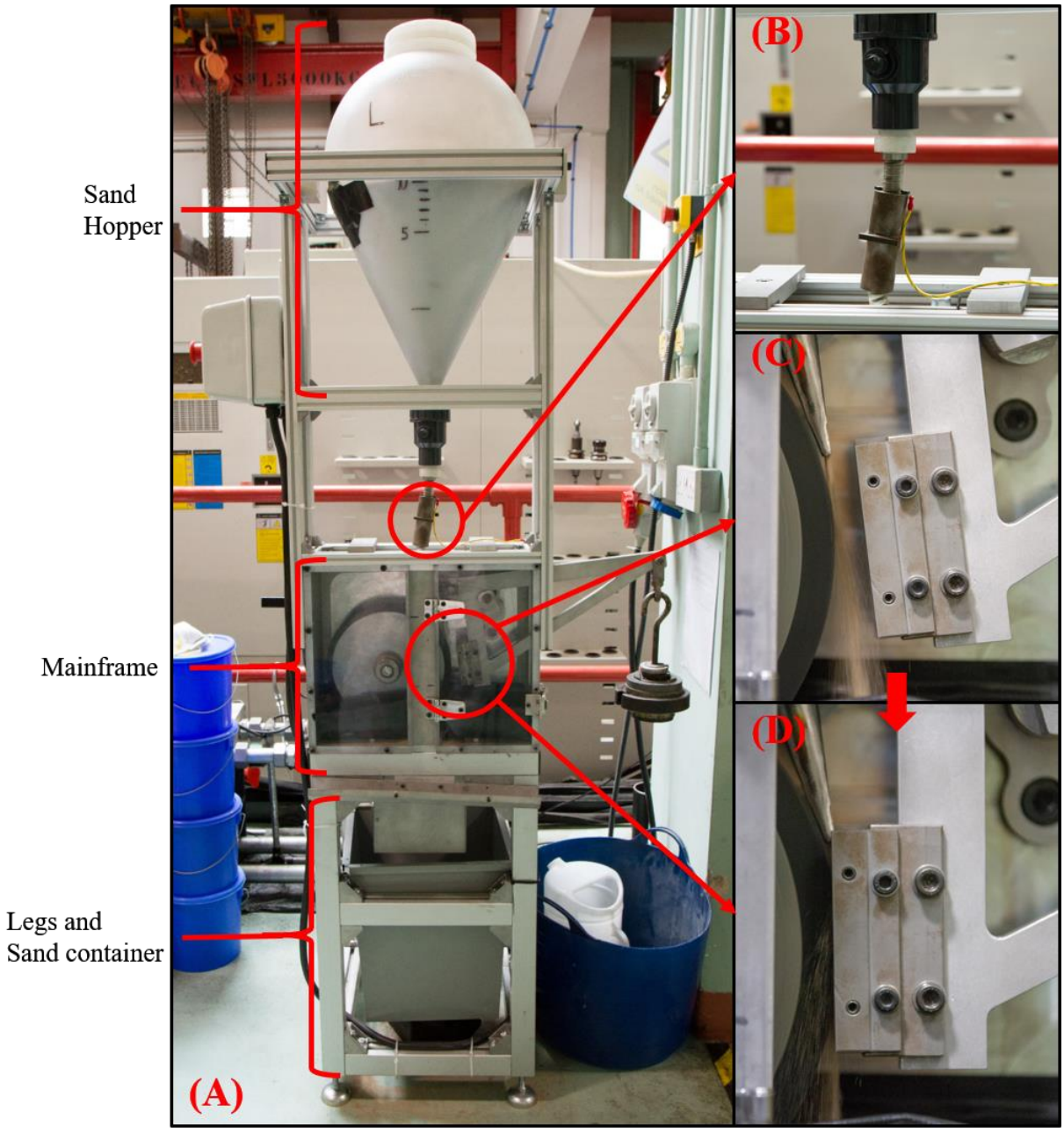

Figure 18 - Final version of the ASTM G65 Dry Sand Rubber Wheel abrasive test rig: (A) Overall vision of the test rig; (B) Detail of the sand flow valve; (C) Standard Samples Holder in the rest position; (D) Standard samples holder in the test position.

3.3. MATERIALS

In order to investigate the effect of the cryogenic treatment on the properties of different commercial alloys, several different types of alloy were studied. Initially, three stainless steels, two being martensitic and one being austenitic, and a low alloy steel were submitted to the

treatment and characterised according to the methodology described in this Chapter. Secondly, a light alloy and an additively manufactured alloy were also submitted to the cryogenic process, tested and compared to the results of the alloys that were not submitted to this treatment. The chemical composition, detailed information and characteristics of the aforementioned alloys used in this research are described in the following sections.

3.3.1. AISI 440C

AISI 440C is a martensitic stainless steel with a high carbon content, high hardness, good corrosion resistance and excellent hardenability. It is usually supplied in the annealed condition with a medium hardness, to facilitate the manufacturing process of the parts, once after treated it can attain a good wear resistance and the highest hardness among all commercial stainless steels' grades. This martensitic stainless steel was chosen to be used as a verification of the cryogenic treatment effectiveness, since the main effect of this treatment is to transform the retained austenite into martensite, which would make the samples submitted to DCT harder than the ones that were only conventionally heat treated. Table 3 presents the chemical composition of the AISI 440C.

Table 3 - AISI 440C chemical composition.

	Carbon	Manganese	Phosphor	Sulphur	Silicon	Chrome	Molybdenum
440C	0.95-1.20	1.00	0.04	0.03	1.00	16-18	0.75

*Values in percentage by weight [wt.%].

This martensitic stainless steel is usually referred as a bearing steel, due to its mechanical properties making it a perfect candidate for making bearings' balls, rollers and races, but it is also used in many other applications in which the high hardness and mild corrosion resistance is desired, such as: moulds & dies, valve components, measuring instruments, gage blocks, surgical tools, pumps and cutlery. Many of these components are subjected to abrasion either directly as a result of their use (e.g. slurry pumps), but also during failure or degradation elsewhere in the system where a lack of abrasive wear resistance would decrease life (e.g. soot from combustion in lubricating oils).

3.3.2. SA508 Gr 4N

The SA508 Grade 4N is a low alloy carbon steel developed to be used in the nuclear industry to manufacture RPV (reactor pressure vessels) and its tubes and connections. Since the life span of a nuclear powerplant is generally determined by the RPV, once it is its main

component and its replacement is not viable, the development of a new material that would make possible to increase the thickness of the RPV and also present better properties than the ones being used up to this time was needed. The materials used in both primary and secondary circuits of nuclear reactor systems are subject to abrasion from debris in the coolant and the liquid metals and salts used in their operation.

This alloy was developed as an upgrade to alloys that already had good properties for this application and were widely used in this industry for more than 30 years, such as SA533 Grade B or SA508 Grade 3. The Grade 4N presents a higher strength and toughness when compared to the cited older alloys. These increased properties are results of the increased hardenability due to the higher Cr and Ni content. The microstructure of this alloy is composed of a mix between martensite and bainite, being that the precipitation and refinement of carbides can be responsible for the changes in the mechanical properties. Table 4 presents the chemical composition of the SAE508 Gr 4N.

Table 4 - SAE08 Gr 4N chemical composition.

	SA508 Gr 4N		**SA508 Gr 4N**
Carbon	0.230	Vanadium	0.030
Manganese	0.20-0.40	Niobium	0.010
Phosphor	0.020	Copper	0.250
Sulphur	0.020	Calcium	0.015
Silicon	0.400	Boron	0.003
Nickel	2.80-3.90	Titanium	0.015
Chrome	1.50-2.00	Aluminium	0.025
Molybdenum	0.40-0.60		

*Values in percentage by weight [wt.%].

The SA508 Gr was selected due to it being a relatively new low alloy steel and its main usage being as a pressure vessel alloy. This application likely means that the parts manufactured with this alloy present an increased thickness that are better suitable to the cryogenic treatments (since a longer soaking time would not increase the effect in the external wall and would make possible to treat the part homogenously). Also, the literature for this low alloy steel does not present enough information about it being cryogenically treated, adding novelty to the results presented in here.

3.3.3. AISI 304L and AISI 316L

AISI 304L and AISI 316L are both austenitic stainless steel alloys. Together, these alloys are the most commonly used austenitic stainless steels, especially due to their excellent corrosion resistance, good mechanical properties and machinability. The main difference between these alloys is the addition of molybdenum to the AISI 316L, which makes it more resistant to corrosion at higher temperatures and in more corrosive mediums (e.g. saline, chloride, bromides). This better corrosion resistance also makes the AISI 316L biocompatible, being used in a number of medical applications.

These alloys are both portraying the letter L after its designation due to it being the lower carbon version of its respective alloy families (AISI 304 and AISI 316). The lower carbon makes it less prone to sensitization, which may occur when these alloys are submitted to higher temperatures for a longer time (welding or even heat treatment). The lower carbon content prevents the chromium carbide precipitation, this way decreasing the chance of corrosion occurring on the grain boundaries that could be deficient in chrome. The chemical composition of the alloys used in this work was analysed and is presented in Table 5.

Table 5 - Nominal chemical composition of the austenitic stainless steel alloys and chemical composition measured.

	Carbon	Manganese	Phosphor	Sulphur	Silicon	Nickel	Chrome	Molybdenum	Nitrogen
304L	0.03	2	0.045	0.03	0.75	8-12	17.5-19	-	0.1
304L*	#	1.15	#	#	#	8.32	18.09	0.26	#
316L	0.03	2	0.045	0.03	0.75	10-14	16-18	2-3	0.1
316L*	#	1.69	#	#	#	10.35	17.07	1.94	#

*These composition values were measured using the Fischerscope XAN. The "#" represents the elements that are too light to be measured using the equipment mentioned, these limitations are explained on Section 3.6.1.

**Values in percentage by weight [wt.%].

These austenitic stainless steels are very versatile, easy to form and weld, which leads it to be used in many different applications according to the level of corrosions resistance needed. The main areas of use are heavy industry (oil, gas, chemical, offshore, marine), food processing, medical equipment, pharmaceutical plants, aerospace, nuclear reactors and many others engineering applications where abrasion regularly occurs.

These alloys were chosen to investigate the effect of a commercial deep cryogenic treatment on an austenitic alloy, since any positive effect would be related to less conventional

effects of the cryogenic treatment. As reported in the literature [37,38], the DCT applied to this series of austenitic stainless steels can form nano-martensite, which may have a positive effect in the wear resistance of this alloys.

3.3.4. Cast Ti-6Al-4V and EBM Ti-6Al-4V

The Ti-6Al-4V (often colloquially known as "Ti64"), which is an alpha-beta titanium alloy, is the most commonly used commercial titanium grade. Its main characteristics are the good strength-to-weight ratio and its high corrosion resistance. It has a density of up to 50% of steel or nickel alloys, therefore having wide application in areas in which the low weight of parts is extremely important. Another important characteristic of this material is its biocompatibility, making it a good candidate to be used in the manufacturing of prosthesis that are in direct contact with bones or tissues. Due to this alloy's poor wear resistance, particularly in sliding (including abrasion) it is usually submitted to surface treatments when a better wear resistance is needed during the application.

In this work, two different types of Ti64 were used, being one the regular cast Ti64 hot roller annealed plate and the other sample obtained through the additive manufacturing process of electron beam melting (EBM) (specifically the Arcam variant). The composition of the Ti64 and the EBM Ti64 used to manufacture the samples are presented on Table 6.

Table 6 - Chemical composition for the cast Ti64 and the EBM Ti64.

	Vanadium	**Aluminium**	**Iron**	**Oxygen**	**Titanium**
Ti64	3.95	6.24	0.18	0.16	Balance
EBM Ti64	3.94	6.45	0.19	0.12	Balance

*Values in percentage by weight [wt.%].

Conventional Ti64 is widely used in the aerospace industry, and also used in areas in which the low weight is considered important, like motorsport or radio-controlled vehicles. EBM Ti64 is a more recent process route but presenting a higher cost and therefore is currently limited in its usages to very specific areas where the cost is not one of the main factors when selecting the material. Examples are in the medical area (prosthesis) and for industrial applications in which the prototypes or specialized parts that cannot be produced using other types of manufacturing techniques, typically due to their complex geometry, are required.

These alloys were primarily selected due to the literature not presenting much information about the effect of the deep cryogenic treatment on the abrasive wear of Ti64 and also lack of a literature that compared the cast Ti64 and the EBM Ti64 directly. The possibility of submitting these alloys (which have the same composition but are produced using different techniques) to the same mechanical tests made it therefore an important research subject. The novelty of the EBM Ti64 being submitted to the deep cryogenic treatment only increased further the importance of analysing this specific material.

3.4. SAMPLE PREPARATION

This section presents the details about the samples used during the abrasive wear test and heat treatments applied in each of the materials.

3.4.1. Standard Samples

The samples were sized according to the respective test standard or, in the cases without a specific standard, with dimensions that best facilitate the subsequent analyses. The samples of AISI 440C were manufactured from a round bar 38.1 mm (1.5 in.) in diameter (a common as supplied size for this material) by slicing in 10 mm thick discs using wire EDM, due to the material high hardness.

Using the same technique, the SA508 samples were obtained from a billet, which was sectioned into small plates in accordance with the samples size requirements of the abrasive wear test standard ASTM G65.

The samples of AISI 304L and AISI 316L were sectioned from a 10 mm thick plate to the dimensions in ASTM G65 using a water jet cutting machine, as this process is capable of cutting this material at a cost less than wire EDM. Figure 19 presents the geometry of an ASTM G65 sample.

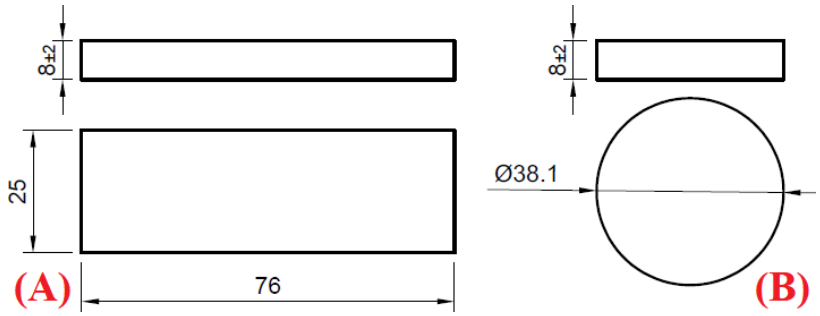

Figure 19 - Samples for the abrasive wear rig: (A) Standard G65 rectangular sample; (b) Circular sample.

The regular cast Ti64 was sectioned out of a bigger plate that had the same thickness as the final sample. The additively manufactured (EBM) sample was processed using an Arcam A2 machine and the used powder had a particle size range of 45-106 µm. This type of machine uses a plasma to atomize the powder and produce the sample and the parameters used were the standard parameters supplied by Arcam V3.2.121. The samples were produced with one of the sides (76 x 8 mm) serving as a base and the schematic from the additive manufacturing process is shown on Figure 20. The EBM obtained samples were roughly to the standard sample size, only needing to be ground on all the side faces to present a better rectangularity.

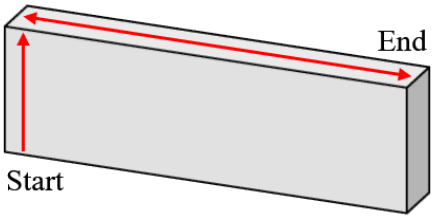

Figure 20 - Schematic of the EBM Ti64 additive process.

The abrasive wear test samples have a flat surface and a ground surface finish. The samples used for hardness, chemical composition analysis and metallography were sectioned from these larger rectangular samples, with geometry suited to each of the analysis methods. It is important to note that all the tests were performed on the same face of each of the materials, i.e. each of the samples used on the characterisation has the same orientation of the samples used in the wear test experiment, that way making sure that the tests are always carried out on the same surface of the material.

3.4.2. Heat Treatments

The engineering alloys used in this research were submitted to commonly used conventional heat treatment prior to the DCT. This is because in commercial and industrial applications the cryogenic treatment is used as an additional treatment, being performed sometime after or as part of the conventional heat treatment cycle and, due to this, a similar approach was taken in this methodology. The exception was the titanium alloys that were not conventionally heat treated (explained later in this section). The aim was not to compare the cryogenically treated samples to the conventionally treated samples, but was to analyse the further effects that the deep cryogenic treatment can present when used in commercial applications.

The prepared samples were first conventionally heat-treated according to the specification of their respective alloys. Half of the samples from each of the alloys were submitted to a cryogenic DCT at different stages of the heat treatment cycle.

The AISI 440C steel samples were subjected to a two-stage austenitizing, 1118 K for 30 minutes and then at 1313 K for 20 minutes. After this heat treatment, the AISI 440C samples underwent a DCT and later a tempering at 463 K for 2 hours.

The SA508 Gr 4N Class 2 steel had undergone austenitization for 2 hours at a temperature of 1153 K, later being submitted to the cryogenic treatment and tempered at 933 K for 2 hours.

The austenitic stainless steels (AISI 304L and AISI 316L) were subjected to an annealing heat treatment at 1228 K for 30 minutes, air cooled to room temperature and later submitted to a deep cryogenic treatment (DCT).

Both of the titanium alloys (cast Ti64 and EBM obtained Ti64) were only submitted to the deep cryogenic treatment after being received, with no additional conventional heat treatment performed. This was deliberate, in order to better analyse the performance of these alloys as "off the shelf" solutions, since this allowed to directly compare a commercial cast Ti64 sample to an EBM 3D printed sample.

The deep cryogenic treatment was performed by Cryogenic Treatment Services Ltd (Newark - UK), which is a research partner, and the parameters utilised were the same as the ones used during their commercial standard cryogenic treatment services for industrial purposes, shown in Figure 21.

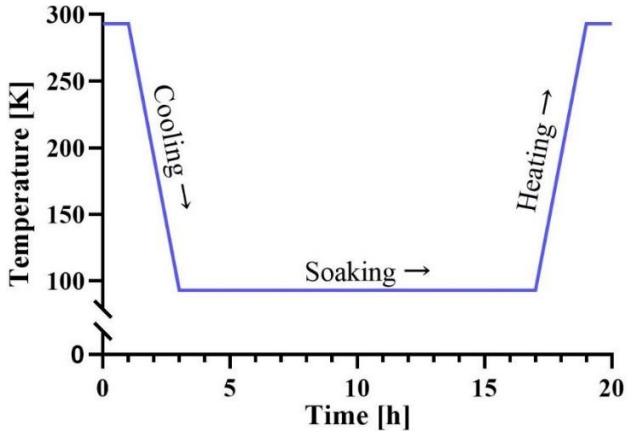

Figure 21 – Deep cryogenic treatment performed in the samples.

During the cryogenic treatment process, the samples were cooled in a chamber with nitrogen atmosphere at a rate of ~2 K/min until the temperature reached 93 K. The temperature in the chamber was maintained at 93 K over a period of 14 hours (soaking), and then gradually returned to room temperature (heating), again at a rate of ~2 K/min. Table 7 presents the sample nomenclature for each of the materials and the final treatment condition it was submitted to.

Table 7 - Sample nomenclature.

Material	Cryogenic Treatment	Designation
AISI 304L	No	SS304
AISI 304L	Yes	SS304CT
AISI 316L	No	SS316
AISI 316L	Yes	SS316CT
AISI 440C	No	A440
AISI 440C	Yes	A440CT
SA508 Gr 4N	No	SA508
SA508 Gr 4N	Yes	SA508CT
Ti-6Al-4V	No	Ti64
Ti-6Al-4V	Yes	Ti64CT
EBM Ti64	No	ETi64
EBM Ti64	Yes	ETi64CT

3.5. DESIGN OF EXPERIMENT DEVELOPMENT

The final experimental parameters for the abrasive wear test were determined after a series of initial tests and results comparisons, this way promoting high likelihood of repeatable and more precise results. The development of the final experimental parameters and the reasons behind it are presented in the two following sections.

3.5.1. Methodology Development Tests

The reliability of the results resulting from an experimental test is a very important factor and to achieve the best repeatability and accuracy of the results obtained on this rig, a series of initial tests were performed. These tests comprised of using the standard specimens for the abrasive wear test made of an inexpensive and easily sourced commercial alloy, being the mild steel EN1A the selected material.

The specimens were manufactured by sectioning various thickness plates of EN1A in the as received condition (without applying any further heat treatment) to the sizes presented on Section 3.4.1 and lather grinding the surface to the standard roughness. To be able to account for the different thickness that the future test samples may have, these samples presented a varied range of thickness, varying inside of the limits determined when designing this test rig (8 ± 2mm). The parameters for the tests were the same as the ones used for most of the alloys used in this research, which are defined as test method A, that has a duration of 6000 revolutions, speed of 200 rpm, a load of 130N and a dwell time of 30 minutes (being the most extensive and also using the highest load of all the standard test). The results for the initial calibrating tests are presented on Table 8.

Table 8 - Results for the initial calibrating tests using the EN1A samples.

Sample	Test Order	Mass Before [g]	Mass After [g]	Mass Loss [g]	Volume Loss [mm^3]
1	1st	134.2031	134.0204	0.1827	23.274
2	2nd	133.9109	133.7128	0.1981	25.236
3	3rd	134.1992	134.0023	0.1969	25.083
1'	4th	134.0204	133.8327	0.1877	23.911
2'	5th	133.7128	133.5133	0.1995	25.414
4	6th	147.3878	147.1987	0.1891	24.089
5	7th	148.7329	148.5289	0.2040	25.987
6	8th	149.2991	149.0914	0.2077	26.459
7	9th	147.7849	147.5825	0.2024	25.783
8	10th	148.4412	148.2443	0.1969	25.083

The results present for the initial calibrating test were as expected and showed that the machine was capable of maintaining a good reproducibility even when the thickness of the samples would vary. The average result for the wear loss of the EN1A samples was 25.032 ± 0.315 mm^3 with a standard variation of 0.997, which is 3.98%. Also, all the samples presented a regular wear scar that was aligned and symmetric, which is what is recommend by the standard. An example of the expected wear scar is presented on Figure 22. Once the calibration was done, the first AISI 304L Stainless Steel samples were manufactured and submitted to the wear test. The results for the AISI 304L initial tests are presented in Table 9.

Table 9 - Results for the AISI 304L initial tests.

Sample	Test Order	Mass Before [g]	Mass After [g]	Mass Loss [g]	Volume Loss [mm^3]
1	1st	145.9651	145.7712	0.1939	24.238
2	2nd	146.3769	146.2193	0.1576	19.700
3	3rd	145.7621	145.6295	0.1326	16.575
4	4th	146.4916	146.3769	0.1147	14.337

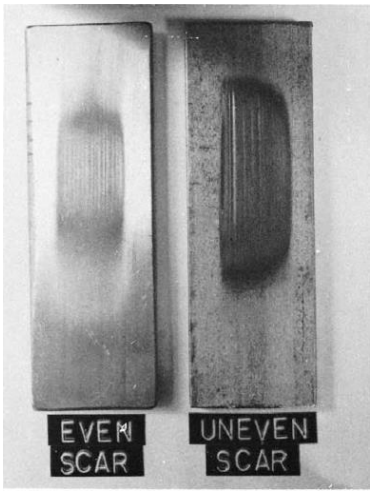

Figure 22 - Example of an even and an uneven wear scar. (Source: ASTM G65)

The results for the initial tests with the AISI 304L did not had a good outcome, because there was a difference in the volume loss as the tests progressed. The results showed that as the tests went on the wear rate would decrease until it reached a limit in which it would be stable (the proper results for the AISI 304L wear can be found in Chapter 6). The only factor that could cause this change in wear rate during the progression of tests was the temperature of the wheel and the metallic parts around it. This problem was only noted during the tests of the stainless steel, having a smaller effect on the other alloys. To minimize the effect of the temperature changes during test, a new test method was developed, one that served the purpose of making the test results more reproducible and easier to check the machine calibration.

After these trials, a new methodology was developed, which consisted of using a calibration sample and a 2000 revolution cycle to raise the temperature of the wheel and the other surrounding components to a more reliable working condition. After this test, the rig would undergo a 10 minutes dwell time and the actual tests could be carried. Also, the new dwell time between the regular 6000 revolutions and 130N test changed from 30 minutes to 40 minutes. To keep the consistency of the work, this test method was adopted in all the tests done in this test rig, even those that did not seem to be too affected by the temperature. The schematic for the abrasive wear test methodology is presented in Figure 23.

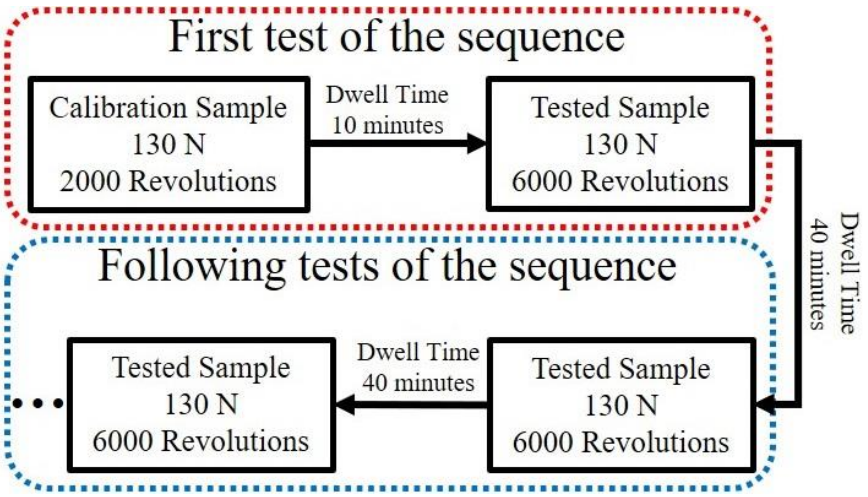

Figure 23 – Abrasive wear test methodology schematic.

The calibration samples were later changed from EN1A plates to a precision ground flat stock made from DIN Grade. 1.2510 (100MnCrW1) tool steel. Even though the EN1A was an inexpensive alloy, the manufacturing of the samples greatly increases its production cost. The solution was replacing it with the precision ground flat stock, once it is supplied with the needed thickness (8 mm), width (25 mm) and surface roughness (3.2 µm), only needing to be sectioned to the needed length. This tool steel bar is manufactured in accordance with the DIN 59350 standard, which guarantees good dimensional tolerances, and is similarly easy to source and relatively low cost (when taking the manufacturing costs into account).

3.5.2. Standard (AFS) and Non-Standard Sand (HST)

The sand used in this research was not the standard sand described in the ASTM G65 standard, once the availability and the cost of this sand made it not viable to be used at the time. Instead, a sand sourced from a local supplier and with similar morphological characteristics was used, which should not affect the results, since all the conclusions derived by comparing the results obtained in the same test rig using the exact same sand batch.

The standard sand used in this type of test is denominated as AFS 50/70 (known as Ottawa Sand), supplied by U.S. Silica. The sand used was a hydraulic fracturing sand supplied by Drilling Services (DSL) denominated HST 40/70. The SiO_2 composition of each sand is present on Table 10 and the grain size (based on sieving methods) presented on Table 11.

Table 10 - Sand SiO_2 percentage.

Sand	% SiO_2	% Loss on Ignition
AFS 50/70	99.70	00.10
HST 40/70	97.80	00.30

Table 11 - Sand grain size.

Sand	Sieve Aperture Size [µm]	% Retained Individual	% Retained Cumulative	% Passing Cumulative
AFS 50/70	425	0.0	0.0	100.0
	300	1.0	1.0	99.0
	212	97.0	98.0	2.0
	PAN	2.0	100.0	0.0
HST 40/70	600	0.0	0.0	100.0
	425	2.1	2.1	97.9
	355	8.1	10.2	89.8
	300	26.7	36.9	63.1
	250	41.3	78.2	21.8
	212	19.6	97.8	2.2
	150	2.2	100.0	0.0
	PAN	0.0	100.0	0.0

These are both silica sands, but as shown on Table 10, the HST sand presents a smaller quantity of SiO_2, once it has 1.90% (in absolute numbers) less silicon dioxide (silica) than the AFS sand, this way presenting a higher quantity of other substances and less purity. Another difference is the grain size of these sand shown on Table 11, once the AFS sand has the majority of its particles (99%) between 212 and 300 µm, the HST sand has a bigger variation, going from 212 to 425 µm for the majority of its particles (97.9%). From this data it is possible to conclude that the HST sand has a bit less SiO_2 and larger sizer particles when compared to the AFS sand.

As explained in more detail in Section 3.5.1, a container of 26 kg of sand was used for 15 abrasive tests of 30 minutes each (~12 kg of sand per test), being the sand added back to the container after each test. The abrasive test wear results did not present any difference with the sand being re-utilised, even though the sand would present a change in colour due to the rubber dust being dispersed from the neoprene rubber wheel and a very small quantity of metallic particles. To verify the possible effect of these rubber and metallic particles in the wear test results, the “used sand” containing these particles was used as an abrasive on some of the trial tests with the calibrating samples, which presented no changes in the wear scar features nor in the wear volume.

After the tests for the work presented in this thesis were carried out, the AFS sand was acquired for a different project (in partnership with one of the University’s commercial partners), so it was possible to compare the HST sand to the AFS sand. Figure 24 presents the picture of the sand samples before test and after abrasive test.

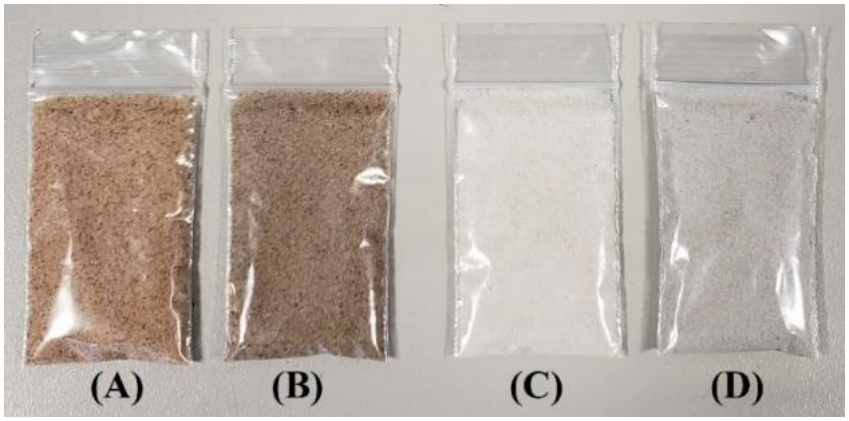

Figure 24 - Sand samples: (A) HST unused; (B) Used HST; (C) AFS unused; (D) Used AFS.

These sands were also analysed using an SEM, before and after being submitted to the abrasive wear test, so the sand particles could be compared. To be able to analyse it on the SEM, the sand particles were held in the sample holder using a double-sided carbon adhesive disc. These particles came from the samples presented on Figure 24 and the SEM images are shown on Figure 25.

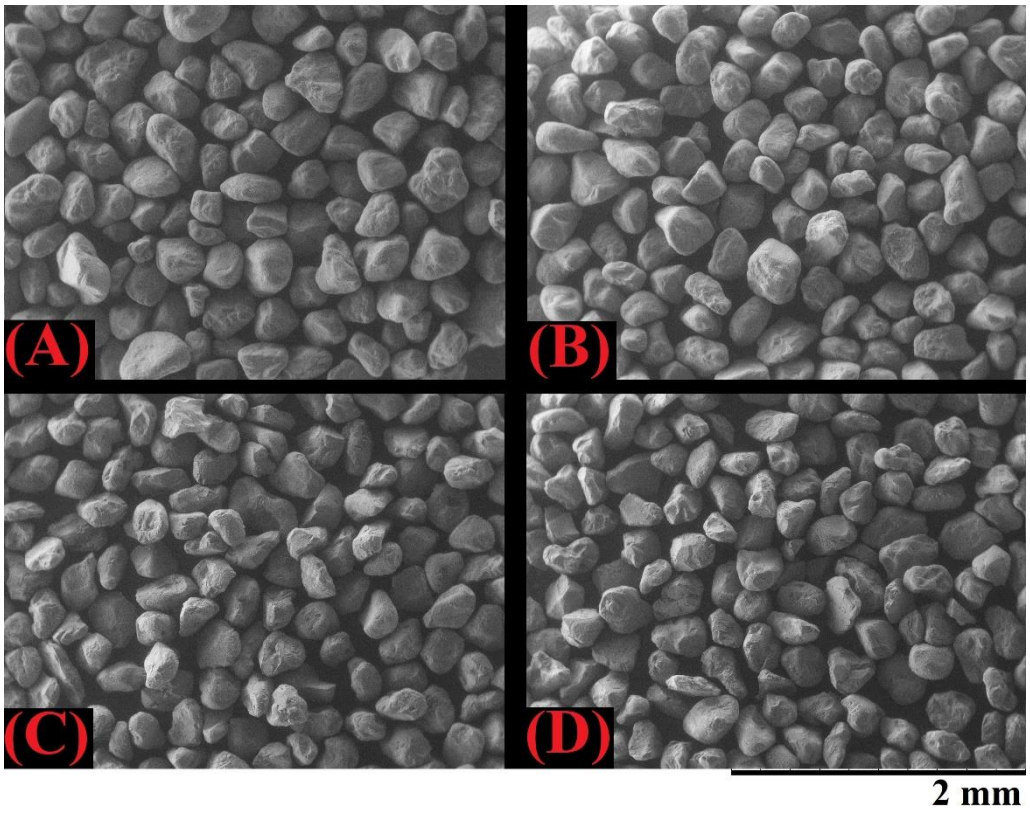

Figure 25 - SEM Sand particles: (A) HST unused; (B) HST used; (C) AFS unused; (D) AFS used.

The SEM comparative image shows the main differences between the two types of sand. When comparing A and C it is possible to note that the grains on A are sharper (presenting

more angular faces) than the grains on C (that are rounder on the overall). Another difference between A and C is that on A the sand particles present a more even distribution, with a smaller variation in size. When comparing the unused sands with its own used counterparts (A with B and C with D) no clear differences can be seen, so it is possible to say that this reused sand presents very similar characteristics to the non-used sand, hence the similar results during the tests.

3.6. ANALYSIS METHODS

This section presents the detailed analysis methods used throughout the development of this research. Focusing on making repeatability possible, every step is explained and the sample preparation, if needed, is also listed.

3.6.1. Composition

The composition of the alloys was analysed using an energy-dispersive X-ray fluorescence machine (a Fischerscope XAN). The limitation with this method is that it is not capable of accurately measuring light elements, therefore being of more use as a qualitative method than a quantitative one. These samples did not need any specific preparation and the tests were conducted on the finished standard samples (presented on Section 3.4.1).

3.6.2. Hardness

Vickers hardness (HV) measurements were performed on every sample used in the wear tests. This type of hardness test was chosen due to its capacity of utilising the same indenter for all the different scales of hardness measurement, being only necessary to change the applied load accordingly.

To minimize the measurement error, five measurements were made on the surface of each of the samples, resulting in a total of 60 measurements for each the researched alloys. The loads chosen (10, 20 or 30 kgf) for each of the materials were based on the size of the indentation, in order to ensure the load presented the best relationship between the size of the indentation and the hardness number. The measurements were performed in the region where the wear scar was likely to be located.

3.6.3. Microhardness

The Vickers microhardness was measured using an automated hardness tester (an EMCOTest Durascan). The measurement was taken using a 16-point matrix (4 by 4). The samples were sectioned and polished, once a flat clean surface is needed for this procedure.

The initial aim was to produce a hardness gradient, from the subsurface of the wear scar to the centre of the sample. Due to the small size of the area affected by the applied load, the measured hardness gradient did not present a significant difference in hardness, therefore the matrix measurement was used as a better suited model. The load used for each sample was dependant on the size of the indentation, being used the smallest load possible for each of the measured samples as with the (macro) hardness measurements.

3.6.4. Roughness

The surface roughness was measured using a column-type surface roughness contact profilometer (a Mitutoyo SJ500), with a 2 µm 60° diamond tip stylus. The samples were submitted to a roughness measurement after being ground, this way ensuring that the surface finish was in accordance with the ASTM G65 parameters.

3.6.5. 3D Non-contact Profilometry

A non-contact profilometer (an Alicona InfiniteFocus SL) was used to measure the samples and generate a 3D surface profile. For these samples, the 5x and 10x objectives were variously used, depending on the size of the wear scar and the required definition/resolution traded off against realistic scanning times for the type of analyses performed, once the full wear scar scan ranges from 15 to 30 minutes when using the 5x lens and can easily reach more than 45 minutes for the 10x lens. The 3D profiles were then used to analyse the wear scar, create a height map and observe the wear scar features in more detail. It also made possible to measure the volume of the wear scar and compare to the volume measured in the more traditional way of using a precision mass scale and the density.

3.6.6. Polishing and Grinding

The metallographic preparation of the samples was conducted following the recommended procedure of from the consumables' supplier. Before being ground and polished, the bigger wear samples were sectioned into cubes (10 mm sides) and hot mounted on a conductive Bakelite resin with carbon filler (to facilitate the electro-etching and the SEM

visualization). The sectioning was done in a precision cutting machine using an abrasive disc, this way generating the least amount of heating or changes in the sectioned samples. The grinding and polishing were done on an automated Buehler Automet machine, as it enables a better control of the parameters (when compared to the manual procedure).

The AISI 304L, AISI 316L and SA508 samples were first ground with a silicon carbide sandpaper (Grit 220, 600 and 1200) lubricated with water, until flat. The samples were then submitted to a second stage of grinding, using a 9 µm diamond suspension on a napless cloth. Finally, a three-stage polish was performed, initially using a 3 µm diamond suspension followed by a 1 µm diamond suspension and then a 0.04 µm colloidal silica suspension.

Due to their high hardness, the AISI 440C samples were prepared using a different method to the steels previously discussed. These samples were initially ground using water-lubricated coarse sandpaper followed by a final grind with a diamond suspension of 9 µm on a diamond epoxy disc. Polishing was performed using a suspension of 3 µm, 1 µm and a 0.25 µm diamond and later a 0.04 µm colloidal silica suspension.

The titanium samples, Ti64 and EBM Ti64, were prepared in the same way, once these alloys present the same chemical composition. The samples were firstly ground for 3 minutes using water lubricated sandpapers (Grit 600, 1200 and 2000) and after were polished for 10 minutes using 9 µm on a diamond suspension on a cloth and finalised with a six minutes final polishing using colloidal silica. The duration of the final step was varied based on periodic inspection of the surface for the desired type of finish.

3.6.7. Etching

Metallographic etching was carried after the grinding and polishing. The etching techniques were carried out in accordance with the techniques shown in the ASM Handbook for the characterisation of each of the alloys. The analysis of the etched surfaces was performed using conventional optical microscopy and SEM. If the samples were not etched appropriately after being polished, they would need to be submitted to the last stage of polishing again to remove the oxide layer or any other impurities in the surface and be stored in a beaker of 100% ethanol.

The AISI 304L and AISI 316L were etched using the same procedures, once the materials are similar enough that the etchants would work properly on both. Since these were

commercial materials, and not high-grade alloys, the hot rolling marks were clearly present on the etched samples, even after it being carefully prepared, especially during the etching using the Vilella's reagent (ASTM E407 designation 80 [62]) to show the microstructure. The etching procedure that presented the best results were using the electro-etching using nitric acid (HNO_3), as described by F. C. Bell & D. E. Sonon [63] on their work. The etching using the Vilella's etchant was completed by swabbing it on the surface of the sample until the etchant effect was noticed (a few seconds up to a minute). For the electro-etching, the samples were submerged on a small glass container filled with the etchant solution (60% Nitric Acid and 40% distilled water) and submitted to a current of nine to 14 mA/cm^2, using a cathode and anode made of stainless steel. This last procedure was carried for up to two minutes, being that the time to etch each sample varies according to the sample size and corrosion resistance.

The AISI 440C sample was etched using the Vilella's reagent and the same procedure as explained on the previous samples. The SA508 was etched by immersing it in a Nital 33% (33% Nitric acid and balance ethanol) solution. The times for each etching procedure vary according to the needed finish, for example a sample to be used for SEM analysis needs to be more etched than the samples used in the optical microscope.

The titanium samples were not submitted to any further etching as the last step of polishing already reveals the microstructure, and the only additional step needed to see the microstructure was to use a cross polarized filter on the optical microscope.

3.6.8. X-Ray Diffraction (XRD)

The X-Ray diffraction was performed on a Bruker D8 Advance diffractometer utilising a Copper K-α energy (40 kV, 40 mA), 0.01 degree of step size, five seconds scan per step and a 30 rpm rotation. The samples utilised on this analysis were ground and polished as specified on Section 3.6.6. These samples were later sectioned to 5 mm thickness, for a better fit in the sample holder. This test was performed by Dr Rob Thornton (an external supervisor of this work) at the University of Leicester.

3.6.9. Scanning Electron Microscopy (SEM)

The scanning electron microscopy was primarily performed in two different SEMs; a Hitachi table top model and a conventional SEM manufactured by FEI. The smaller SEM was used to obtain the images that did not require high magnification (over 1000 times) and the FEI

SEM was used for the more detailed images. The samples used in this method did not need any specific preparation, being the only conditions that the sample is conductive and free of any dirt or volatile substance. The Hitachi SEM was used at the Leonardo Tribology Centre (Sheffield) and the FEI SEM was that installed at the University of Leicester.

3.6.10. Transmission Electron Microscopy (TEM)

The only material analysed by this technique was the AISI 304L, presenting only one samples of each condition (conventionally heat treated and cryogenically treated). The samples used in this procedure were sectioned using a focused ion beam microscope (FIB) and later thinned to the needed specification using a scanning transmission microscope (STEM), this way achieving a thickness of approximately 80 nm and dimensions of 12 x 8 microns. The transmission electron microscope (TEM) used was a Jeol JEM-F200 and the TEM setup and data acquisition was performed by Dr Jiahui Qi (a postdoctoral researcher at the Department of Materials Science and Engineering, The University of Sheffield). The selected area diffraction patterns obtained were analysed with the help of the CrysTBox diffractGUI software, in its version 2.21.

3.7. ABRASIVE WEAR

The wear test methodology developed for this work is based on ASTM-G65 [58]. The equipment (Chapter 3.2) and the samples (Figure 19) were developed in accordance with the dimensions and specifications of this same standard. As presented on Section 3.5, initial tests were performed before defining the final methodology for the abrasive wear tests used on this research. Five tests were performed on each of the materials for each type of treatment, i.e. five tests for each material as received and five tests for each material submitted to the cryogenic treatment. In order to obtain the wear volume, the samples were weighed on a precision scale (precision of 0.1 mg) before and after they were tested. The wear surfaces and scars were analysed using microscopy techniques and profilometry.

3.8. METHODOLOGY SUMMARY

A methodology to evaluate the effect of the commercial deep cryogenic treatment in a range of engineering alloys was developed. The engineering alloys were selected to represent a variety of the most commonly used alloys, presenting different types of structures and composition, being these chosen alloys: martensitic stainless steel (AISI 440C), low alloy

carbon steel (SA508 Gr 4N), stainless steels (AISI 304L & AISI 316L) and light alloys (Ti64 and EBM obtained Ti64).

To verify the effect of the DCT in the wear resistance of the above-mentioned alloys, an abrasive wear test rig was developed based in the ASTM G65 standard. The Dry-sand/Rubber-wheel test method was chosen due to it being a commonly used test method in industry and presenting a well-developed documentation. To better customize the test rig to the available space, the budget and the test needs, it was decided to design and build a new test rig instead of acquiring a commercial one. To calibrate the test rig, achieve a standard wear scar pattern and define the test parameters, EN1A calibration samples were made a submitted to several tests, being these samples used only to calibrate the test rig (not undergoing any further advanced analysis). This designed and built test rig presents the same dimensions as specified by the ASTM G65 standard, using the standard neoprene rubber wheel and a non-standard type of sand (HST sand, characterised in this chapter).

Samples of each alloy were manufactured according to the ASTM G65 specification, being of rectangular shape presenting 8±2 mm thickness and 26 x 75 mm area. Due the being supplied in a solid bar, the AISI 440C samples were the only round samples (Ø 38.1 mm). These samples were later conventionally heat treated (apart from the titanium samples that were no submitted to a conventional heat treatment) and half of the samples of each alloy were submitted to the same type of commercial deep cryogenic treatment.

These samples were also used in all of the mechanical characterisation tests, this way guaranteeing that the samples submitted to the abrasive wear tests were the same as the ones that were characterised by the mechanical tests. The advanced analysis methods like metallography, X-ray diffraction and TEM, were performed in smaller samples sectioned from the standard samples aforementioned. Each of these smaller samples were prepared according to need of each of the specific advanced characterisation method.

The results of the tests and characterisation methods were grouped according to each type of material and the comparison between the cryogenically treated samples and the ones that were not submitted to the DCT are presented in the following chapters. The development of this methodology led to consistent repeatable results, which made the analysis of the effect of the cryogenic treatment in the abrasive wear resistance of the chosen alloys possible.

4. WEAR OF MARTENSITIC AND LOW ALLOY STEEL

This chapter presents the collected data, analysis and initial conclusions related to the abrasive wear tests conducted on the martensitic AISI 440C (A440 and A440CT) and the low alloy steel SA508 Gr 4N (SA508 and SA508CT). The mechanical tests' results are presented for all the studied samples, followed by a comparison between the conventionally heat treated and the cryogenically heat treated group. The wear scar is analysed in detail and all the presented results for these alloys are discussed. A summary with the important discoveries and points of note is at the end of the chapter.

4.1. TEST RESULTS

The test method presented in Section 3.6 was performed on the martensitic and low alloy steels, the acquired data was analysed in detail to identify any trends, and initial conclusions proposed related to the effect of the cryogenic treatment in the wear resistance of these alloys. This section contains the summarized data for each of the tests performed on the martensitic and low alloys steels used in this research.

4.1.1. Hardness and Microhardness

The hardness test is a simple, quick and well-known test used to analyse the mechanical properties of the alloys. In this work, this test was mainly used to certify the uniformity of each group of samples and the possible difference between the conventionally heat treated and the cryogenically treated samples. The hardness chosen for this work is the Vickers hardness test, that presents results in kg/mm^2.

The martensitic samples (AISI 440C) were submitted to the Vickers 30 kgf test (HV30), while the softer low alloy steel samples were submitted to the Vickers 10 kgf test (HV10). The applied loads were chosen according to the size of the diamond shaped indentation left in the analysed surface and the details of this Vickers hardness test are presented in Section 3.6.2. The surface tested was the same used for the ASTM G65 abrasive wear test, being this the larger area (25 mm X 76 mm). Table 12 presents the Vickers hardness results for the martensitic and low alloy steel samples.

Table 12 - Martensitic (HV30) and low alloy steel (HV10) Vickers hardness values.

Sample	Cryogenic Treatment	Average Hardness [kg/mm^2]	Standard Deviation (σ)	Standard Error ($\sigma_{\bar{x}}$)	% Standard Error
A440	No	631.1	51.1	10.4	1.65%
A440CT	Yes	750.1	26.8	5.5	0.73%
Sample	**Cryogenic Treatment**	**Average Hardness [kg/mm^2]**	**Standard Deviation (σ)**	**Standard Error ($\sigma_{\bar{x}}$)**	**% Standard Error**
SA508	No	276.8	5.3	1.0	0.35%
SA508CT	Yes	277.3	6.9	1.3	0.45%

The Vickers hardness results presented in Table 12 showed a small Standard Error, being 1.65% the biggest value found, this way showing that these measured values present a good repeatability and that the samples' hardness distribution is uniform (across the sample area and between different samples) and well represented by these results. The SA508 Gr 4N samples did not present any measurable difference between the conventionally heat treated and cryogenically treated samples, while the AISI 440C samples showed a noticeable difference between the two sample conditions. All the samples presented a low Standard Error for the measurements obtained, this way affirming that these results are reliable and have a good repeatability. Table 13 presents the microhardness results for the alloys studied in this chapter.

Table 13 - Martensitic (HV1) and low alloy steel (HV1) Vickers microhardness values.

Sample	Cryogenic Treatment	Average Hardness [kg/mm^2]	Standard Deviation (σ)	Standard Error ($\sigma_{\bar{x}}$)	% Standard Error
A440	No	648.3	14.6	3.7	0.56%
A440CT	Yes	761.8	9.2	2.3	0.30%
Sample	**Cryogenic Treatment**	**Average Hardness [kg/mm^2]**	**Standard Deviation (σ)**	**Standard Error ($\sigma_{\bar{x}}$)**	**% Standard Error**
SA508	No	283.9	8.4	2.1	0.74%
SA508CT	Yes	287.9	5.6	1.4	0.48%

The microhardness results for the samples presented a similar result to the hardness measurements presented in Table 12. The results for the SA508 Gr 4N samples also produced a slightly higher value for the cryogenically treated samples. There was a low value of the Standard Error (less than 1%) for both groups of conditions. For the AISI 440C samples, the cryogenically treated group presented a hardness and microhardness significantly higher than the conventionally heat treated group, showing that the cryogenic treatment did had a positive effect on this mechanical property. The analyses of these results are presented in Section 4.2.

4.1.2. Wear Volume

The ASTM G64 rubber-wheel/dry-sand abrasive wear test was performed in the samples as detailed in Section 3.7. The SA508 Gr 4N was submitted to the Method A test (130 N & 6000 cycles) as per the ASTM G64 standard, while the AISI 440C was submitted to different types of test, being the first one the standard's Method A and the second one the modified method A, in which the sample was submitted to 12000 cycles in total. The doubled test duration was chosen to promote an increase in the wear volume (compared to the standard's Method A), this way increasing the wear scar depth and size. The modified Method A test duration was limited to 12000 cycles, due to the limitation of the test rig's sand container volume, thus being the longest test duration possible in this rig without any further modification. The outline for the test methods used is shown in Table 14 and the results for the ASTM G65 abrasive wear test are presented in Table 15.

Table 14 - Outline of the ASTM G65 test methods for the martensitic and low alloys steels.

Sample	Test Method	Revolutions	Load Applied [N]
A440	A	6000	130
A440CT	A	6000	130
(**M**)A440	Modified A	12000	130
(**M**)A440CT	Modified A	12000	130
SA508	A	6000	130
SA508CT	A	6000	130

Table 15 - Martensitic and low alloy steel abrasive wear test results.

Sample*	Number of Tests	Cryogenic Treatment	Mass Loss [mg]	Volume Loss [mm^3]	Standard Deviation (σ)	Standard Error ($\sigma\bar{x}$)	% Standard Error
A440	5	No	0.01578	2.023	0.452	0.202	9.99%
A440CT	5	Yes	0.01578	2.023	0.502	0.224	11.09%
(**M**)A440	4	No	0.03185	4.083	0.287	0.143	3.51%
(**M**)A440CT	4	Yes	0.03050	3.910	0.540	0.270	6.91%
SA508	5	No	0.12288	14.988	0.494	0.221	1.47%
SA508CT	5	Yes	0.12313	15.103	0.714	0.319	2.11%

* The (**M**) identifies the results from the modified test (12000 cycles).

The results obtained for the SA508 Gr 4N samples presented a small Standard Error and a good repeatability, being that all the tests (in the same group of treatment condition) show similar values. The results for the AISI 440C samples did not give a similar result, once the standard Method A had a Standard Error that was higher than 10% of the value measured, which can therefore be considered as a non-reliable result. For the modified test using 12000 cycles the results present a smaller Standard Error. For all of the measured samples there were

no noticeable differences in the Volume Loss between the conventionally heat treated and the cryogenically treated group (among each of the alloys and tests groups), once this difference was smaller than the standard deviation of the measured values.

4.1.3. Microstructure

The metallography was performed in both of the alloys and for each of the conditions as explained in detail in Section 3.6. The type of image, Optical or SEM, was chosen in a manner that would facilitate the presentation of the most important features of each alloy, this way facilitating the better understanding of these features and differences (if present). The typical microstructure (obtained using SEM) for the AISI 440C samples is shown in Figure 26.

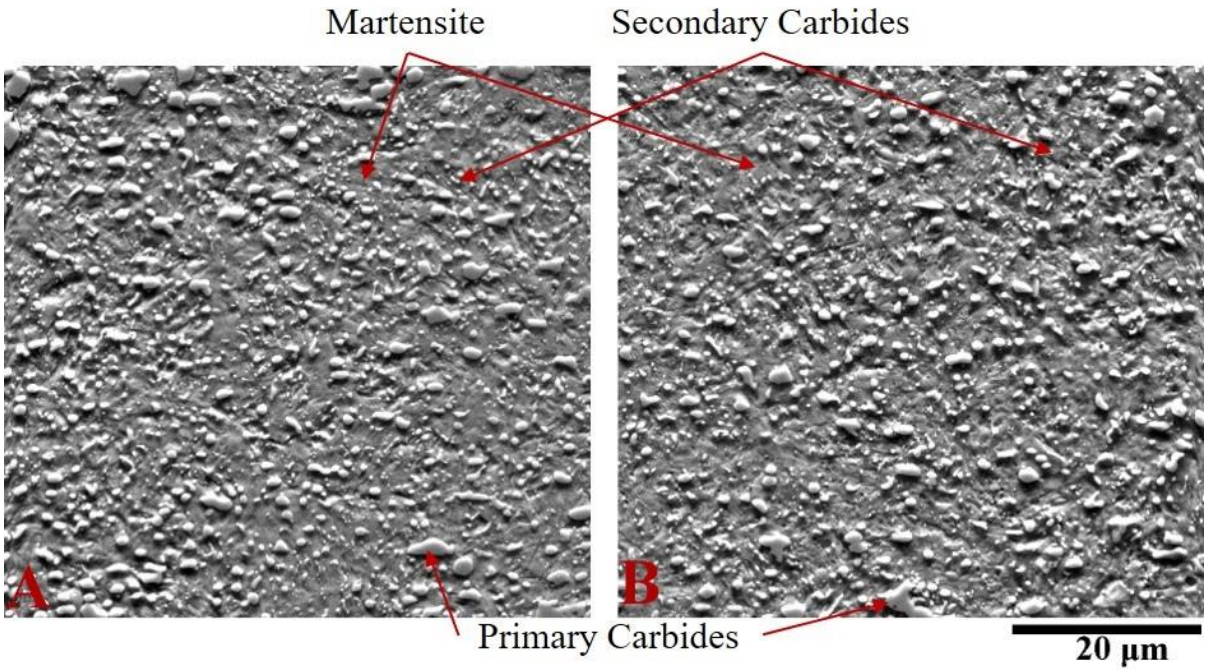

Figure 26 - Microstructure of the AISI 440C: (A) A440; (B) A440CT.

The SEM images for the A440 and A440CT samples present a very similar structure and pattern, showing a combination of a martensitic matrix with the presence of primary and secondary carbides. The carbides are shown in the image as the higher, brighter and oblong structures distributed across the whole image, being divided in to two main groups, the primary carbides (bigger) and the secondary carbides (smaller, more rounded shapes). The martensitic matrix is presented by the grey area under the carbides, presenting its characteristics angular shapes.

The images shown in Figure 26 were analysed using the software ImageJ to measure the average size of the carbide particles present in both samples. In ImageJ, the images with the same area were submitted to a fine-tuning in contrast (to better differentiate the carbide from the matrix) and measured using the "Analyse particles" function, this way measuring the average area of the particles present in each of the samples. By analysing these images, it is not possible to affirm that the cryogenic treatment affected the carbides that are present in these samples, once there is no clear difference in the area (A440: 0.475 ± 0.258 μm; A440C: 0.432 ± 0.252 μm) nor distribution of the carbides when comparing the conventionally treated to the cryogenically treated sample. Figure 27 presents the typical micrographs for the SA508 Gr 4N samples.

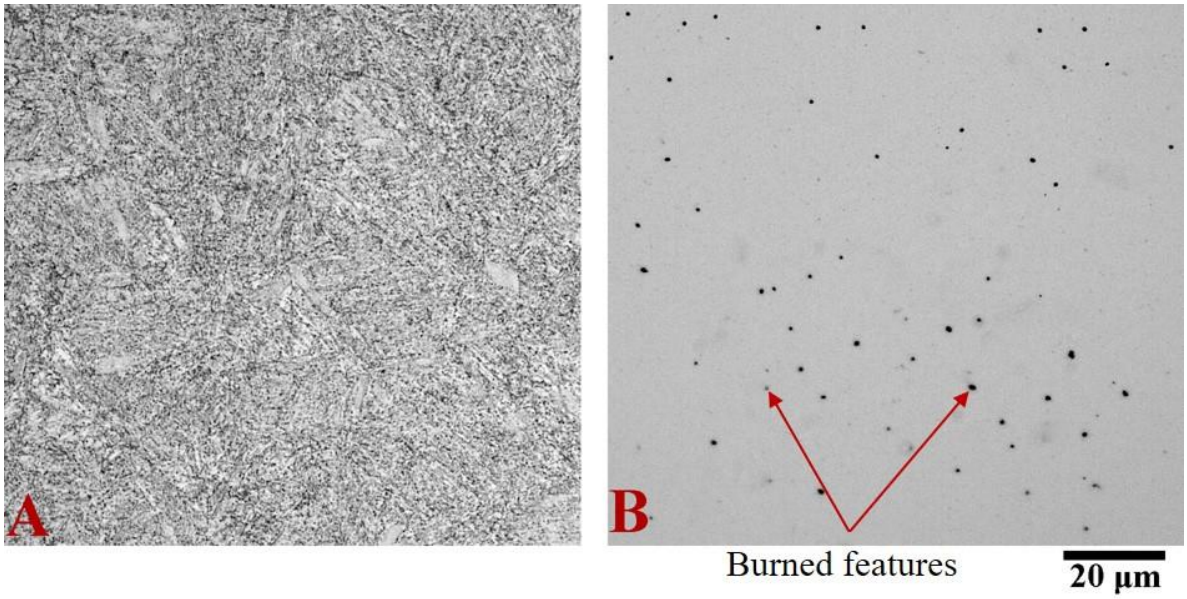

Figure 27 - Microstructure of the SA508 Gr 4N: (A) SA508; (B) SA508CT.

The SA508 Gr 4N sample presented very different reaction to the etchant which it was submitted to, being that the conventionally heat treated etched as expected and the cryogenically sample was only slightly affected by the etchant, probably due to an increase and corrosion resistance as a result of the cryogenic treatment. Figure 27 (A) present the typical microstructure for the conventionally heat treated samples being mainly composed of a very fine tempered martensitic structure, that is homogeneous and present throughout the sample.

Figure 27B illustrates an unexpected interaction between the etchant used for the metallography of these samples and the cryogenically treated samples. The only visible difference between the unetched polished sample and the etched one is the appearance of the black round dots that can be seen in the image, resultant from the polishing of the samples and

made clear due to the burning effect of the etchant in the edges present in the material. Since it is important to analyse the changes that may occur in the microstructure of the studied alloys, the etching duration of the cryogenically treated sample was increased from the initial time (3 minutes) to 60 minutes and still no effect other than the appearance of the black dots could be seen. Due to this effect, the comparison between the conventionally heat treated sample and the cryogenically treated sample cannot be performed, but a new and unexpected effect of the cryogenic treatment in this alloy was found.

4.2. COMPARISON OF CONVENTIONALLY HEAT TREATED VS CRYOGENICALLY TREATED

A basic statistical analysis of the experimental data was performed to better understand the possible patterns and differences that were found. To verify the hypothesis that the results for the conventionally heat treated samples and the cryogenically treated sample were similar, a double tail unpaired T-test was used, being that the higher value of the t-value and the increased significance (p-value ≥ 0.95) indicates that the results are significantly different and that the cryogenic treatment did present a difference in the measured parameter. The p-value higher or equal to 0.95, which is equal or higher than 95% confidence, is a value commonly used in engineering to determine how accurate a result would be, meaning that there is only a five percent chance that the results found (in this case) would be similar to one another. Since the p-value is not being limited to 0.95, the real value of p-value will be presented. The results for the unpaired two tailed t-test for the AISI 440C samples are presented in Table 16 .

Table 16 - Unpaired two tailed t-test: AISI 440C tests results comparing the conventionally heat treated to the cryogenically treated samples.

Test	t-value	Significance (p-value)	Mean Difference	SE Difference	Significantly Different?
Hardness	9.880	<0.001	118.8	12.0	Yes
Microhardness	26.18	<0.0001	113.5	4.3	Yes
Volume Loss	0.000	0.999	0.000	0.302	No
Volume Loss (**M**)	0.566	0.592	0.173	0.306	No

* The (**M**) identifies the results from the modified test (12000 cycles).

The results given in Table 16 for the Vickers hardness and microhardness tests shows that there is a significant difference between the cryogenically treated and the conventionally heat treated samples. For both of these tests the t-value is a high number and the confidence level is above 99.9%, indicating that there is no relevant uncertainty (less than 0.01%) related to the difference presented in these results, this way confirming that the cryogenic treatment did increase the hardness value of the tested material.

The wear results did not present any difference between the two different wear test methods when comparing the conventionally heat treated and the cryogenically treated samples. The wear for the unmodified Method A was exactly the same for both of the treatment groups, this way presented no t-value and no mean difference. The modified Method A presented a small difference between the mean values for each group of tests, that showed to not be relevant due to its small t-value and low significance (p-value). Even though the cryogenic treatment presented an increase in the hardness of this material, the abrasive wear results could not be efficiently used to measure this difference, and this limitation of the test that will be discussed later in this chapter. Table 17 presents the results for the unpaired two tailed t-test for the SA508 Gr 4N samples.

Table 17 - Unpaired two tailed t-test: SA508 Gr 4N tests results comparing the conventionally heat treated to the cryogenically treated samples.

Test	t-value	Significance (p-value)	Mean Difference	SE Difference	Significantly Different?
Hardness	0.345	0.731	0.567	1.641	No
Microhardness	1.532	0.138	3.875	2.530	No
Volume Loss	0.296	0.774	0.115	0.388	No

The statistical analysis results presented in the previous table for the SA508 samples shows that there is no measurable difference between the cryogenically treated and conventionally heat treated samples for this material. Even in the tests in which the p-value presented a confidence of over 70%, the mean difference was smaller than its own standard deviation, meaning that it is not a relevant value and that the hypothesis that the cryogenic treatment affected these samples is not true.

The following boxplot graphs were plotted to help on the visualization and comparison of the previously present data. Figure 28 shows the results for the Vickers hardness tests for both of the alloy groups studied in this chapter.

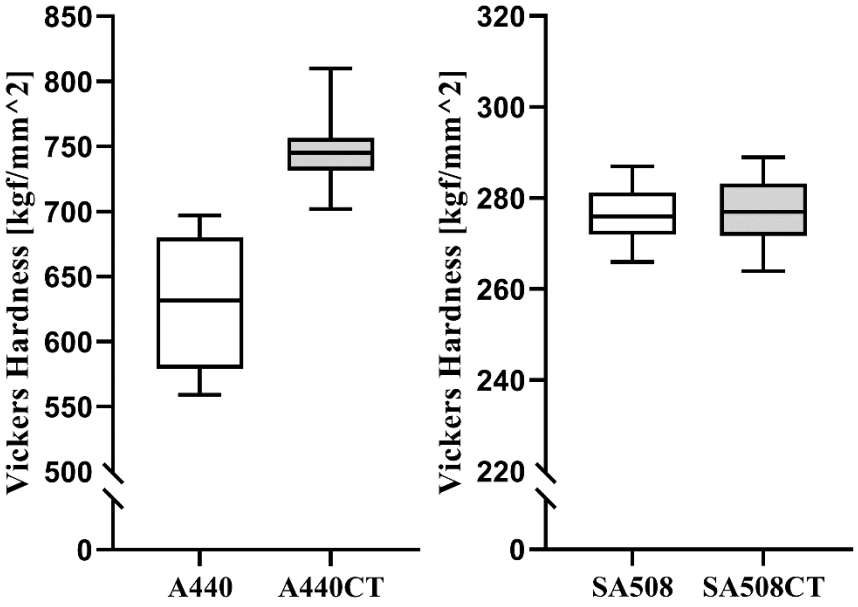

Figure 28 - Martensitic (HV 30) and low alloy steel (HV 10) samples Vickers hardness.

The boxplot plot graphs for the AISI 440C samples clearly illustrates the difference in hardness present in these two different groups and the error bars do not overlap. Due to the hardness being measured on every single sample (6 different samples for each condition) and the value being so high (which means that the indentations were small and a therefore more difficult to measure accurately than a bigger indentation), the scatter of the values are larger than the other measurements presented in this work, while still presented a low Standard Error (lower than 2%) and a Standard Deviation that is smaller than 8.1% for the conventionally heat treated and 3.6% for the cryogenically treated. For the AISI 440C, it can be concluded that the hardness increased for the cryogenically treated samples and that these same samples' hardness measurement also presented a lower Standard Deviation, meaning that these results are more homogenous.

The results for the SA508 Gr 4N samples are very similar for both of the tested groups, being that the difference in hardness is negligible (less than 2%) and both of the Standard Deviation are very similar, being the one for the cryogenically treated samples 0.6% higher. Based on these results, it is concluded that the cryogenic treatment did not present any measurable change in the hardness for the SA508 Gr 4N samples. Figure 29 illustrates the results for the Vickers microhardness tests for the samples of this chapter.

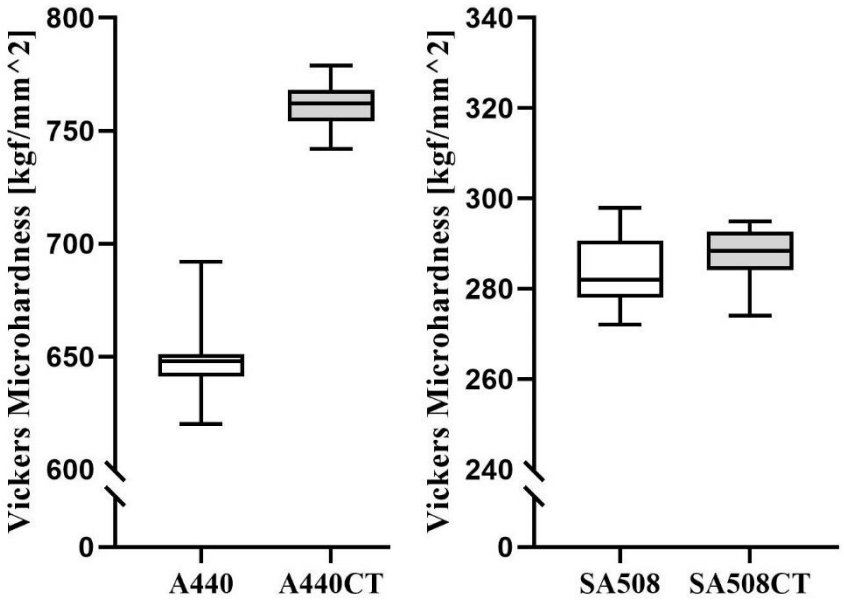

Figure 29 - Martensitic (HV1) and low alloy steel (HV1) samples Vickers microhardness.

The results for the Vickers microhardness of the AISI 440C samples demonstrated in the previous graphs also show the difference that the cryogenic treatment had in this material, once it is presented that the difference between the cryogenically treated and conventionally heat treated samples for this measurement is of at least 16.84%. Also, in the cryogenically treated group the scatter of the data is smaller than the one for the conventionally heat treated samples, meaning that there is less variation of results in the measurement done (the value of the Standard Deviation of the A440CT group is 62% of the A440 group).

Even though there is a small difference (4.7%) in the hardness and microhardness "Mean Difference" (of the cryogenically treated group and conventionally heat treated group), the total increase in hardness is similar when taking the Standard Deviation of the difference (SE difference in Table 16) into account, being the minimum measured difference between the two tested groups of 16.92% for the Vickers hardness and 16.84% for the Vickers microhardness.

The SA508 and SA508CT samples did not present any measurable difference in the microhardness and it can be clearly seen in the graphs presented, the only main difference in the results being the slightly smaller (~1% smaller) Standard Deviation shown by the cryogenically treated samples. This way, the cryogenic treatment did not present any measurable difference for the microhardness measured in this alloy. Figure 30 illustrates the results for the ASTM G65 abrasive wear test (Method A and Modified Method A) performed in AISI 440C samples.

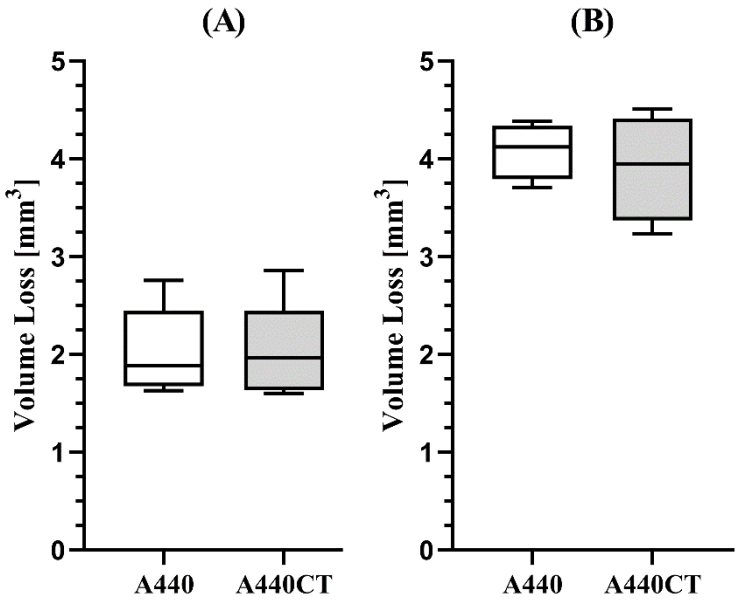

Figure 30 - Martensitic steel samples abrasive wear volume loss [mm^3]: (A) Method A (6000 cycles); (B) Modified Method A (12000 cycles).

The results presented for the ASTM G65 abrasive wear test for the AISI 440C samples shows that there are no relevant differences between the wear resistance of the cryogenically treated and the conventionally heat treated samples. The samples submitted to the Method A present a very low wear rate (due to the high hardness of the material), this way not making it possible to measure any difference between the two different conditions. Since the value of the volume loss is so small, any variation in this value makes the standard deviation relatively high, this way making it very difficult to point to differences and to affirm that there is a relevant effect.

Submitting these same samples to the modified wear test, this time with double the number of the cycles (12000) than standard (6000), did not show any effect, since it only linearly increased the removed volume by a factor of 2 (which is the same factor that the cycles were increased). This way, the same problems encountered with the previous test remain, in which the Standard Deviation is a small number, but is considered a high relative number when compared with the, also small, volume loss. These tests were more useful to determine the limits of this type of abrasive wear test, in which there is a low load and three body abrasion, meaning that this test cannot be used to quantify the abrasive wear resistance of a material that is considered to be of very high hardness. Figure 31 shows the results for the volumes loss of the SA508 Gr 4N samples.

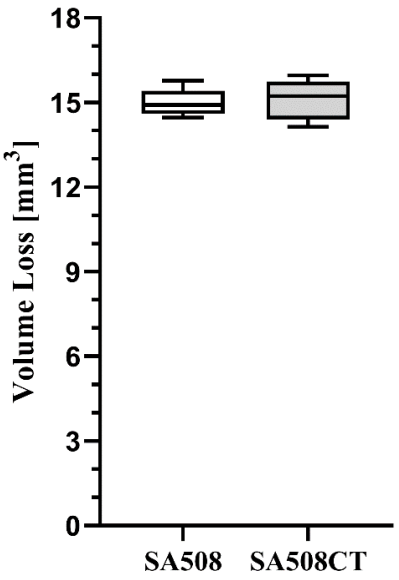

Figure 31 - Low alloy steel samples abrasive wear volume loss [mm^3].

The results highlighted by Figure 31 show that the cryogenic treatment did not increase the wear resistance for the SA508 Gr 4N samples. Both values of volume loss are similar and, even though the average wear volume of the cryogenic samples are slightly higher than for the conventionally heat treated samples, the t-test showed that the premise is false and thus the value should be considered as similar, which is presented in the graph as the scatter of the data being in the same region.

4.3. WEAR SCAR ANALYSIS

The detailed analysis of the wear scar aims at better understanding the mechanisms that affected this property and the influence that the different heat treatment may have on it. The wear scar analysis of the alloys studied in this chapter is presented below.

4.3.1. AISI 440C Standard Test Method (6000 cycles)

The typical wear scar for the A440 samples is pictured in Figure 32A, showing the wear scar main regions in the details B and C. Once the samples presented in this subchapter (Figure 32 & Figure 33) are the ones submitted to the standard Method A test, the wear scars are very shallow and, due to this are difficult to analyse satisfactory.

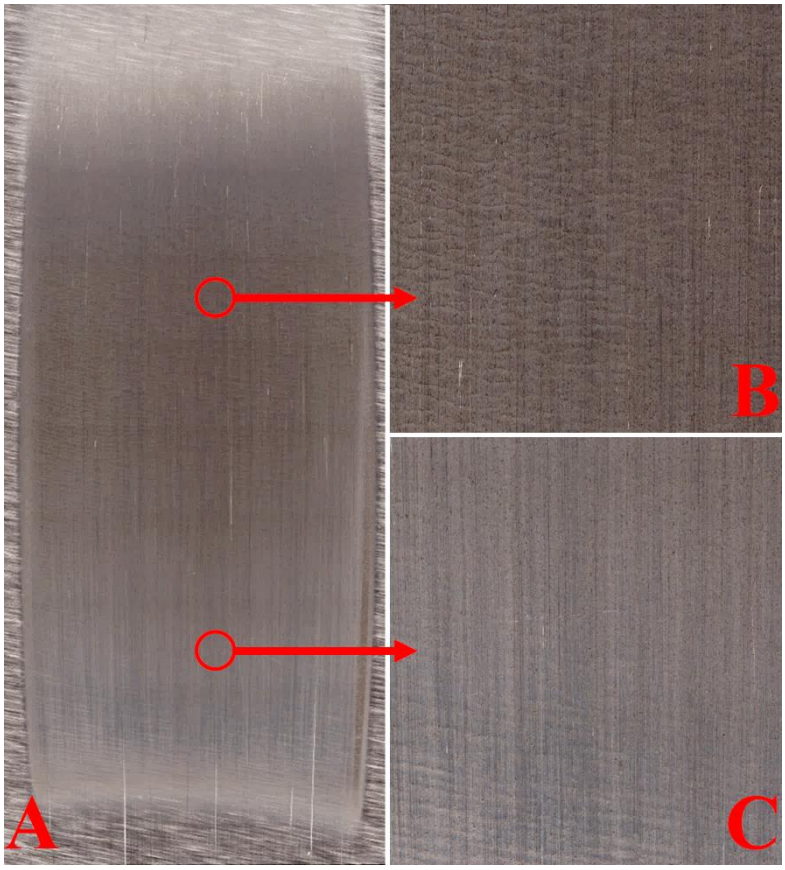

Figure 32 - AISI 440C standard test method (6000 cycles): (A) A440 typical shallow wear scar; (B) Central region rolling marks; (C) Bottom region scratches.

Even though these (AISI 440C samples) were round samples, which are not in accordance with the ASTM G65 standard, the wear scars shown were always regular and within the continuous central region of the sample (not reaching the circular edges of the specimen), this way being similar in overall shape to the other wear scars studied in this research and the ones presented in the ASTM standard.

The standard wear scar shape is seen in these samples, being composed of a rectangular shape with parallel sides and a symmetrical shallow parabolic shape in the lower part of the wear scar (bottom of Figure 32A). The central region (Figure 32B) presents faded rolling marks, characterised by wavy marks, mixed with light scratches, being the highest wear depth also present in this region. Light scratches are seen in the lower region of the wear scar showed in Figure 32C, mainly due to the lower pressure exerted by the rubber wheel in the extremities of the wear scar, due to this the grains do not roll and only lightly scratch the surface instead of removing material. A similar wear scar is found in the cryogenically treated samples, an example of which is shown in Figure 33.

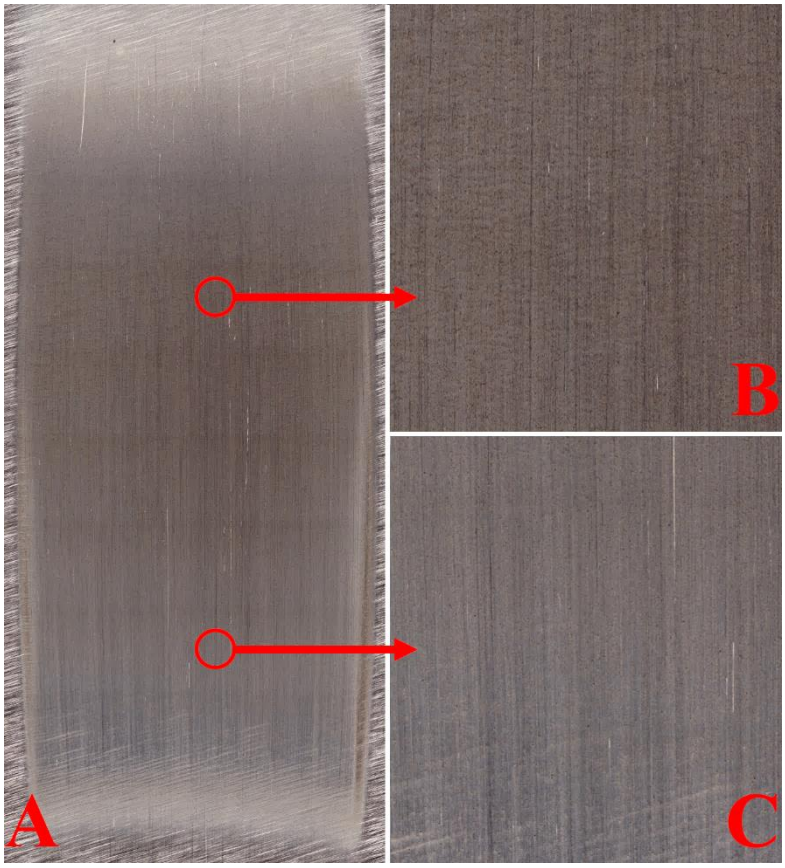

Figure 33 - AISI 440C standard test method (6000 cycles): (A) A440CT typical shallow wear scar; (B) Central region rolling marks; (C) Bottom region scratches.

The wear scars of the cryogenic samples were very similar to the ones of the conventionally heat treated samples, showing light wavy marks in the central region (Figure 33B) and scratches at the bottom area (Figure 33C). These light marks are due to the high hardness of the material and will be discussed more in depth at the end of the chapter.

4.3.2. AISI 440C Modified Test Method (12000 cycles)

The abrasive wear test was repeated for the AISI 440C samples due to the low wear volume (shallow wear scar) that resulted from the standard tests, with the new tests having double the cycles (12000) of the previous test. The typical wear scar for the new A440 samples is pictured in Figure 34, which also illustrates the details of the wear scar.

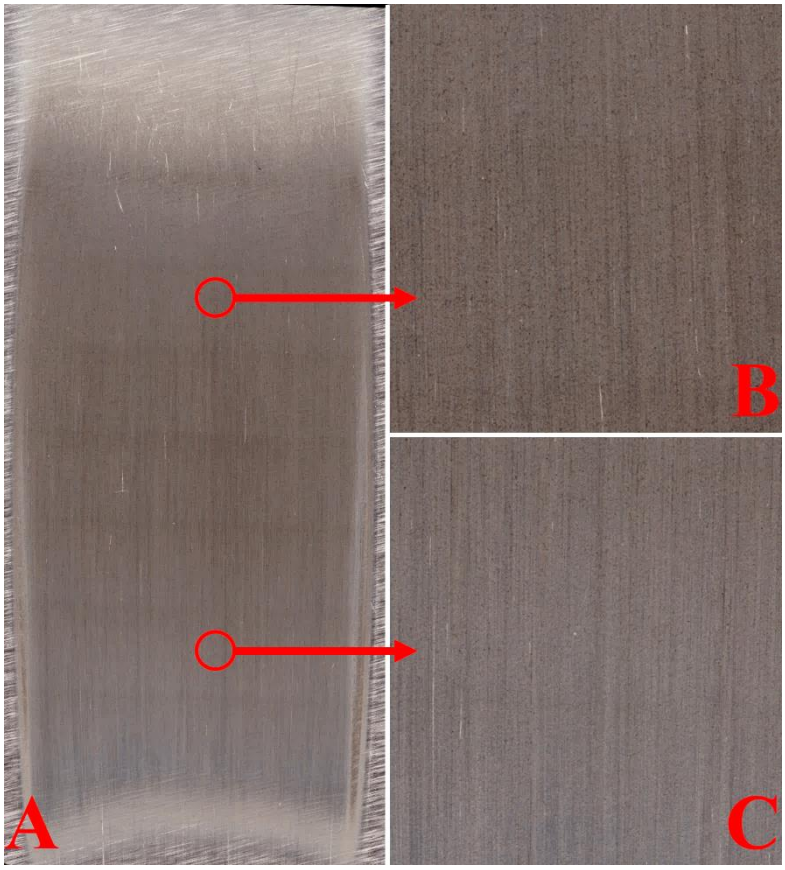

Figure 34 - AISI 440C modified test method (12000 cycles): (A) A440 typical wear scar; (B) Central region rolling marks; (C) Bottom region scratches.

The wear scar for the A440 samples is similar to the ones present in the previous test, having the same expected standard features, but this time being not as shallow. According to the result presented by the removed wear volume, this wear scar is twice as deep as the previous ones. The features inside of wear region (Figure 34B) are slightly different, presenting less wavy marks in the central area and a few more scratches. In the bottom region (Figure 34C) the same light scratches appear. There are no other major differences and, even though this wear scar is deeper, it can still be considered as a shallow wear scar for this type of test.

The wear scar was sectioned in two perpendicular directions, being one along the wear scar (cross-section, in the same direction as the wear occurred) and the other in the direction across the wear scar. The SEM images of the section across the wear scar were analysed and did not present enough details, since most of the images only showed light waves, not presenting all the stages of the wear. The cross-section images presented the whole of the wear process (as shown in the analysis below), which made it the chosen method for the wear scar analysis performed in this research. This way, the detailed analysis of the wear scar and the region below it was done using SEM images of the cross-section of the central region of the

wear scar, in which the wear is more severe and the features of the affected area can be better seen. These sample were sectioned from one of the wear samples used in the abrasive wear test and prepared according to the metallography sample preparation described in Section 3.6. After, it was etched and the images were acquired using the SEM. The details of the wear scar cross-section for the A440 sample are illustrated in Figure 35.

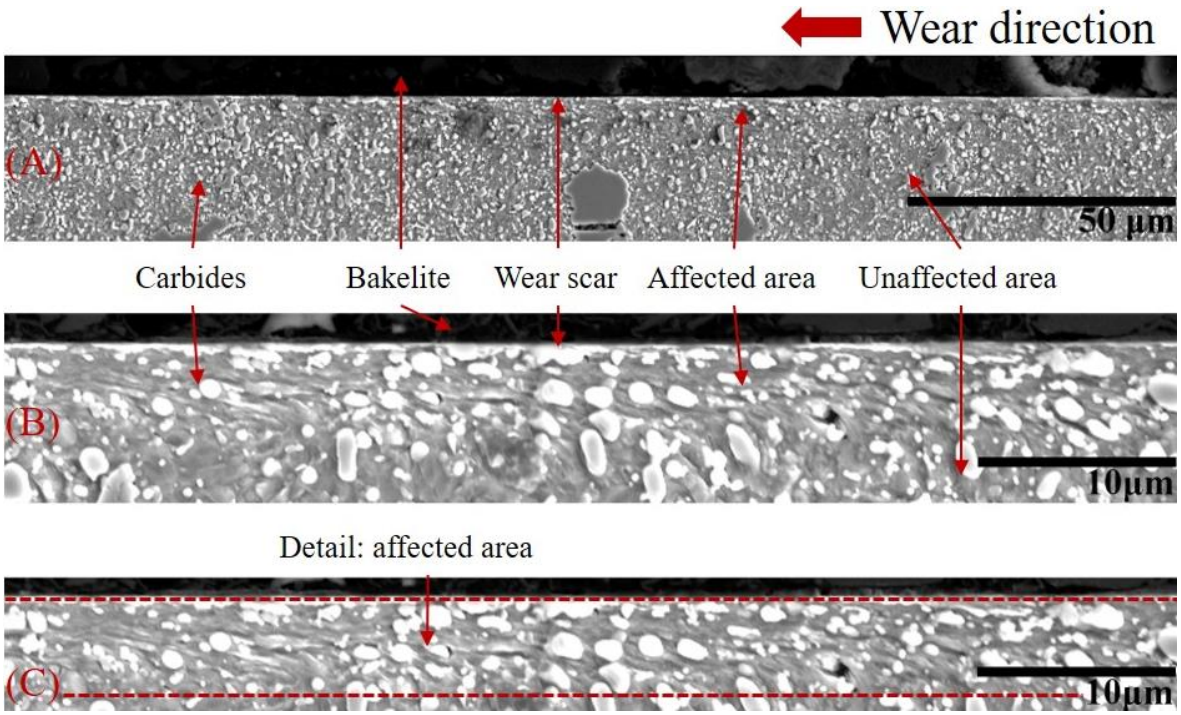

Figure 35 - A440 wear scar (12000 cycles) cross-section SEM detail: (A) 1000x magnification; (B) 4000x magnification; (C) Affected area detail.

Figure 35A shows the lower magnification image, at 1000x, which is better to visualize the small thickness of the wear scar itself and the subsurface area just below it, called the affected zone. The region under the affected zone is the regular matrix of the material, presenting the same microstructure as previously seen in Figure 26, which has primary and secondary carbides distributed through the whole region. The darker area on top is the Bakelite mounting, which is used during the process of polishing and etching. The darker areas in the alloy matrix are a result of over-etching that happened in some small portions of the analysed region and, since it does not present any significant information, should be disregarded.

The wear scar region, seen in Figure 35B, is marked by a brighter layer, which is a result of the material suffering heavy plastic deformation in the direction of the wear to a point that part of this material is removed, characterising the wear. Once the wavy marks seen in the wear scar (Figure 34) were very faded and the magnification of this images are very high (up

to 4000x), there are no signs of waves. Also, the material being removed did not leave any clear crater, showing that the process of removing material is very slow and also needs many cycles to happen, agreeing with the volume of material removed that was previously presented in Section 4.1.2. The region below it pictured in Figure 35C and marked between the red dashed lines, called the affected zone, shows how deep the plastic deformation that came from the top of the scar went, presenting a plastic deformed region that would later be worn if the wear process kept going indefinitely. This region shows how the deformation of the matrix leads to the formation of the brighter layer present in the top of the wear scar, being it a result of the rearrangement of the carbides and the matrix itself. The cryogenically treated samples' wear scar and details are illustrated in Figure 36.

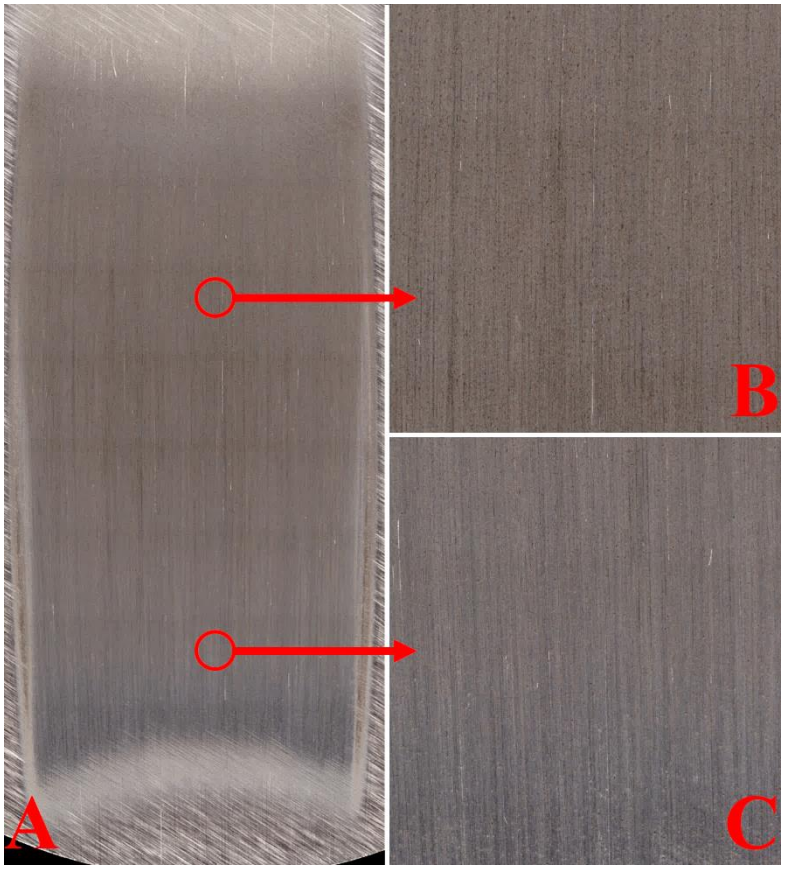

Figure 36 - AISI 440C modified test method (12000 cycles): (A) A440CT typical wear scar; (B) Central region rolling marks; (C) Bottom region scratches.

The wear scar for the cryogenically treated 440C sample has similar characteristic to the conventionally heat treated one. In Figure 36B the light wavy marks and scratches are present and well distributed across the central region. The bottom of the wear scar, Figure 36C, shows just the light scratches, similar to the ones found previously. By examining this image,

there are no notable differences between this wear scar and the one presented in Figure 34. The detailed cross-section of the wear for the A440CT is pictured in Figure 37.

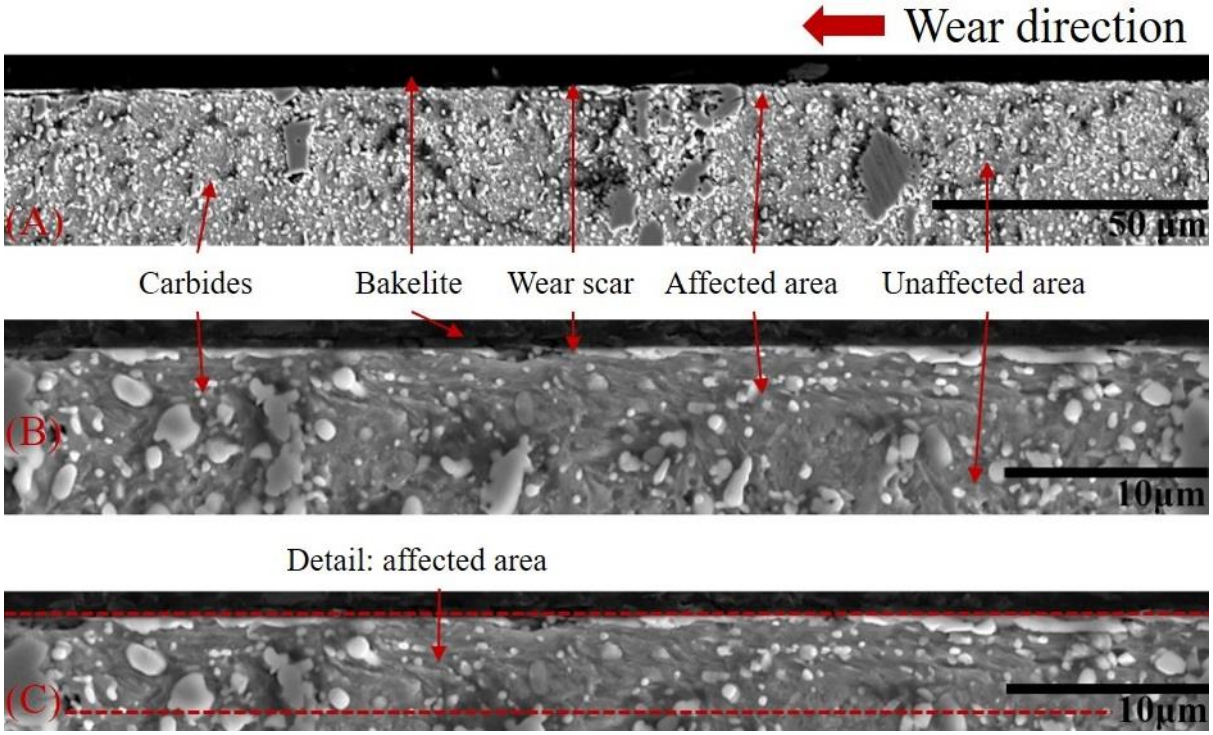

Figure 37 - A440CT wear scar (12000 cycles) cross-section SEM detail: (A) 1000x magnification; (B) 4000x magnification; (C) Affected area detail.

The SEM obtained images of the wear scar cross-section illustrates the effect of the wear in the surface and subsurface of the material. As seen in the previous cross-section image, the surface is composed of a lighter layer of plastically deformed material (Figure 37A & B), followed by the immediate subsurface in which the affected zone (plastically deformed material in the direction of the wear shown between the red dashed lines in Figure 37C) is seen. The darker regions marked in the images are a result of the burning effect of the etching, which was used to better show the matrix and the carbides dispersed in it.

When comparing the cross-section of the conventionally heat treated samples with the one shown in Figure 37 for the cryogenically treated sample, no major differences are seen. The same pattern repeats, in which the top layer is plastically deformed until the material is slowly removed and, during this process, the subsurface also suffers some of the plastic deformation which provokes dislocation of the matrix and carbides in the direction of the wear. Due to the wavy marks being very shallow, no major waves are present in the cross-section images, once this material has an elevated hardness and does not show a deep wear scar.

4.3.3. SA508 Gr 4N

The same method of analysis utilised in the last section was repeated in this section, first showing the overall shape and feature of the wear scars and later analysing in more detail the cross-section of the same wear scar region. For the SA508 Gr 4N samples, the cross-section images were obtained using a light microscope. The typical Alicona obtained images for the wear scar surface of the SA508 samples is illustrated in Figure 38.

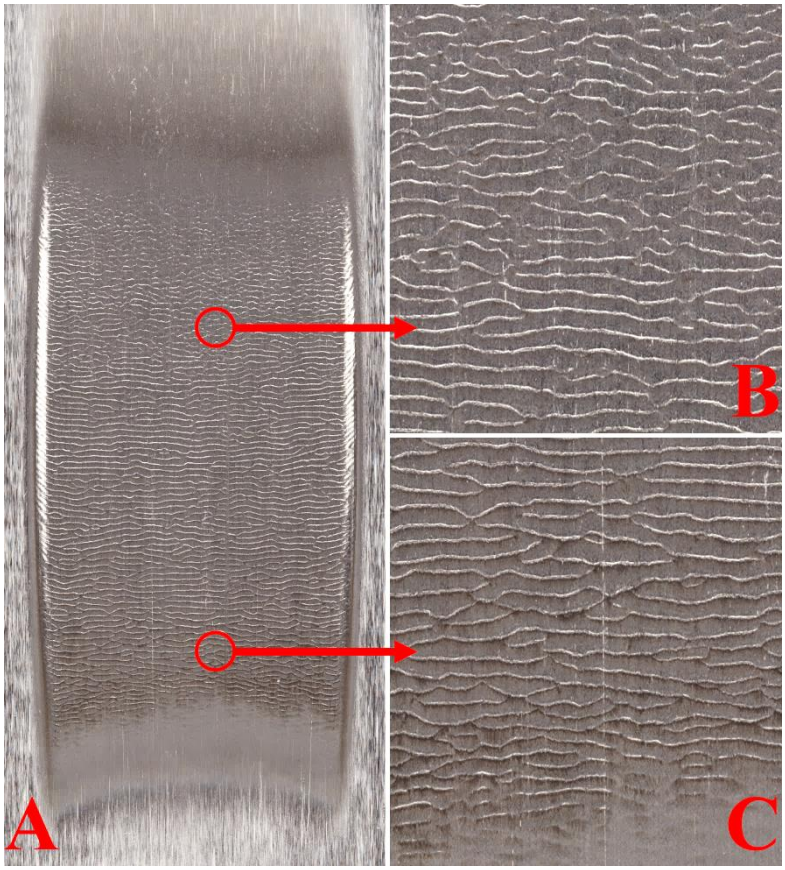

Figure 38 - (A) SA508 typical wear scar; (B) Central region rolling marks; (C) Bottom region rolling marks.

The characteristic wear scar for the SA508 was uniform and well aligned, having all the desired qualities of the wear scar described in the ASTM G65 Standard. These wear scars are different from the previous alloy, since it presents defined wavy marks that are easier to be identified and are present from the top of the wear scar to the bottom of it.

As it is pictured in Figure 38B, the central region which has the deepest depth of the wear scar and, commonly, the highest deformed region, presents deep three body abrasion waves and very few scratches, meaning that the material in this region suffered heavy plastic deformation before it was removed and that the abrasive (sand grains) rolled during its time in

contact with the sample surface. The same pattern repeats throughout the whole length of the wear scar, being also present in the bottom region (Figure 38C), which is the lowest load region. The fewer scratches are a result of a better three body abrasion, meaning that the wear test occurred as intended and that the material does not have a high resistance to this type of wear. The cross-section of the central region of this wear scar is illustrated in the following micrograph (Figure 39).

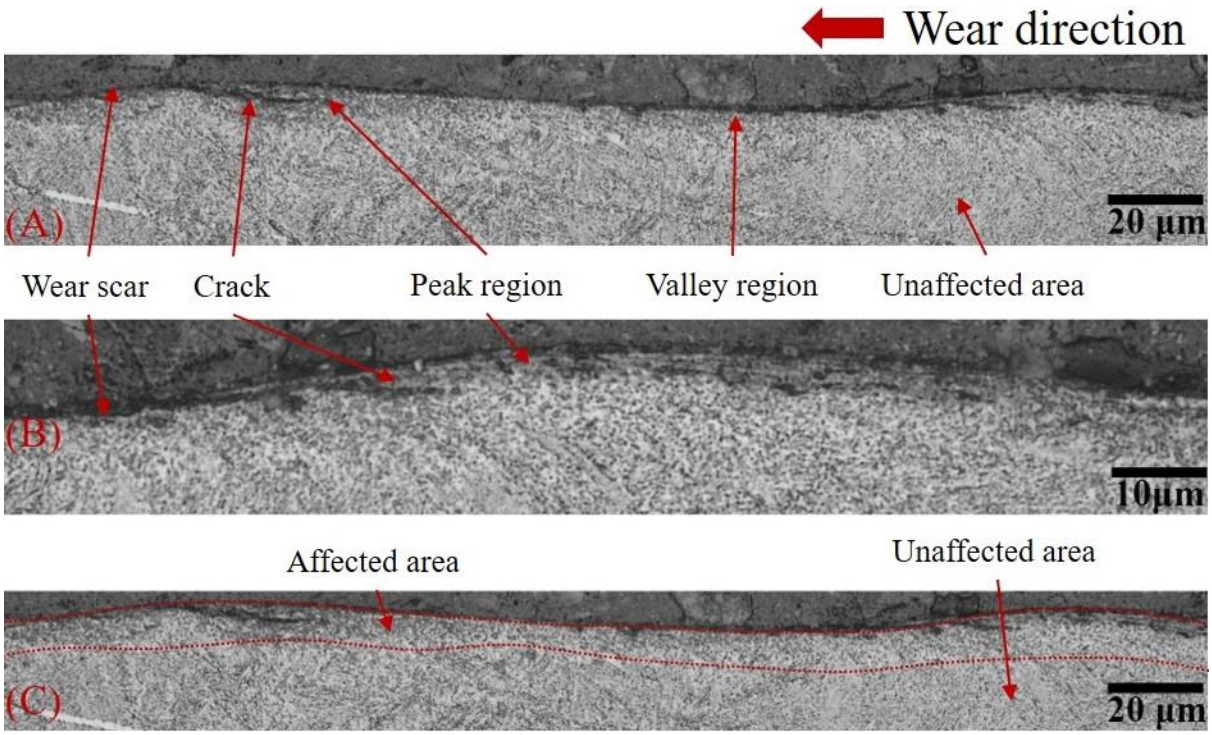

Figure 39 - SA508 wear scar cross-section micrograph detail: (A) 500x magnification; (B) 1000x magnification; (C) Affected area detail.

The wave marks are very clear and well demonstrated in the images of the cross-section of the wear scar, showing how the peak regions and valley regions are different. The wear scar is formed by two main regions; being the valleys that are a result of the removed material, and the peaks, which generate the cracks and later become valleys. Below the top of the wear scar, there is the affected region and, below it, there is the unaffected matrix of the material.

The material in the peak region suffers plastic deformation until it cracks at the corner of the peak, leading this crack to increase until the other side of this same peak and, consequently, leading to this material being removed. This phenomenon repeats several times until the peaks are transformed in valleys, being a cascade event and leading to the wear of the surface region. Figure 39B illustrates a peak that has cracks and a lifted edge on the left hand side. The affected region is shown in between the red dashed lines in Figure 39C. To facilitate

the understanding of the cracks formed in the peak region, zoomed SEM images were taken and are shown in Figure 40.

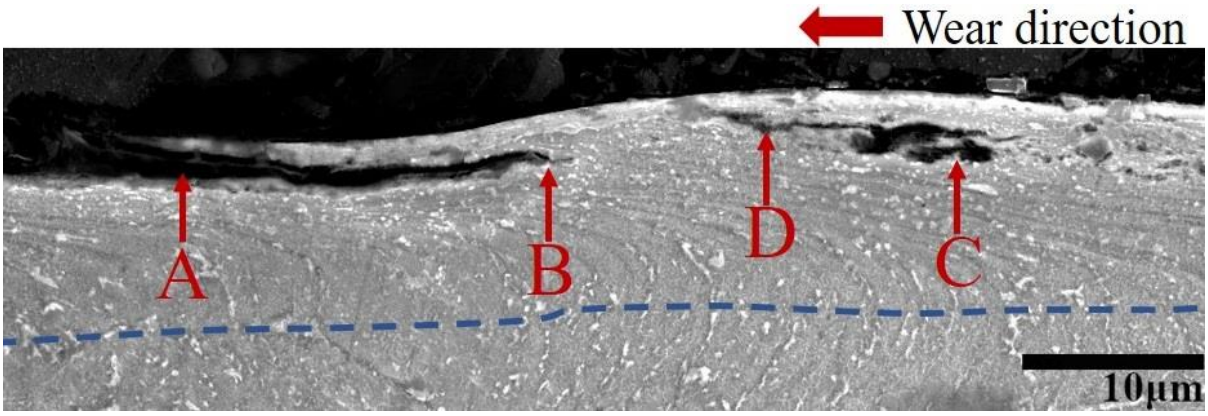

Figure 40 - SA508 SEM cross-section: crack formed in the peak region (4000x).

The peak pictured in Figure 40 shows two stages of the crack, the one on the left the stage in which the material is so deeply deformed that one of the sides of the cracked region is not attached to the surface anymore (Figure 40A), which eventually leads to this material being removed as the crack grows to the side that is still attached to the surface (Figure 40B). On the right side of the peak is seen the formation of the crack (Figure 40C) due to the high level of plastic deformation that the region is submitted to. This deformation forms a peak that leads to the formation of the crack near the central region (Figure 40D), growing until it reaches the same point as show on the left side of the image. The higher regions (peaks) are more prone to the formation of cracks due to it being submitted to an increased applied pressure (due to the smaller area and being in more contact with the abrasive due to it being higher) and, consequently, suffering an amplified plastic deformation.

These cracks result in large quantities of material being removed each time from the higher regions, dislocating the peak effect and forming new peaks while the old peak regions are transformed valleys of removed material. This continued effect during the abrasive wear of the studied alloy that forms the waves shown in Figure 38, being these the aftermath of the repeated process of forming peaks and valleys.

The region below the wear scar itself, called the affected region, shows the material being deformed in the direction that the wear particles move. This region is bigger inside of the peaks and smaller in the valley regions, as illustrated by the heights identified as A & B and blue dashed line delimiting the end of the affect area and the beginning of the alloy unaffected matrix in Figure 40.

The same type of analysis was done for the cryogenically treated sample to verify and compare the possible differences in the wear scar surface and its cross-section region. Figure 41 illustrates an example of the typical wear scar for the samples submitted to the abrasive wear test.

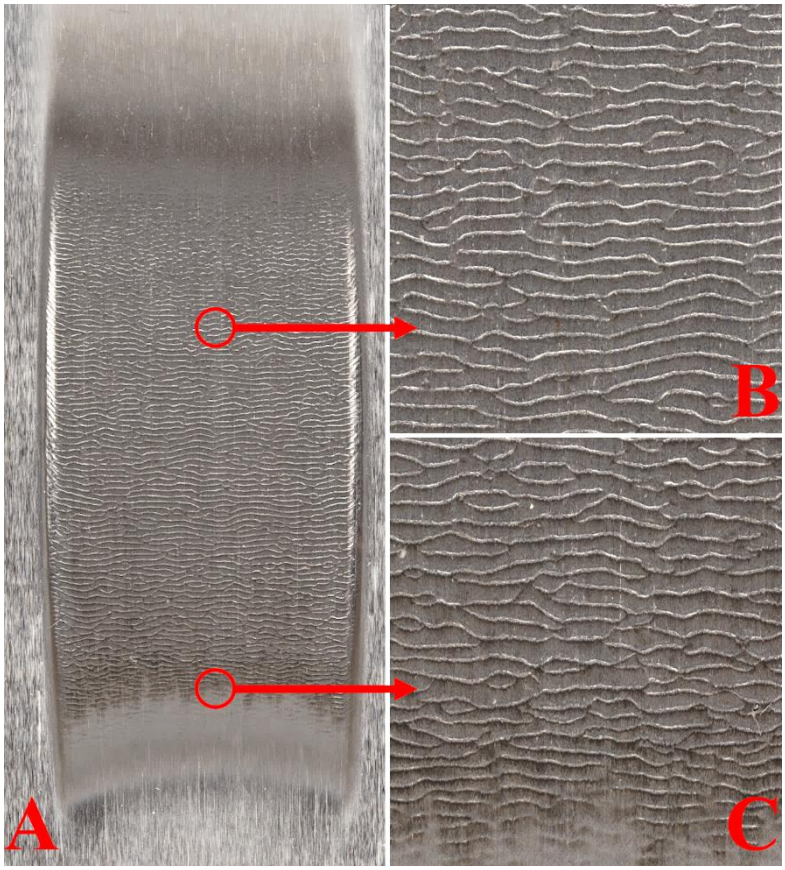

Figure 41 - (A) SA508CT typical wear scar; (B) Central region rolling marks; (C) Bottom region rolling marks.

This wear scar shows the same features as the one for the conventionally heat treated sample, presented in Figure 38. This wear scar is uniform and as expected, showing all the desirable features for a wear test conducted according to the ASTM G65 standard. The central region of the wear has the prominent wavy marks that are a result of the three-body abrasion combined with an increased plastic deformation, as explained previously. These wavy marks are present throughout the whole length of the wear scar, only decreasing in the lower region of the wear scar due to the lower applied load, as seen in Figure 41C. The wear scars for the conventionally heat treated (SA508) and cryogenically treated (SA508CT) are very similar and, when comparing the wear regions, no important difference is noted.

The analysis of the cross-section of the wear scar for this sample is illustrated in Figure 42. In this analysis it was not possible to identify the affected layer nor the matrix, due to the

material not reacting to the etchant, as explained in Section 4.1.3. Other than the features of the microstructure, the characteristics of the wear region are well defined.

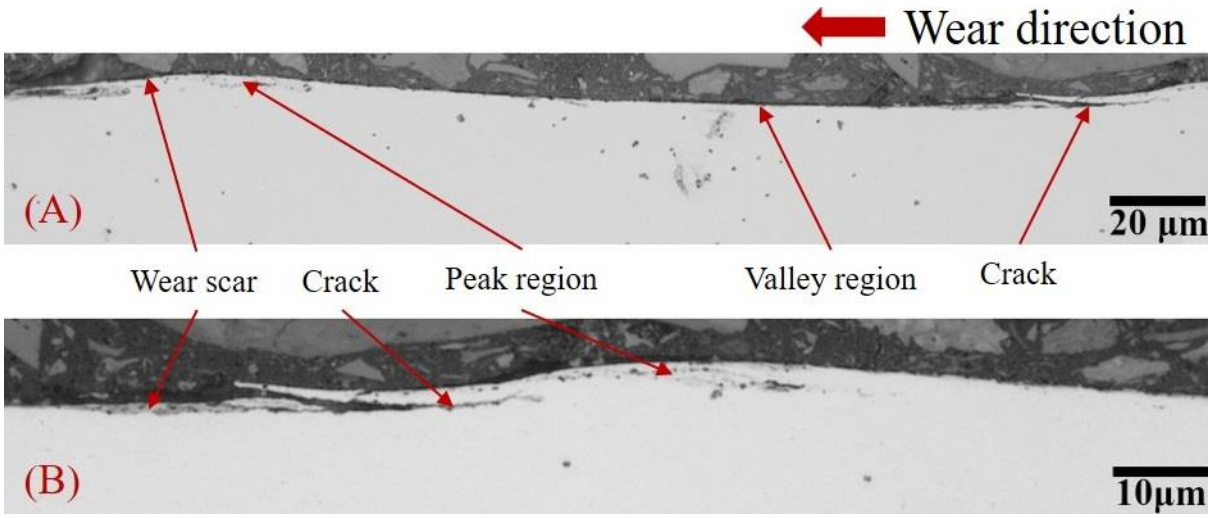

Figure 42 - SA508 wear scar cross-section micrograph detail: (A) 500x magnification; (B) 1000x magnification.

The wavy shapes are well defined and are seen in Figure 42A, being composed of lower and higher regions. The left side of the peaks present deformed and crack regions that show a separation from the wear scar surface, also previously seen in Figure 39. There are no visible cracks or separated areas in the lower region. The darker round dots and shapes present in the matrix are a result of the etching that burns the edges of the voids generated during the polishing of this material. In Figure 42B a detailed peak is seen, which is shown in more detail in the SEM obtained image in Figure 43.

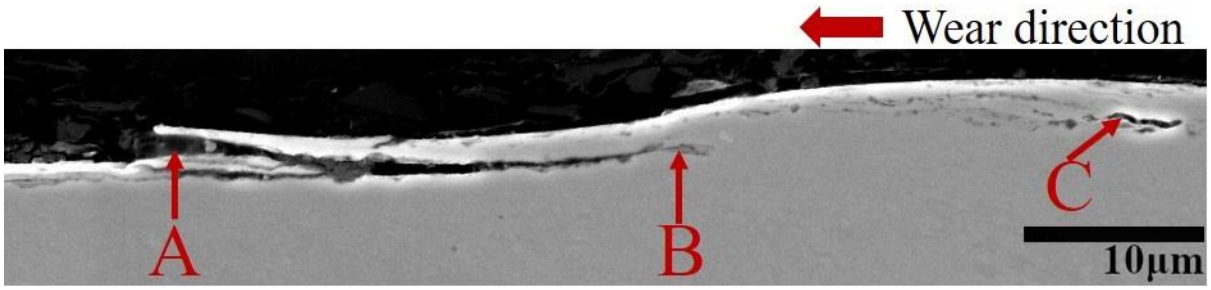

Figure 43 - SA508C SEM cross-section: crack formed in the peak region (4000x).

The separation of the material occurs the same way as explained for the previous sample, being the separated region marked in Figure 43A and the continuous crack propagation in Figure 43B. The formation of the new crack is also seen in Figure 43C, being this time in earlier stage than the one shown in Figure 40C. There is no clear difference when comparing the mechanism acting in the wear of the SA508 and SA508CT samples.

4.4. MARTENSITIC AND LOW ALLOY STEEL DISCUSSION

The ASTM G65 dry-sand/rubber-wheel abrasive wear test was used to determine the effect of the cryogenic treatment in the abrasive wear resistance of the AISI 440C martensitic steel. Samples were produced from a round bar, heat treated, sectioned and prepared according to the ASTM standard specifications, differing only in the shape, which was circular instead of the rectangular that is advised by this standard. After, the samples were analysed using a mass scale to quantify the volume loss and advanced microscopy to inspect the wear scar.

Martensitic steels are well known for being susceptible to one of the earliest reported beneficial effects of the cryogenic treatment, which consists of transforming the retained austenite present in the alloy matrix into martensite [9,13,64,65]. In the case of the AISI 440C, there are reports in the literature that referrer to increases of up to 7% [65] in hardness and another which presents a wear resistance that was increased by 21.8% [9], which led to the choice of this material as a strong candidate to serve as quality standard for the cryogenic treatment process itself. In addition to this, there is little research presented in the literature on the abrasive wear resistance of this material when submitted to low load three-body abrasion which is the type of wear tested in this work.

The first test that this material was submitted to was Vickers hardness, which presented an increase of 18.9% (Table 12 & Table 13) for the cryogenic treated samples when compared with the conventionally heat treated samples, agreeing with the literature and meaning that the cryogenic effect did have a positive effect in the mechanical properties of this alloy. The main feature seen in the metallography of this alloy was the primary and secondary carbides, which were distributed across the whole martensitic matrix (Figure 26). When comparing the carbides in both treatment groups, the microstructures did not show any difference, thus the cryogenic treatment did not affect the carbide size nor distribution for this specific alloy.

The AISI 440C samples were submitted to the abrasive wear test, initially following the Method A as defined by the standard and due to the high hardness of these alloys, but not much material was removed and thus measuring of the wear was considered inconclusive. As an effect of the increase in hardness, a general increase in wear resistance was expected as previously reported in the literature [66], but not to the extent of the initial results, therefore the standard test method was modified with the aim of producing enough measurable wear to discern between the samples. After increasing the duration of the abrasive wear test by 100%,

the wear scar was still not deep enough to produce a statistically conclusive result, once the average of the results presented a small difference (4% less wear for the cryogenically treated, Table 15), but due to the increased value of the Standard Deviation of these measurements, the confidence was not high enough and the difference measured was considered not significant (Table 16).

Based in the results presented in the ASTM G65 [58] for a range of alloys, it is seen that increased hardness alloys (which present lower wear volume) tend to present a proportionally higher value of Standard Deviation when compared to alloys with higher wear volume, this way making more difficult comparisons of this nature. Taking this into account, a different type of test (e.g. pin on disc) should be used to compare small difference in harder materials, like the AISI 440C, albeit for a different wear mechanism(s).

The SA508 Gr 4N is a recent steel developed for use in the manufacturing of nuclear pressure vessels. Due to the environment it is submitted to during its usage, good mechanical properties and corrosion resistance are needed. Samples of this alloy were submitted to the deep cryogenic treatment and later submitted to the tests, so its results could be compared with the only conventionally treated.

As with all the samples, the first results for the SA508 Gr 4N were the hardness and the microhardness (Table 12 & Table 13), which showed that there is no measurable difference when comparing the cryogenically treated and the conventionally heat treated samples. The results of these tests showed a very small Standard Deviation (smaller than three percent in all cases) for all the samples, confirming that the samples a uniform hardness distribution.

This material had very defined wavy marks in the entire region of the wear scar (Figure 36 & Figure 38), which are a characteristic of the three-body abrasion mechanism, evidencing that the abrasive wear occurred during the test as intended. One important characteristic of this wear scar were the very prominent waves that populated the centre of the wear scar, which when analysed with the aid of the cross-section images (Figure 37 & Figure 39), showed severe plastic deformation. Due to these features being very visible, the analyses of the different stages of the surface wear were facilitated. As a result of to the heavy plastic deformation presented on its surface and the wear volume of this material being considerably high, this alloy is considered as being very susceptible to abrasive wear.

One of the most important discoveries in this research regarding the SA508 Gr 4N is linked to an unexpected result during the etching of this alloy. The conventionally heat treated samples were etched as per the guidelines commonly found in the literature and the results were as expected, revealing the desired microstructure and features (Figure 27). The unexpected result originated when submitting the cryogenically treated samples to the same etching procedure as the conventionally heat treated samples, which surprisingly had not visible effect in the surface of the SA508CT samples. The etching time was modified from three minutes to 60 minutes and repeated two more times (after the sample being ground and polished again), showing the exact same result for all the repeats: no changes were found in the surface of the alloy.

Even though this beneficial effect was not expected, it is highly desirable, since the corrosion resistance is a notably desirable parameter for this alloy due to its application in nuclear pressure vessels [67,68]. Since the characterisation of the corrosion resistance of alloys is out of the scope of this research, no further investigation in to this subject was performed. The next steps taken relative to the research and development of this new found feature are presented in the Future Work section (Section 8.1).

The microstructure could not be thoroughly analysed due to the previously described inability to etching the SA508CT samples, meaning that the differences in the microstructure, if any, that could occur due to the effect of the cryogenic treatment (like redistribution and change in size of carbides) could not be verified. Based on the results for the hardness (Table 12 & Table 13) and abrasive wear tests (Table 15), it is concluded that the cryogenic treatment did not present any measurable difference in the mechanical properties when compared to the non-cryogenically treated samples, since the only found difference was the increased corrosion resistance of the SA508CT samples to the 33% nitric acid and 67% ethanol solution.

4.5. MARTENSITIC AND LOW ALLOY STEEL SUMMARY

This section presents the summary of the findings for the AISI 440C and SDA508 Gr 4N alloys.

- The hardness and microhardness results showed that each of the groups had a uniform hardness across its samples. When comparing the cryogenically treated samples to the conventionally heat treated ones, only the AISI 440C samples had an increase in hardness and microhardness for the treated group.
- The wear scar produced by the standard Method A in the abrasive wear test of the AISI 440C samples did not result in a wear scar with well-defined features, being necessary to change the test by doubling the length of its duration.
- There were no measurable differences in wear volume for the AISI 440C and SA508 Gr 4N samples.
- The microstructure of the AISI 440C samples did not show any noticeable difference when comparing the conventionally heat treated and the cryogenically treated samples.
- The SA508 Gr 4N increase in corrosion resistance is an important factor for its specific application as a nuclear pressure vessel alloy, leading to the need of future investigation to research this newly found result.

5. WEAR OF LIGHT ALLOYS

This chapter presents the measured data, analysis and conclusions related to the abrasive wear tests conducted on the Cast (Ti64 and Ti64CT) and the EBM obtained Ti-6Al-V (ETi64 and ETi64CT). The mechanical tests' results are presented for all the studied samples, followed by a comparison between the untreated and the cryogenically heat treated group. The wear scar is analysed in detail and all the presented results for these alloys are discussed. A summary with the important discoveries and points of note is at the end of the chapter.

5.1. TEST RESULTS

A test programme was performed (as detailed in Section 3.6) on the Cast Ti64 and EBM obtained Ti64 to acquire data and trends related to the wear resistance of these alloys. This section presents the summarized data for each of the tests performed on the light alloys used in this research.

5.1.1. Hardness and Microhardness

The hardness test selected was the Vickers hardness method with an applied load of 20 kgf (HV20). This load was chosen due to the size of indentation and the expected bulk hardness of the alloys. Both alloys were tested in one session and the samples were selected at random and both of the larger sides (25 x 76 mm) were tested for hardness. Each of the six samples of each material and condition was tested four times, totalling 24 measurements for each group. The results are presented in Table 18.

Table 18 - Light alloys Vickers Hardness (HV 20) values.

Sample	Cryogenic Treatment	Average Hardness [kg/mm^2]	Standard Deviation (σ)	Standard Error ($\sigma\bar{x}$)	% Standard Error
ETi64	No	373.65	6.28	1.28	0.34%
ETi64CT	Yes	376.48	6.24	1.27	0.34%
Ti64	No	383.42	6.09	1.24	0.32%
Ti64CT	Yes	386.09	5.68	1.16	0.30%

The hardness results are as expected for these types of alloys, and the measurements have excellent repeatability. Due to the number of measurements performed, and the relatively small standard deviation presented, the standard error was always lower than 0.5% of the total hardness value.

These samples were also submitted to a Vickers microhardness measurement, as it is essential to verify if any factors may influence the hardness measurement, like grain size, matrix hardness and/or precipitates. The HV 0.1 was chosen because it was the smallest test force (0.1 kgf) that would still present a measurable and reliable indentation. For this measurement, a matrix of nine points was used, being conducted on the same surface and region as the corresponding wear test. The results for the microhardness measurements of both conditions are presented in Table 19.

Table 19 - Light alloys Vickers microhardness (HV 0.1) values.

Sample	Cryogenic Treatment	Average Hardness [kg/mm^2]	Standard Deviation (σ)	Standard Error ($\sigma_{\bar{x}}$)	% Standard Error
ETi64	No	340.79	6.89	2.30	0.67%
ETi64CT	Yes	341.43	7.85	2.62	0.77%
Ti64	No	341.36	8.22	2.74	0.80%
Ti64CT	Yes	341.65	6.81	2.27	0.66%

The microhardness results have a small standard deviation and an excellent standard error, once it is smaller than 1% of the measured microhardness for all the obtained values. Both sets of results (hardness and microhardness) are reproducible and present an excellent standard deviation and standard error.

5.1.2. Wear Volume

The abrasive wear test was conducted as described in Section 3.5. The Cast Ti64 samples used the Test Method A (6000 cycles) and the EBM Ti64 samples used Test Method A (6000 cycles) as well as Test Method B (2000 cycles), due to its lower resistance to wear abrasion (explained in more detail in Section 5.2). The outline for the ASTM G65 tests is shown in Table 20. For this test, all the samples were chosen at random and the results are presented in Table 21.

Table 20 - Outline of the ASTM G65 test methods for the martensitic and low alloys steels.

Sample	Test Method	Revolutions	Load Applied [N]
ETi64*	A	6000	130
ETi64CT*	A	6000	130
ETi64	B	2000	130
ETi64CT	B	2000	130
Ti64	A	6000	130
Ti64CT	A	6000	130

*First tests done, extreme wear scar.

Table 21 - Light alloys abrasive wear test results.

Sample	Number of Tests	Cryogenic Treatment	Mass Loss [mg]	Volume Loss [mm^3]	Standard Deviation (σ)	Standard Error ($\sigma\bar{x}$)	% Standard Error
ETi64	4	No	49.285	11.125	0.729	0.364	3.28%
ETi64CT	4	Yes	50.425	11.383	0.536	0.268	2.36%
Ti64	5	No	67.360	15.205	0.801	0.401	2.63%
Ti64CT	5	Yes	67.120	15.151	0.490	0.245	1.62%

All the sample groups presented a Standard Error smaller than 4%, being that the Standard Error for the cryogenically treated samples was always lower than the ones presented by the untreated sample groups. It is important to note that the statistics shown (standard deviation, standard error and percentage standard error) were calculated using the Volume Loss parameter, which is the standard method for reporting the wear material loss.

5.1.3. Grain Size and Porosity

The grain size was measured using the images obtained from an optical microscope (cross-polarised) for each material and each of the conditions, and the results are presented in Table 22. The main details, features and differences in the microstructure are shown in Section 5.4.

Table 22 - Light Alloys grain size.

Sample	Cryogenic Treatment	Average Intercept [µm]	ASTM Grain Size [G]
ETi64	No	1.635	15.2
Eti64CT	Yes	1.678	15.1
Ti64	No	3.034	13.5
Ti64CT	Yes	3.006	13.5

The porosity of the light alloy samples was measured to understand better the wear behaviour of the EBM Ti64, which is described in more detail in Section 5.3. One polished sample of each condition (totalling two samples with the same area dimensions) were scanned using an optical microscope and the Clemex system (image acquisition & software) to quantify and analyse the pores present. The results are presented in Table 23 and clearly show that EBM Ti64 is significantly more porous (6.8x more pores per area) than the cast equivalent.

Table 23 - Light Alloys pore count.

Sample	Pore average length [µm]	Pore average area [μm^2]	Pores per area [pores/ μm^2]	Pore % of total area
Cast Ti64	10.05	56.65	0.239E-06	0.00136%
EBM Ti64	17.74	253.49	1.626E-06	0.04121%

5.1.4. Microstructure

The samples of both titanium alloys were prepared for metallography as explained in detail in Section 3.6. Due to the nature of these alloys, there was no need to further etch the samples to analyse the microstructure and the effect of the wear in the subsurface. Also, comparing the microstructure of the cryogenically treated and the untreated samples, it is possible to verify if the treatment affected the microstructure. Figure 44 presents the general microstructure obtained using cross-polarised lens in an optical microscope for each of the Cast Ti64 samples.

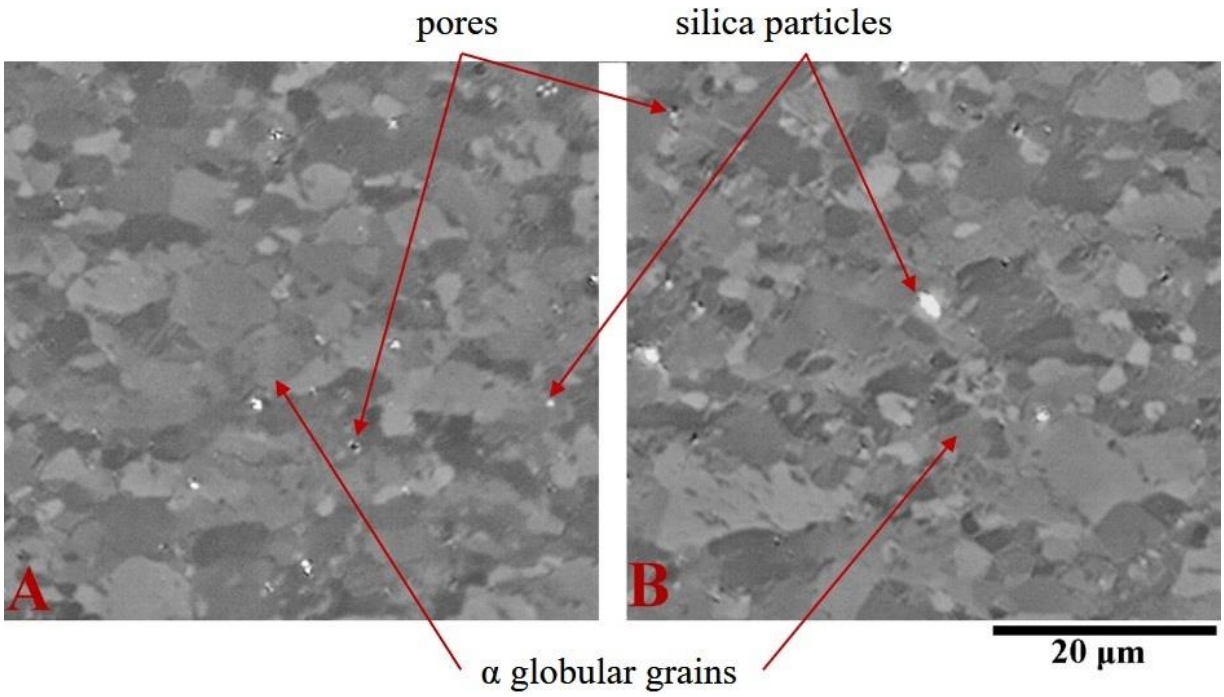

Figure 44 - Microstructure of the Cast Ti64: (A) Ti64; (B) Ti64CT.

The micrographs presented shows that both images are very similar, being composed of rounder α globular grains of similar average sizes, as it is common for this type of titanium alloy that was submitted to hot rolling. These images were also used to calculate the average grain size (presented in Section 5.1.3), which showed that for the both conditions of the material studied (untreated and cryogenically treated) the average grain size is very similar, which when tested using a two tail t-test (Table 24) was confirmed that the values are similar and the 3% difference can be considered negligible.

The micrographs also show some round white spots, which are silica particles that got stuck inside of the pores during the final stage of polishing and when submitted to a high intensity light appear as white dots. The few pores present in these samples can be seen as dark

rounder spots. No effects that would occur due to the cryogenic treatment can be seen, since the micrographs are very similar, this way concluding that for the Cast Ti64 the cryogenic treatment did not present any effect on the microstructure.

The EBM obtained Ti64 samples were prepared using the same procedure as the previous samples and as explained in the methodology and the microstructure obtained using cross-polarised lens in an optical microscope is presented in Figure 45.

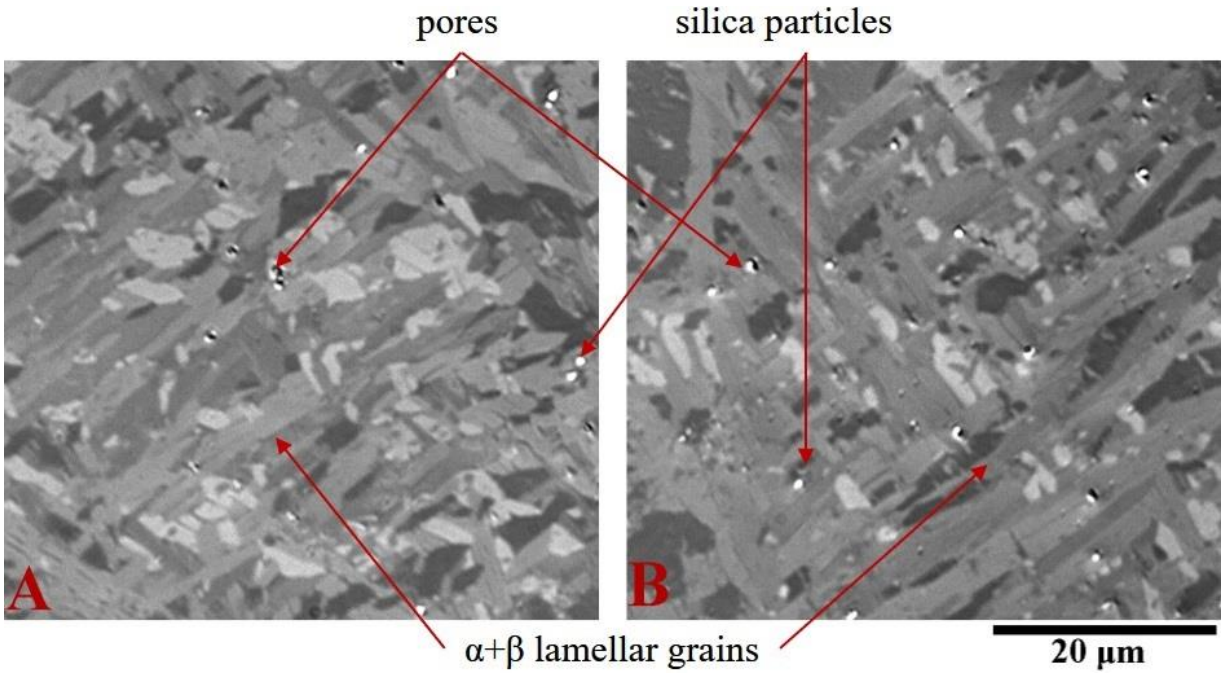

Figure 45 - Microstructure of the EBM Ti64: (A) ETi64; (B) ETi64CT.

This image shows very similar microstructures for both of the conditions, being these composed of α+β lamellar grains, which are the common microstructure found on Ti6-4Al-4V samples obtained by Electron Beam Melting. These lamellar structures come from a bigger β grain that forms during solidification and later cools down forming the α+β lamellar grains presented here. These micrographs were used to calculate the grain size (presented in Section 5.1.3), which had similar values and the difference between them can be considered negligible due to the t-test results present in Table 25.

5.2. COMPARISON OF UNTREATED AND CRYOGENICALLY TREATED

Understanding the results and its trends is the main part of the results analyses and evaluation, and the statistical analyses is the tool that makes this type of analyses possible. One of the tests that can be used to verify a hypothesis is the double tail unpaired T-test, that show

if a set of data is similar to another set of data, in this case comparing the conventionally treated samples to the cryogenic treated samples. Table 24 and Table 25 presents the t-test results for the Cast Ti64 and the EBM Ti64 samples respectively.

Table 24 - Unpaired two tailed t test: cast Ti64 tests results comparing the untreated to the cryogenically treated samples.

Test	t-value	Significance (p-value)	Mean Difference	SE Difference	Significantly Different?
Microhardness	0.000	>0.999	0.00	3.48	No
Hardness	1.472	0.148	2.58	1.75	No
Grain size	0.196	0.854	0.03	0.14	No
Volume Loss	0.130	0.899	0.05	0.42	No

Table 25 - Unpaired two tailed t test: EBM Ti64 tests results comparing the untreated to the cryogenically treated samples.

Test	t-value	Significance (p-value)	Mean Difference	SE Difference	Significantly Different?
Microhardness	0.095	0.925	0.33	3.51	No
Hardness	1.530	0.133	2.83	1.85	No
Grain size	0.747	0.497	0.04	0.06	No
Volume Loss	0.568	0.590	0.26	0.45	No

The tests illustrated in the two previous tables show that there are no quantifiable differences between the cryogenically treated samples and the untreated samples for all the tests that were performed. Even though the t-value is higher in some of the tests (hardness for both materials), it does not present a significative p-value, this way meaning that the initial premise (that both group of samples present different results) cannot be verified. These trends and results are analysed in more detail in the following paragraphs.

Verifying the homogeneity of the samples is a fundamental part of gathering results that are reliable and reproducible, being the hardness testing a straightforward way of doing so, due to it being a simple and well-known test. Figure 46 presents the comparative results of the hardness measure for the titanium samples on both conditions. All the samples were tested in a random manner and on both sides, this way guaranteeing that the hardness was uniform across all the samples. Comparing the results for ETi64 and ETi64CT, it can be assumed that the cryogenic treatment did not present any measurable increase in the hardness of this material. Even though the average hardness of the ETi64CT samples is a slightly higher than the one for the untreated samples, the error bars of both results overlap and the t-test showed that there is no relevant difference in the results, this way showing that hardness values for both conditions are approximately the same. A similar case occurred with the Ti64 and Ti64CT, in which the

cryogenically treated sample presented an average hardness value that is a bit higher than the untreated sample, but is also inside of the area of the error bars and similar t-test results.

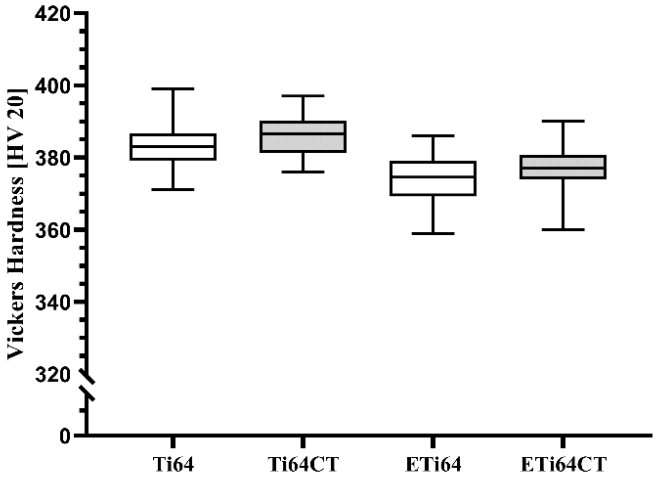

Figure 46 - Titanium samples Vickers Hardness (HV 20).

Figure 47 presents the comparison of the results of the microhardness measurements for the titanium samples. Due to the smaller load applied to measure the microhardness, the indentation size is also smaller and a slightly bigger range of error occurs (when comparing to the previous hardness measurement). The previous trend is repeated and no measurable differences can be found when comparing the conventional and the cryogenically treated samples, which indicates that, for the Ti-6Al-4V, the cryogenic treatment applied presented no measurable differences in the hardness and microhardness.

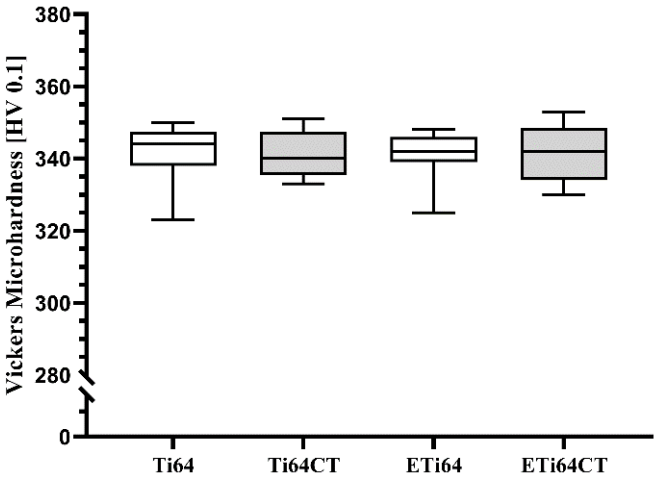

Figure 47 - Titanium samples Vickers Microhardness [HV 0.1].

A comparative box chart of the titanium samples' wear volume is shown in Figure 48. The graph shows that the cryogenic treatment did not present any measurable increase in abrasive wear resistance for these materials, once both groups (Cast and EBM) of box charts are in the same regions, the error bars overlap and the t-test did not show any relevant difference between the sample groups (untreated and cryogenically treated). Also, when doing a t-test for this group of data, the initial hypothesis (that the values for the cryogenic samples differ from the untreated samples) is denied due to the high value of the P-Value.

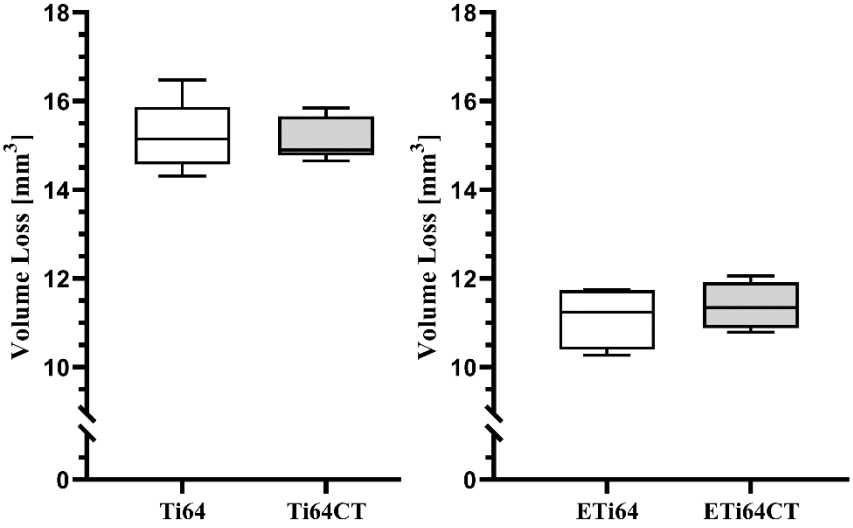

Figure 48 - Titanium samples abrasive wear volume loss [mm^3].

As there are no measurable differences in the untreated and the cryogenically treated samples for both of the materials, they were divided into two groups to be better analysed, now comparing only the Cast Ti64 and the EBM Ti64, regardless of the treatments applied to it. When comparing the EBM Ti64 to the Cast Ti64, it is possible to conclude that the volume loss on the EBM is roughly 70% of the wear volume of the Cast Ti64 samples, regardless of the abrasive wear test of the EBM Ti64 lasting only one third (2000 revolutions) of the duration of the cast Ti64 test (6000 revolutions).

5.3. WEAR SCAR ANALYSIS

This chapter presents the analysis of the typical wear scar of each of the light alloys' group samples. Figure 49 shows the typical wear scar for the titanium samples submitted to the abrasive wear test method A (130N and 6000 cycles).

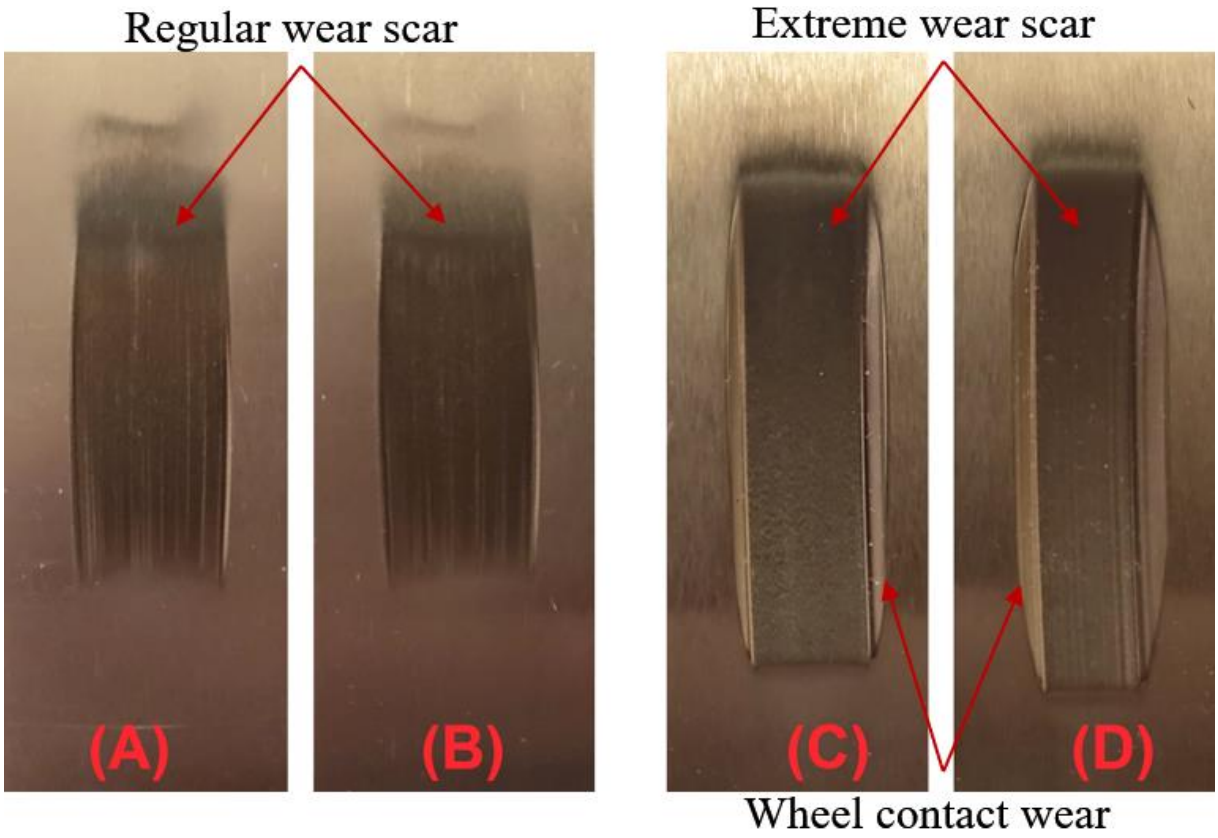

Figure 49 - Typical wear scar for the abrasive wear test method A: (A) Ti64; (B) Ti64CT; (C) ETi64; (D) ETi64CT.

While the conventional cast Ti64 and Ti64CT presented a regular wear scar for the abrasive wear test, the ETi64 and ETi64CT samples showed an extreme case of wear, having very deep wear scars and also wear marks caused by the contact of the rubber-wheel's rubber with the sample (marked as "wheel contact wear" in Figure 49). Figure 50 shows the height map for the ETi64 and ETi64CT samples.

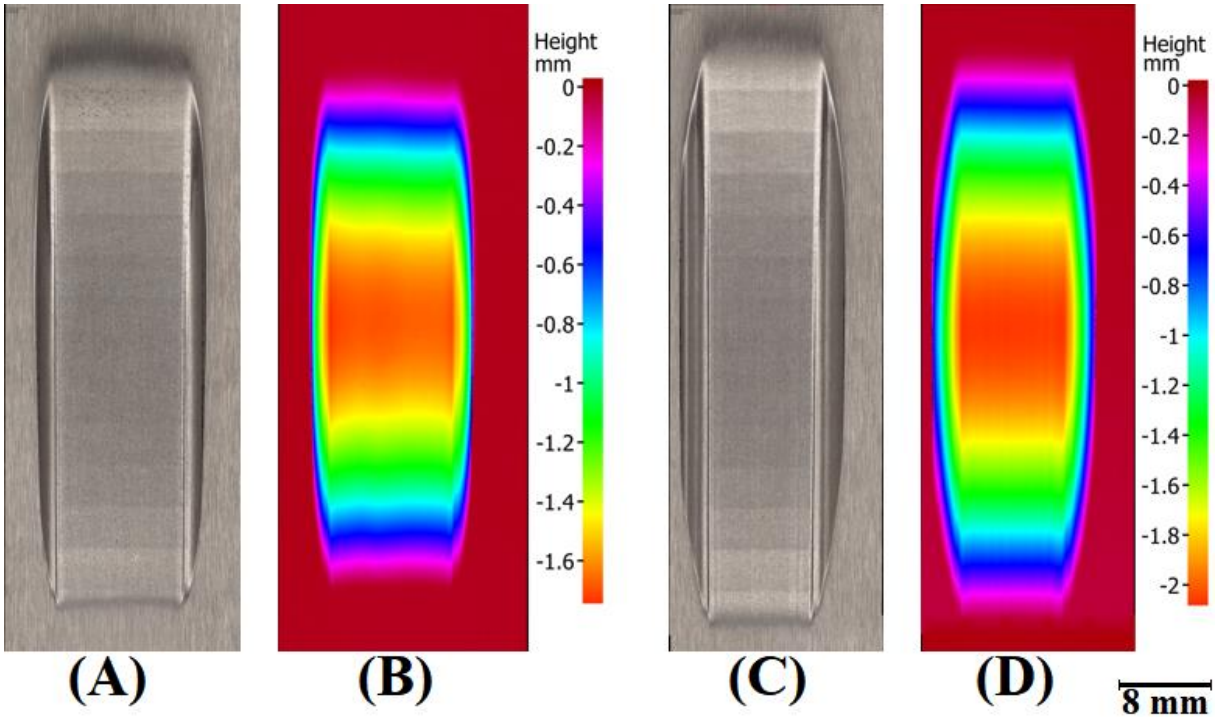

Figure 50 - EBM Ti64 extreme wear scar: (A) ETi64; (B) ETi64 heightmap; (C) ETi64CT; (D) ETi64CT heightmap.

The extreme wear exhibited by EBM obtained samples occurred when these samples were submitted to the method A of the abrasive wear test. The wear scar is deep enough such that the flow of sand became concentrated in the middle of the contact zone, leaving both corners of the rubber wheel without sand and, this way, allowing the rubber to come in contact with the titanium sample. The contact of the wheel with the samples surface damaged the corners of the wheel and rendered the results to not be comparable, once the wear scar did not present an even shape. Due to the test being performed first on ETi64 (causing the initial rubber wheel corner damage), it showed a wider wear scar than the one measured on ETi64CT. Due to this extreme wear behaviour and the damage caused to the rubber wheel, the EBM obtained samples were then submitted to a less aggressive abrasive wear test (Method B), having the duration of the test reduced to 1/3 (2000) of the total revolutions.

5.3.1. Cast Ti64 Wear Scar

The Ti64 and Ti64CT presented very similar wear scars, which can be seen in Figure 51 and Figure 53, respectively. These wear scars have rolling wear marks (detail B) in the centre accompanied by very few longer scratches that appear mainly in the bottom region of the wear (detail C).

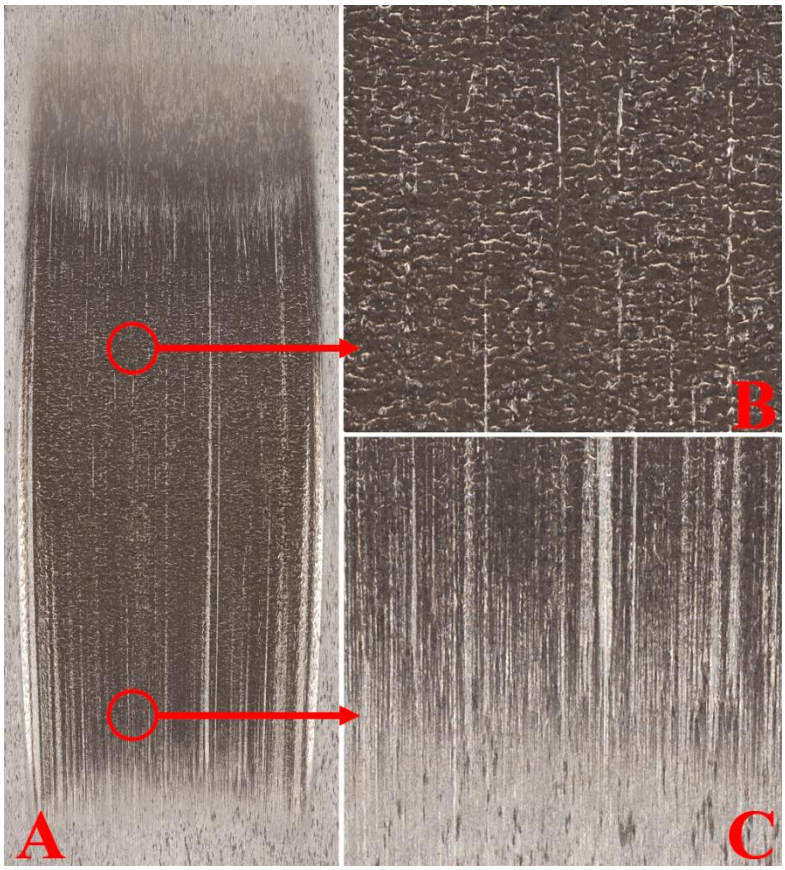

Figure 51 - (A) Ti64 typical wear scar; (B) Rolling marks; (C) Scratches.

The roughly horizontal wavy marks resulted from three-body abrasion and appear due to the rolling motion of the abrasive on the surface of the wear scar region. The scratches at the bottom were due to the start of a two-body abrasion mechanism, so the particles do not roll and deeper scratches are formed instead of the waves.

Figure 52 presents the cross-section of the central region of the wear scar, obtained using a conventional microscope and cross-polarized lens. Part (A) of Figure 52 presents a less zoomed image of the wear scar, showing the wear scar (interfacing with the Bakelite used to mount and prepare the sample) which presents waviness resulted from the rolling and an affected are just below the wears scar. This affected area is the result of the material resisting

the forces applied by the wear particles, this way having a plastically deformed region. Below the affected area, and moving toward the central region of the sample, the regular unaffected microstructure of the material is seen. These micrographs also show a few pores and the remnant silica particles used to polish the region.

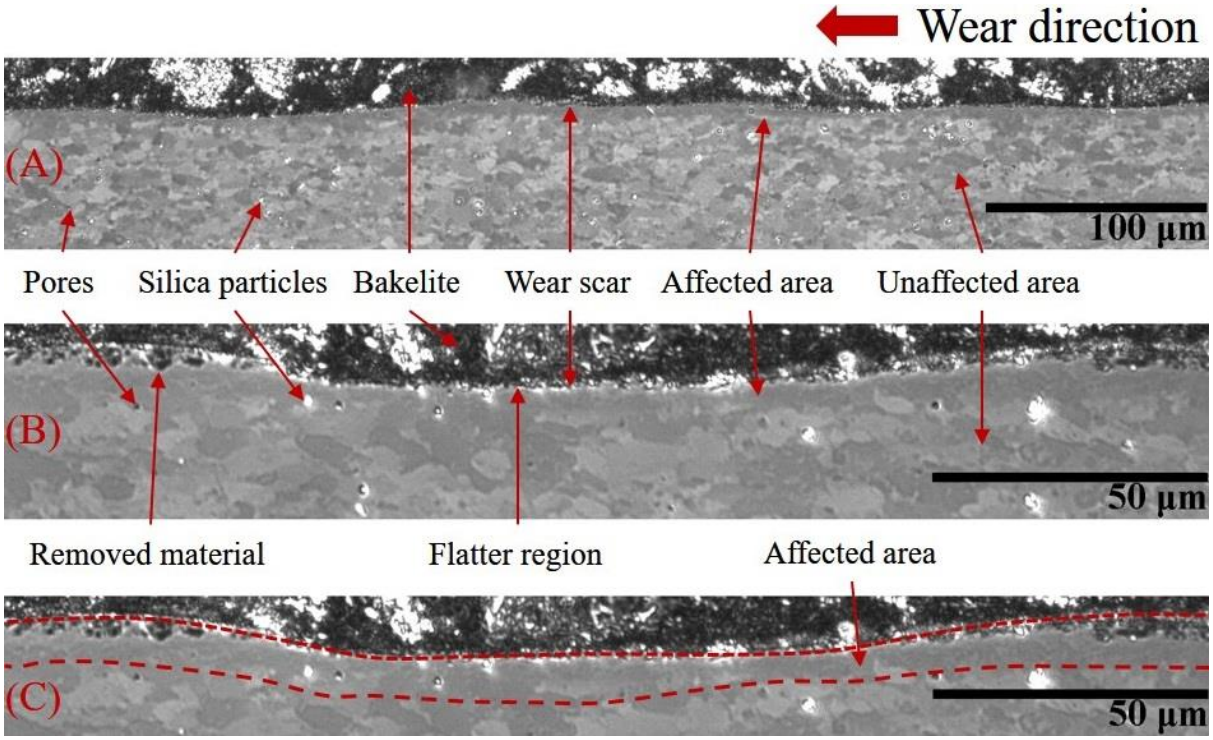

Figure 52 - Ti64 wear scar cross-section micrograph detail: (A) 20x micrograph; (B) 50x micrograph; (C) Affected area detail.

The (B) section of Figure 52 presents a similar region but with an increased magnification, this way presents the wear scar in more detail. The top of the wear scar is a mixed region, presenting regions in which the material is only deformed and regions in which the material was removed due to the higher amount of deformation it was submitted to. The combination of these two regions create the wear scar with several wavy marks and flatter regions, being the top of the wave the region in which the material is in the initial phase of being removed and the bottom flat regions are the ones in which the material was already removed, this way creating the wear evolution for this material. Figure 52C presents in detail the affected region.

To be able to analyse and compare the effect of the cryogenic treatment in the wear scar of these alloys, the same techniques used in the images present so far in this chapter were used in the Ti64CT sample. Similar mechanisms and wear scar can be seen on the cast Ti64 samples submitted to the cryogenic treatment, as present in Figure 53.

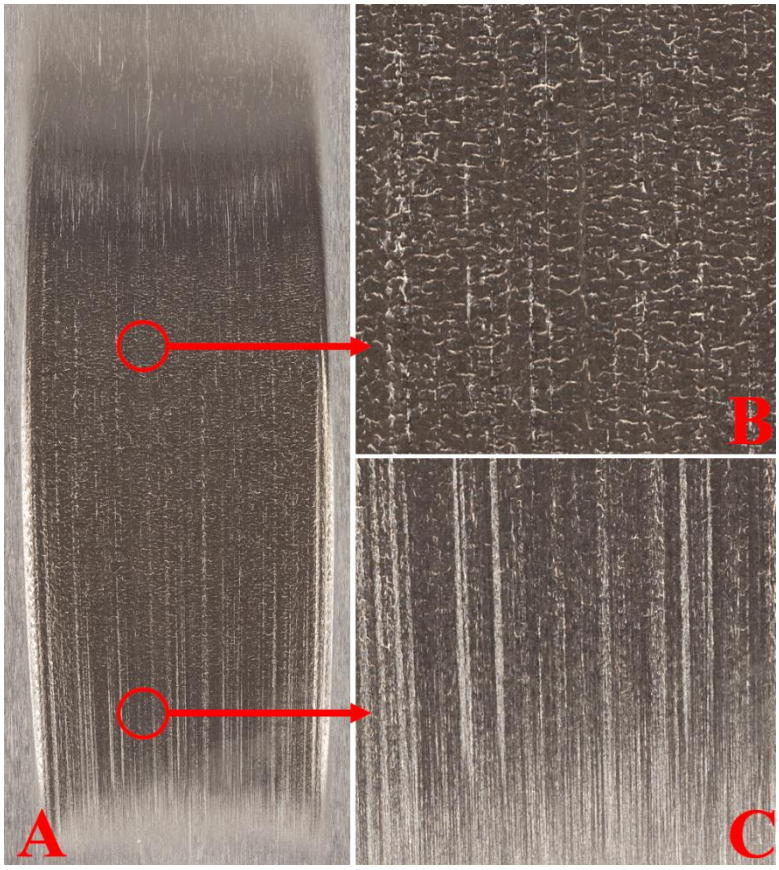

Figure 53 - (A) Ti64CT typical wear scar; (B) Rolling marks; (C) Scratches.

As explained in Section 3.7, the primary type of wear expected by the ASTM G65 abrasive wear test is the low-stress three-body abrasion, which agrees with the results found on most of the wear scars generated in this work. The deeper scratch marks represent a considerably smaller part of the wear scar and can be attributed to the poor wear resistance of the titanium alloy, facilitating the appearance of scratches due to ploughing happening. This phenomenon can be seen more frequently on the EBM obtained samples as presented in Section 5.3.3.

Figure 54 presents the cross-section of the wear scar for the cryogenically treated sample of Cast Ti64. The same features presented in Figure 52 can be seen in this image, like the small pores, silica particles, wear scar and wear affected area. When comparing with the previous cross-section image, no notable differences can be seen, being that this micrograph also presents the wavy wear scar and the same wear behaviour as previously explained. Figure 54 also presents three sections, being section (A) a wider field of view image to better show the wave and the affected area, section (B) showing in more detail the wear scar and the regions

in which the material has been removed and section (C) with the dashed line facilitating the delimiting of the affected area, in which the subsurface material is plastically deformed.

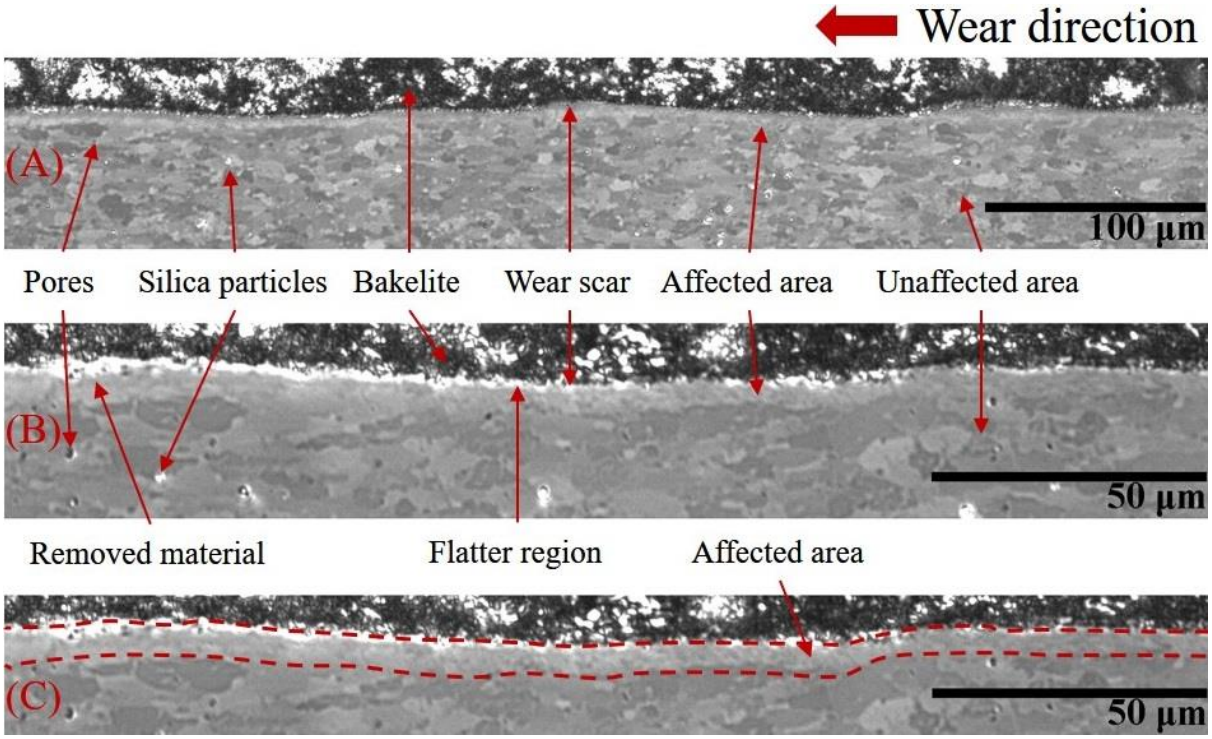

Figure 54 - Ti64CT wear scar cross-section micrograph detail: (A) 20x micrograph; (B) 50x micrograph; (C) Affected area detail.

The analyses of the wear scar presented in this chapter agrees with the previous test results, in which the cryogenically treated samples did not present any difference when compared to the untreated sample. The wear scar, subsurface and microstructure presented by both sets of samples are very similar and presents all the same patterns, thus no particular difference can be seen.

5.3.2. EBM Ti64 Extreme-Wear Scar

The EBM Ti64 initial tests showed an extreme case of wear, as shown in Figure 50, and for that matter is not going to be accounted for the wear volume measurement and the extensive wear scar analysis, once this type of wear does not represent the intended wear for this type of abrasive wear test. Figure 55 shows the wear in more detail for the typical extreme wear in the EBM Ti64 samples.

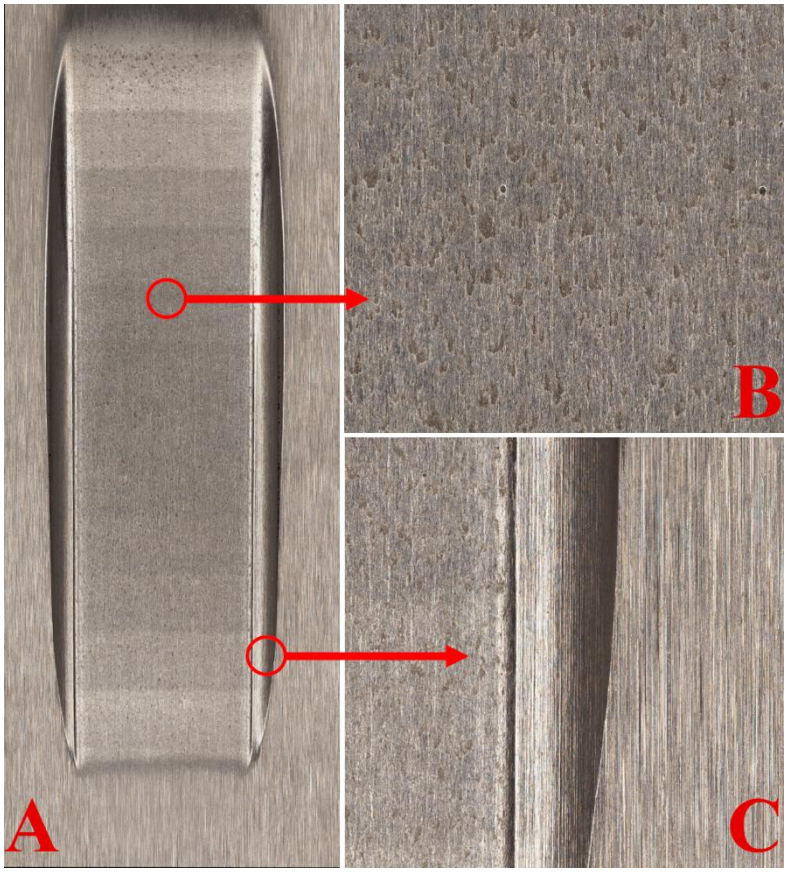

Figure 55 - (A) Typical extreme wear scar for ETi64; (B) Detail of the inner wear scar; (C) Detail of the wear scar sides.

This wear scar in Figure 55B does not present the rolling marks as seen previously, being the marks shown flatter with less features. This is likely due to the rubber on the circumference of the wheel being held by its corner while it touched the sample without sand in the interface, this way the sand in the centre of the wear scar did not had the needed pressure applied to it and just “polished” the central region instead of producing the intended wear mechanism. The sides of the wear scar (Figure 55C) is not as crisp as seen on the previous wear scars, this time the sample also removed material from the rubber wheel producing a rounded

and uneven edge. Figure 56 presents the extreme wear scar for the samples that was submitted to the cryogenic treatment.

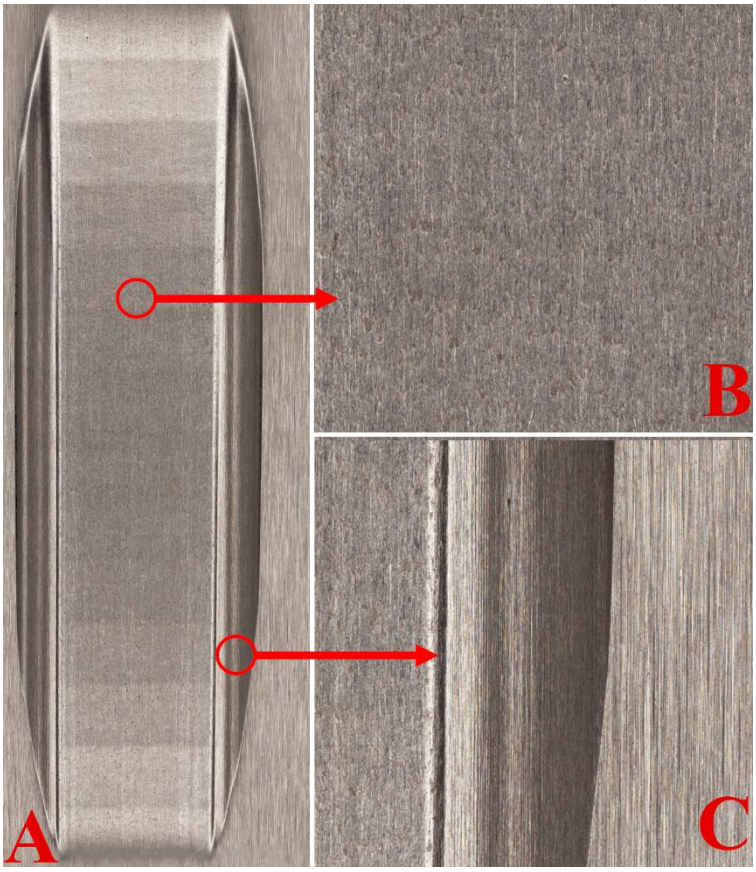

Figure 56 - (A) Typical extreme wear scar for ETi64CT; (B) Detail of the inner wear scar; (C) Detail of the wear scar sides.

As the previous extreme wear sample, this wear sample was not used to measure the wear difference. Similar characteristics to the untreated ETI64 sample can be found, being the polished central area (Figure 56B) and the rounded edges (Figure 56C). This wear scar presented a more polished central area and a bigger rounder edge, being these features due to the wheel's rubber already being damaged when this test started. The idea behind this second extreme wear test was to investigate if the same wear pattern would happen to the cryogenically treated sample, this way using the already damaged wheel would not play an important role in the final wear scar (since the damage to the rubber was not extreme). Due to these results, the parameters were changed (as presented in Section 3.7), the wear test was repeated and the results are presented in Section 5.3.3.

5.3.3. EBM Ti64 Wear Scar

The updated wear test for the EBM obtained Ti64 samples were performed and the wear scars presented a more regular shape and a better definition of the wear mechanisms. The typical wear scar for the ETi64 samples is present in Figure 57.

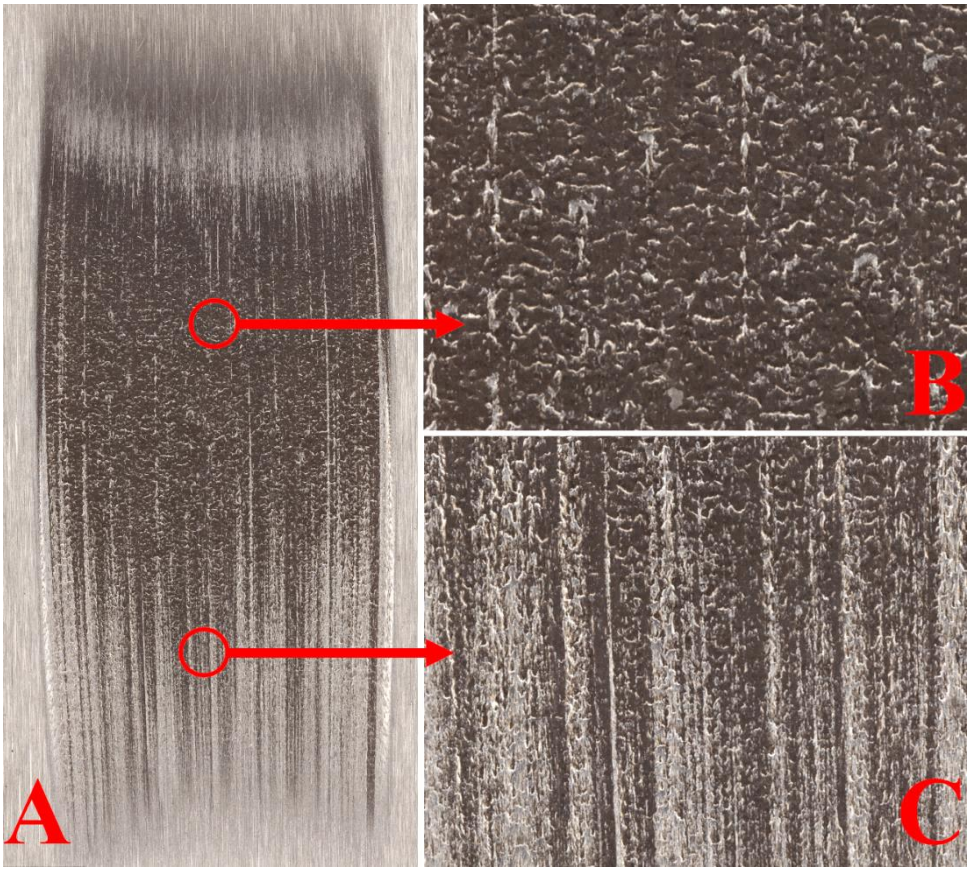

Figure 57 - (A) ETi64 typical wear scar for; (B) Rolling marks; (C) Scratches.

This time, the wear scar presented is similar to the one presented by the Cast Ti64 samples, in which the top section of the wear scar (detail B) shows rolling marks in the shape of waves and a concentration of scratches in the bottom part of the wear scar (detail C). The main difference between the two types of material (cast and EBM) is that the EBM obtained Ti64 present a bigger quantity of scratches from the central region of the wear scar, even presenting scratches that start on the top region and finish in the bottom of the wear scar. Even though the brighter areas (scratches) appear to be higher than the darker areas, it is actually lower, being the scratches deeper than the wavy marks from three body abrasion wear.

The analyses of the cross-section of the ETi64's wear scar is presented in Figure 58, being composed of two micrographs acquired using cross-polarised lens in a conventional microscope. Two different magnifications were used, being (A) using 20x lens and (B) & (C) using a 50x lens.

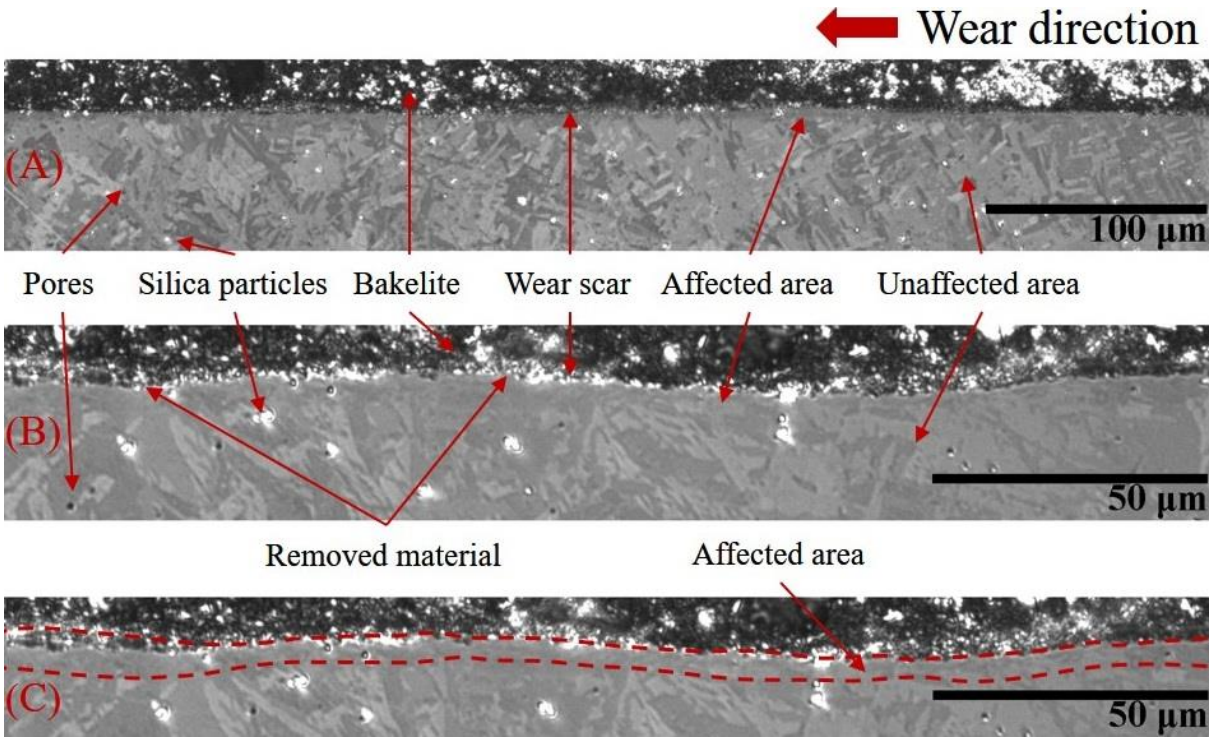

Figure 58 - ETi64 wear scar cross-section micrograph detail: (A) 20x micrograph; (B) 50x micrograph; (C) Affected area detail.

Figure 58 presents a wear scar with patterns that are similar to the ones presented by the Cast Ti64 samples (Figure 52 & Figure 54), once it has lower and higher areas that compose the wavy marks. The main difference here is that the top of the waves (shown on detail A & B) is not as high as the Cast Ti64 samples and the wear (removed material) is more uniform across the whole surface, not presenting a well-defined "flat region", but instead presenting a shape similar to a sinusoidal wave (better seen on detail A). Even though the grain shape is very different from the Cast Ti64, the plastic deformed region can be clearly seen and defined just below the wear scar. Another notable difference is the increased occurrence of pores and the number of these pores that present a larger diameter when compared to the Cast Ti64 samples, which were confirmed and quantified by the results presented in Table 23.

Figure 59 presents the typical wear scar for the cryogenically treated EBM Ti64 (A) samples and the detailed central region (B) and bottom region of the wear scar (C).

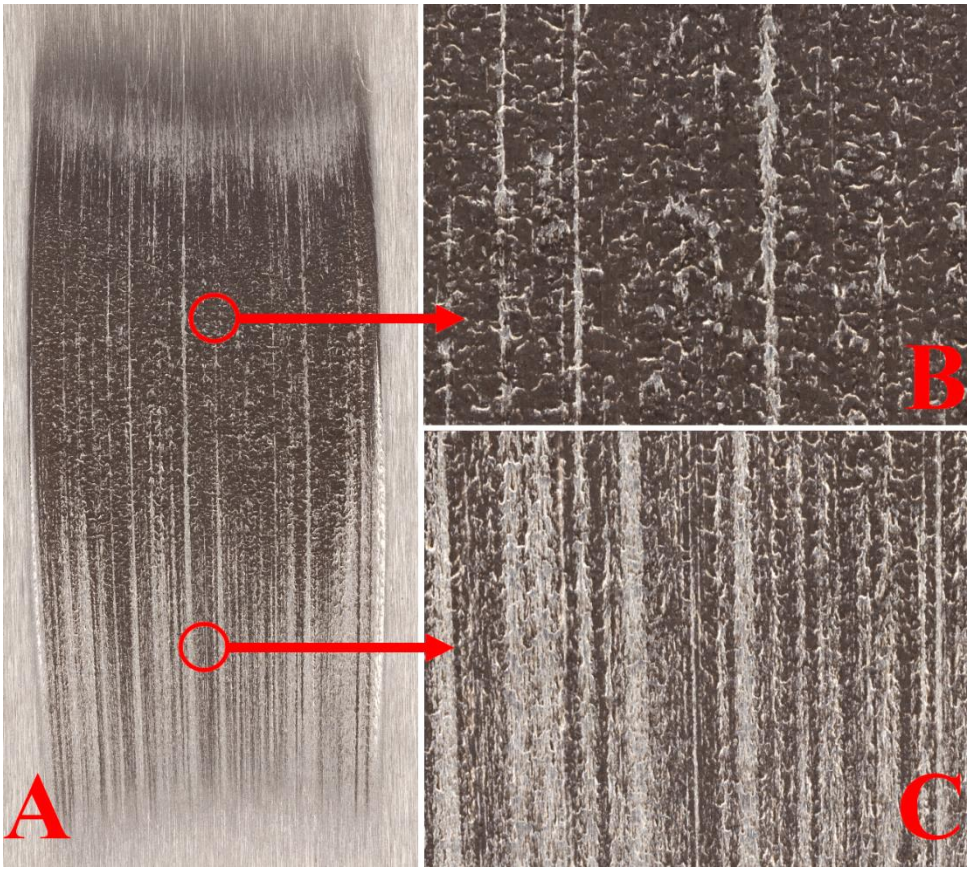

Figure 59 - (A) ETi64CT typical wear scar for; (B) Rolling marks; (C) Scratches.

There is no recognisable difference between the cryogenically treated (Figure 59) and the non-treated EBM Ti64 (Figure 57) samples when analysing the wear scars. The deeper scratches can be seen throughout the wear scar and a bigger concentration of it happens after the middle section of the wear scar. This bigger and deeper scratches occur due to two main factors, one being the lower resistance of the titanium alloys to wear and the second being the higher occurrence of pores in the EBM obtained samples (as shown and analysed in Section 5.1.3 & Section 5.1.4).

The details of the ETi64CT wear scar cross-section are shown in Figure 60. These micrographs are similar to the ones of the EBM Ti64 untreated samples, having no clear difference when comparing both micrographs. Once again, the sinusoidal shape is present, with several waves and a wear pattern (removed material, detail A & B) across the whole top section of the wear scar. The microstructure close to wear scar region also shows the same type of plastically deformed region that follows the direction of wear, presenting below it an unaffected region in which the regular microstructure is seen.

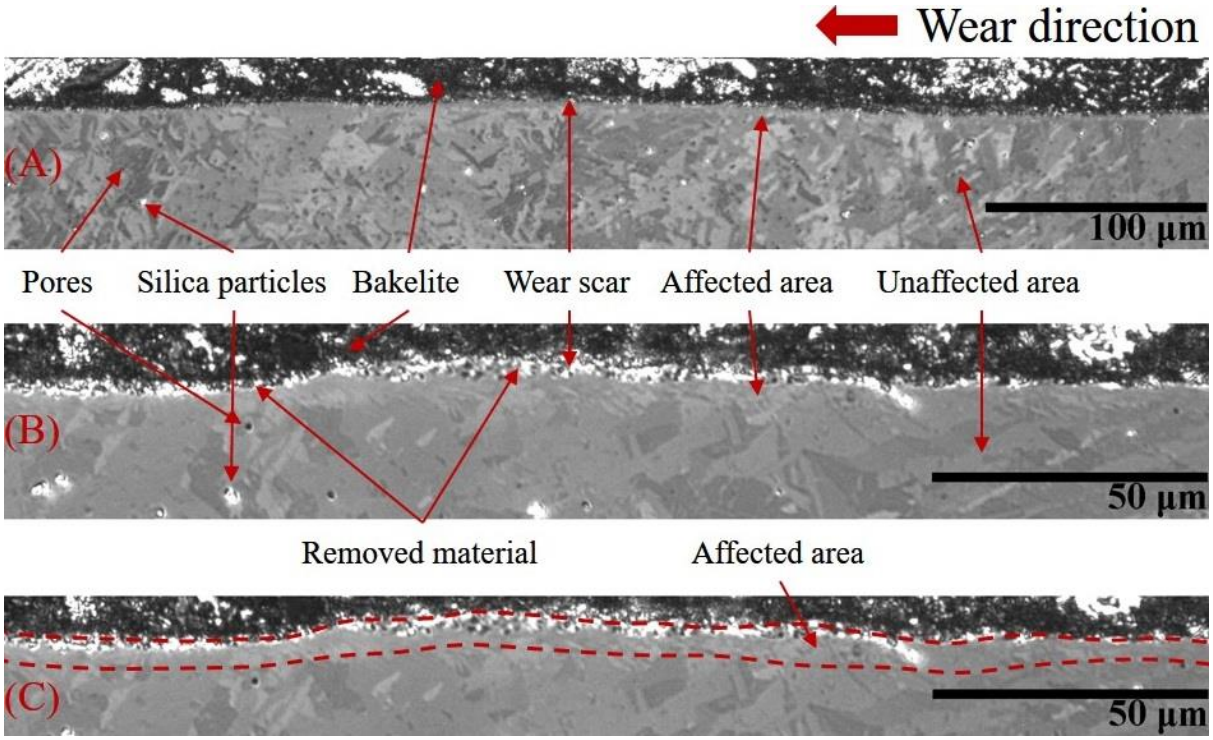

Figure 60 - ETi64CT wear scar cross-section micrograph detail: (A) 20x micrograph; (B) 50x micrograph; (C) Affected area detail.

The increased number of pores and the bigger pores sizes increase on the surface the chance of the sand grains getting entrapped in the material's surface, this way preventing other sand grains from rolling and thus facilitating the occurrence of ploughing. Once this phenomenon starts to occur, the section of material removed leaves an even bigger pore, which entraps more sand particles and the ploughing happens as cascade event until the end of the wear scar. It is possible to note that the amount of scratches increases after the middle section of wear scar, which occurs due to the increased pressure applied in the middle section of the scar (since this is the region normal to the wheel diameter, this way applying more pressure). The difference in the wear scar can be easily seen when comparing the EBM obtained (Figure 57 & Figure 59) and the Cast Ti64 (Figure 51 & Figure 53) samples.

5.4. LIGHT ALLOYS DISCUSSION

Samples of Ti-6Al-4V (Ti64) titanium alloy were manufactured using two different methods, being a more conventional hot rolled annealed plate and an additively manufactured sample obtained using Electron Beam Melting technique on an Arcam machine. The plate was sectioned into the standard ASTM G65 samples and the EBM samples were printed with the desired dimensions, both having half of the samples submitted to cryogenic treatment and, finally, all of the samples were ground as per the standard needs.

There is a lack of information in the literature about the effects of the cryogenic treatment in the mechanical properties of the Ti64, being that some of the research found claims that the cryogenic treatment affects the mechanical properties like hardness and wear resistance [25,40], while more recent research asserts that the cryogenic treatment does not affect the Ti64 microstructure in any way, also not resulting in any significant changes in hardness [69]. In this work, the titanium samples were tested without any further heat treatment other than the cryogenic treatment itself, being the material treated as an "off-the-shelf" solutions, thus no custom parameters were used in the printing of the EBM samples (detailed in Section 3.4.1).

Once the samples were prepared as explained previously, it was submitted to the Vickers hardness testing, to verify the consistency of it. As shown in Table 18 and Table 19, all the groups of samples presented a good repeatability, meaning that are no relevant differences in samples that are part of the same group. These results also confirmed that the cryogenic treatment did not affect the hardness in any measurable way for the cast or EBM obtained samples, agreeing with the results found by the more recent work previously referred [69].

The analysis of the microstructure of the material is important because different heat treatments or manufacturing methods can produce different types of microstructures. The cast Ti64 microstructure was composed of the commonly seen α globular grains (Figure 44) and, when comparing untreated and the cryogenically treated samples, there were no perceptible difference among then, even having very similar grain size (Table 22). The EBM samples showed an increased number of pores (having 6.8 times as many pores than the cast sample, Table 23), but the cryogenic treatment also did not present any relevant difference in the grain size (Table 22) or in the lamellar α+β microstructure showed by these samples (Figure 45). It

is important to note that the features like porosity and grain size can be changed by selecting different parameters during the manufacturing process of the EBM samples.

The abrasive wear test is the main test used in this work to judge the effect of the cryogenic treatment in the studied alloys. In the case of the EBM samples, the initial standard Method A caused the samples to experience extreme wear, making a wear scar so deep that the sand flow was concentrated in the centre of it and led to the wheels contacting the side of the samples (Figure 50), wearing the sample and the rubber patch of the wheel at the same time. Owing to this, new parameters were set and the test for the EBM samples was changed to a less aggressive test, having one third of the total duration of the other tests (defined as Method B in the ASTM G65). After changing the duration, the abrasive wear test presented good and repeatable results, which made the untreated samples and cryogenic samples results comparable, showing that the cryogenic treatment did not affect the abrasive wear resistance of this material (Table 21). The test for the cast Ti64 samples was the standard Method A, which when comparing the untreated and cryogenically treated samples also did not show any significant difference in the results.

When comparing the wear scar for the cast Ti64 (Figure 51 & Figure 53) and the normal wear scar for the EBM Ti64 (Figure 57 & Figure 59) a clear difference is seen, being that the first presents less scratches and more of the rolling wavy marks while the later shows more scratches, being these scratches a result of the bigger quantity of pores in the surface of the sample, which increases the chance of ploughing happening in the surface instead of the desirable three body abrasion. Comparing the different groups (treated and untreated) of each material, no difference of mechanism is apparently seen in the wear scar surface or its cross-section, concluding that the cryogenic treatment did not affect the mechanisms that act in the wear of these alloys in any notable way.

Although not the main focus of this work, it is also useful to compare the performance of the untreated EBM titanium to the untreated conventionally cast Ti64. Even though the tests duration of the EBM samples were submitted to were different (being one a third of the other), the comparison of it being an option of "of-the-shelf" (i.e. not tailoring the EBM parameters to a specific application) solution is still valid and worth to take into consideration. The customization of the parameters of an EBM printing is both time and budget consuming (once it would need many tries and tests), which should be considered when choosing an engineering alloy as a solution to a specific application. This way, when directly comparing these two

variants of the alloy as “ready solutions”, the cast Ti64 presents an advantage over the EBM obtained, once that for the same hardness, it presents a volume loss significantly smaller than its counterpart, being that when the same parameters for the abrasive test were applied to the EBM sample, extreme wear occurred in this alloy. This is perhaps intuitive, due to the difference in porosity, but is useful to have quantified nonetheless.

5.5. LIGHT ALLOYS SUMMARY

This section presents the summary of the findings for the cast Ti-6Al-4V and the EBM obtained Ti-6Al-4V, which is shown in the following list:

- The Vickers hardness and microhardness tests results for both variants of the alloy when comparing their respective untreated and cryogenically treated groups did not present any significant difference.
- The EBM samples presented an average of 6.8 times as many pores per unit area than the cast Ti64 samples.
- There were no apparent differences in the grain size or in the microstructure's features when comparing the untreated and cryogenically treated groups of each of the light alloys.
- The wear volume for the abrasive wear test also did not present any measurable difference between the untreated and treated groups.
- The EBM obtained samples have significantly worse abrasive wear resistance than the more conventional cast Ti64 alloy.
- The wear scars for the EBM samples showed a combination of three body abrasion (rolling marks) and ploughing, that resulted in deep long scratches along the wear scar length. The cast Ti64 samples showed more of the wavy marks and fewer smaller scratches.

6. WEAR OF AUSTENITIC STAINLESS STEELS

This chapter presents the data, analysis and conclusions related to the abrasive wear tests conducted on the AISI 304L (SS304 and SS304CT) and the AISI 316L (SS316 and SS316CT) austenitic stainless steel. The mechanical tests' results are presented for the aforementioned samples, followed by a comparison between the conventionally heat treated and the cryogenically heat treated group. The wear scar is analysed in detail and all the results presented for these alloys are discussed. A summary with the important discoveries and points of note is at the end of the chapter.

6.1. TEST RESULTS

To be able to acquire data and trends related to the wear resistance of these alloys, the tests detailed in Section 3 were performed in the austenitic stainless steel selected alloys. This section presents the data for each of the performed tests.

6.1.1. Hardness and Microhardness

To verify the uniformity of the samples that were used in all the tests, an initial hardness test was performed in a Vickers hardness machine. The load chosen for these materials was the 10 kgf, which was the one that showed the clearer indentation and had the appropriate size to be measured. This test was performed in every single sample, on both sides of these samples and in different areas of the surface, as explained in Section 3.6. The results for the Vickers hardness performed in the Austenitic Stainless Steel samples are presented in Table 26.

Table 26 - Austenitic stainless steels Vickers hardness (HV10) values.

Sample	Cryogenic Treatment	Average Hardness [kg/mm^2]	Standard Deviation (σ)	Standard Error ($\sigma\bar{x}$)	% Standard Error
SS304	No	182.19	6.18	1.13	0.62%
SS304CT	Yes	187.01	5.00	0.91	0.49%
SS316	No	167.12	5.70	1.04	0.62%
SS316CT	Yes	167.52	6.42	1.17	0.70%

The hardness results for both groups of alloys (AISI 304L and AISI 316L) showed that the samples were uniform and that the values are inside of what is expected for these alloys. The lower Standard Error of these measurements is a result of the high number of repeats (30 in total for each alloy and each condition) and the low standard deviation (scatter of the measured values) that these measurements presented. The analysis of the results also had a

small standard error (being this always smaller than 1%), which means that these results have an excellent repeatability. Table 27 shows the results for the Vickers microhardness test performed in the alloys studied in this chapter.

Table 27 - Austenitic stainless steels Vickers microhardness (HV0.5) values.

Sample	Cryogenic Treatment	Average Hardness [kg/mm^2]	Standard Deviation (σ)	Standard Error ($\sigma_{\bar{x}}$)	% Standard Error
SS304	No	191.61	6.61	1.65	0.86%
SS304CT	Yes	194.55	6.75	1.69	0.87%
SS316	No	177.37	5.33	1.33	0.75%
SS316CT	Yes	179.85	5.92	1.48	0.82%

The results for the microhardness, as the ones previously shown for the hardness, also present a good repeatability (Standard Error for these results is also always smaller than 1%) and are as expected for this kind of material. The load applied was chosen taking the standard in consideration, so the size of indentation was a limiting factor. If a load that is too light is used, the indentation size is deemed too small and the error that comes from measuring this indentation becomes too big, this way increasing the deviation of the results.

6.1.2. Wear Volume

The modified ASTM G65 Dry-Sand/Rubber-wheel was conducted on the specimens for both alloys, in the cryogenically treated and also in the conventionally heat treated conditions. The parameters used in this test were the ones described in the standard Method A, being a normal load applied of 130 N and a duration of 6000 cycles. The summary of the parameter for each material and condition is illustrated in Table 28.

Table 28 - Outline of the ASTM G65 test methods for the austenitic stainless steels.

Sample	Test Method	Revolutions	Load Applied [N]
SS304	A	6000	130
SS304CT	A	6000	130
SS316	A	6000	130
SS316CT	A	6000	130

The samples were weighted after being submitted to the abrasive wear test and the mass loss was calculated. These results are found in Table 29.

Table 29 - Austenitic stainless steels abrasive wear test results

Sample	Number of Tests	Cryogenic Treatment	Mass Loss [mg]	Volume Loss [mm^3]	Standard Deviation (σ)	Standard Error ($\sigma\bar{x}$)	% Standard Error
SS304	5	No	100.260	12.533	0.822	0.368	2.93%
SS304CT	5	Yes	68.240	8.530	1.016	0.454	5.33%
SS316	5	No	71.940	8.992	0.254	0.113	1.26%
SS316CT	5	Yes	68.820	8.602	0.290	0.130	1.51%

The results presented for the abrasive wear test of the AISI 316L had a low Standard Error (always smaller than 2%), while the results for the same test for the AISI 304L presented a higher Standard Error (smaller than 5.5%). Even though the result for the Standard Error of the AISI 304L samples is somewhat bigger than for the ones of the AISI 316L, these sample still presented a good repeatability of results and the trends resulting for the heat treatment are still clearly seen. This increased ranged of values for the wear resistance of the AISI 304L can be due to the samples being manufactured from a commercial alloy, which can present some variation in the mechanical properties.

6.1.3. Grain Size

The grain size was measured using a SEM image of the microstructure of one etched sample from each material in each of the conditions, as per the methodology shown in Section 3.6. The results for the austenitic stainless steels grain size measurements are presented in Table 30.

Table 30 - Austenitic stainless steels grain size.

Sample	Cryogenic Treatment	Average Intercept [µm]	ASTM Grain Size [G]
SS304	No	27.602	7.1
SS304CT	Yes	26.891	7.1
SS316	No	21.681	7.8
SS316CT	Yes	22.135	7.7

6.1.4. Microstructure

The AISI 304L and AISI 316L samples were sectioned and prepared according to the methodology presented in the Methods (Section 3.7). These materials presented a challenge due to the presence of the rolling marks in the microstructure of these alloys. After being ground and polished until no blemishes (scratches or other unwanted features) could be seen under an optical microscope, these samples were submitted to the etching procedure, which

initially showed more of the rolling marks than the actual microstructures of the alloys, as illustrated in Figure 61. As it is shown in this image, the rolling marks are waves that prevent the microstructure from being seen clearly, these marks are very obvious in Figure 61B. Another effect also happens due the interaction of these waves with the etchant, which etches the lower regions of the waves more than the rest of the microstructure, leaving a cluster of holes as seen in Figure 61A. It is important to note that these waves could only be seen after etching the samples, so the fine-tuning of the etching was an important part of being able to see the microstructure properly in these samples. The methods and parameters used are presented and explained in Section 3.6.7.

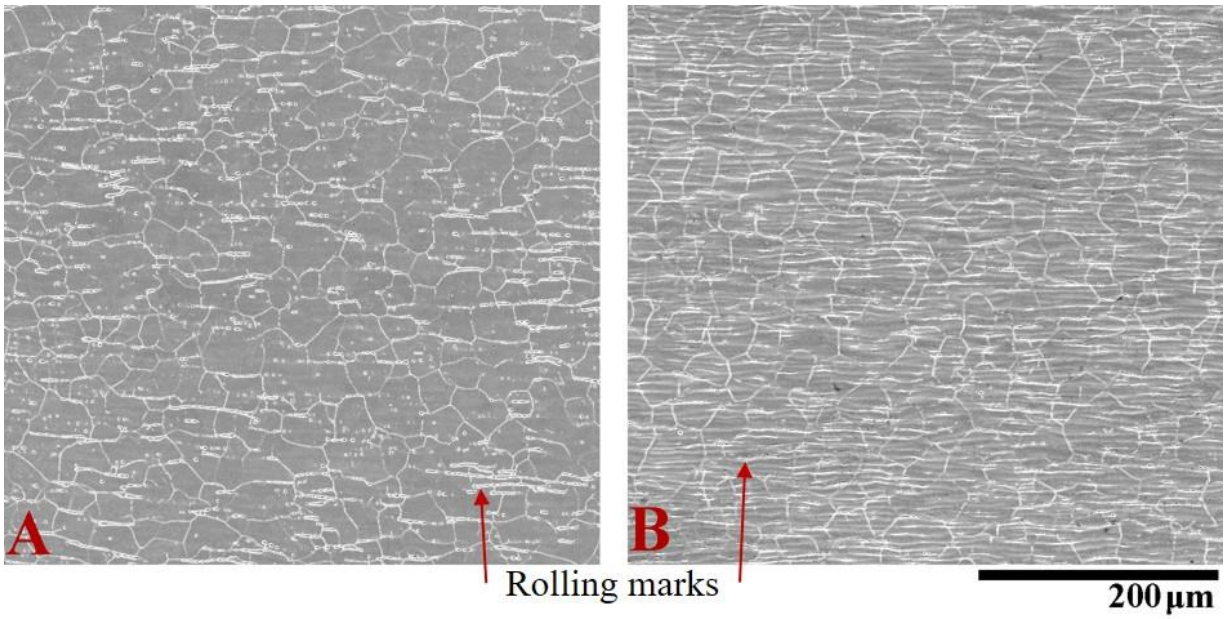

Figure 61 - Typical SEM image of the microstructure presenting the rolling marks:
(A) AISI 304L; (B) AISI 316L.

After finding the optimum parameters for the etching, the microstructure of the Stainless Steel samples was analysed using an SEM. Figure 62 illustrates the typical microstructures for the AISI 304L in conventionally treated and cryogenically treated conditions.

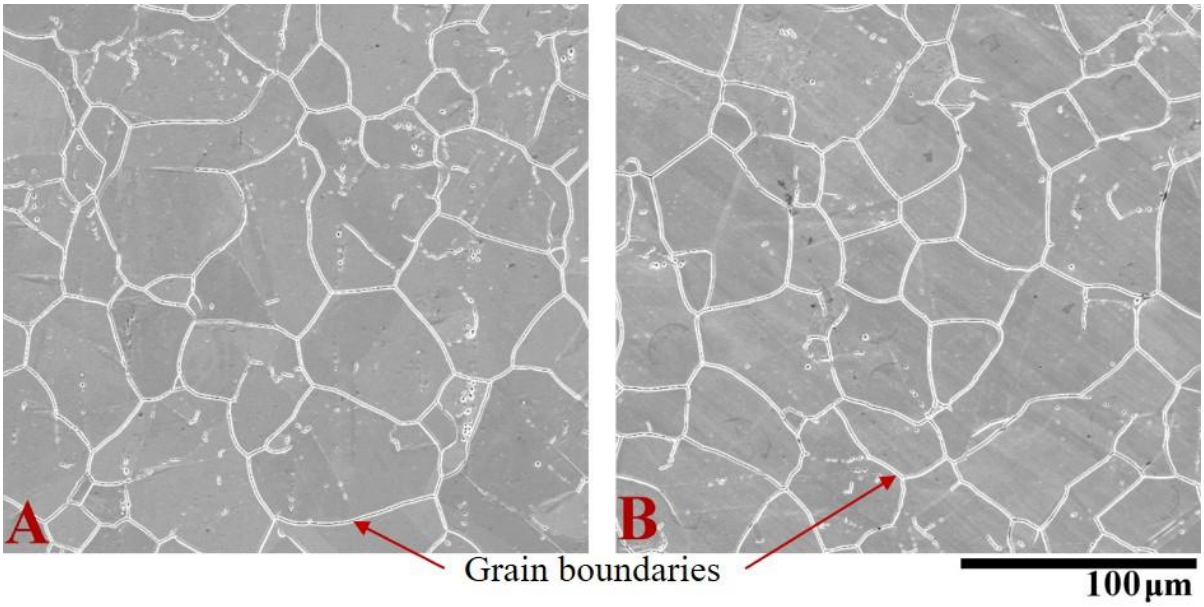

Figure 62 - Microstructure of the AISI 304L: (A) SS304; (B) SS304CT.

From Figure 62, is seen that there are still some minor burned areas due to the etching effect in the waves that resulted from rolling, but the microstructure of both conditions is clearly seen and were used to measure the grain size (Table 30). When comparing both of the microstructures, no clear difference is seen, meaning that for these alloys the cryogenic treatment did not affect the size and format of the grains. Also, no precipitate of any kind is seen. Similarly, Figure 63 shows the typical microstructure for the AISI 316L samples used in this research.

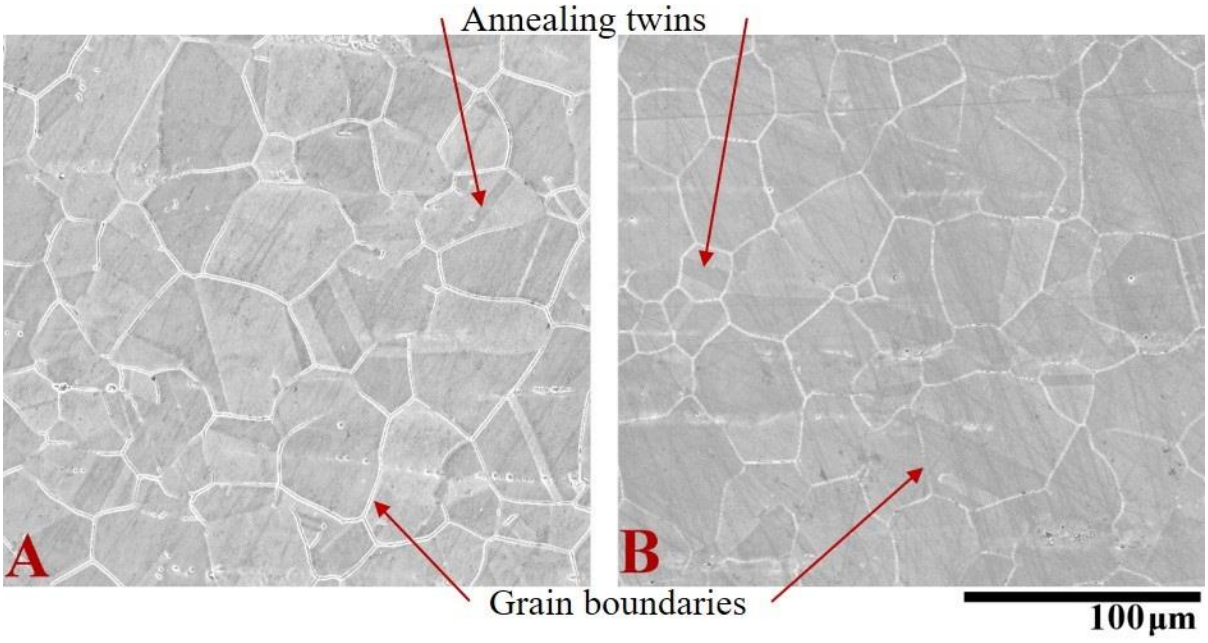

Figure 63 - Microstructure of the AISI 316L: (A) SS316; (B) SS316CT.

The microstructures for the AISI 316L samples do not present as much of the burned areas as the previous image, which makes the image clearer and the grains better defined. Another feature that is seen in these microstructures is the presence of annealing twins, that are structures present inside of the grains, which have straight sides and occur due to growth accidents during the recrystallization. Since both images for these materials present a very similar microstructure, the cryogenic treatment did not produce any change to the microstructure that can be seen with the advanced microscopy techniques presented in this section.

6.1.5. X-Ray Diffraction

The metallographic analysis presented in Section 6.1.4 showed that there is no visual difference when comparing the conventionally heat treated and the cryogenically treated samples, even though the deep cryogenic treatment presented a positive effect on the wear resistance. To further verify the phases present in the stainless steel alloys, an X-ray diffraction analysis was performed in each of the groups of the materials studied in this chapter, being the samples analysed sectioned from parts of samples used in the abrasive wear test. The results for the AISI 304L samples and AISI 316L samples are presented in Figure 64 and Figure 65, respectively.

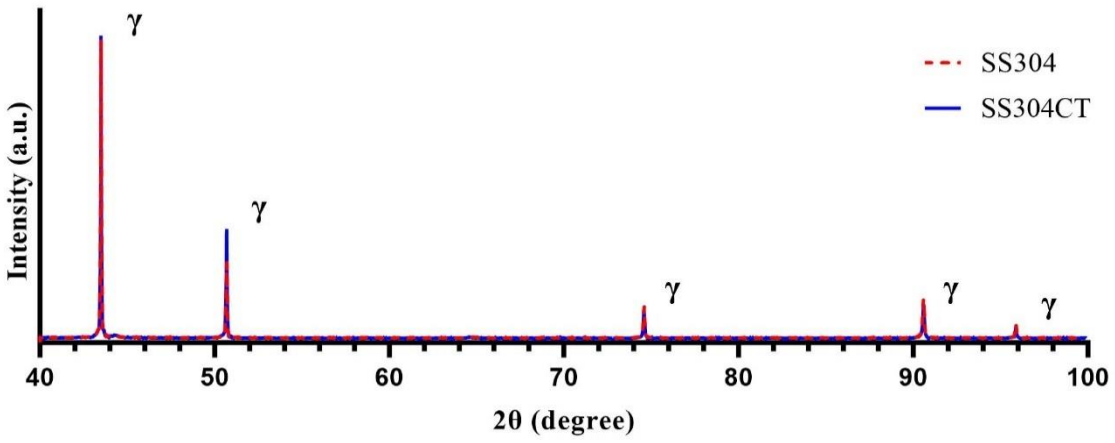

Figure 64 - AISI 304L X-ray diffraction spectra. The deep cryogenic treated curve is presented as a solid blue line and the conventionally heat treated as a red dashed line.

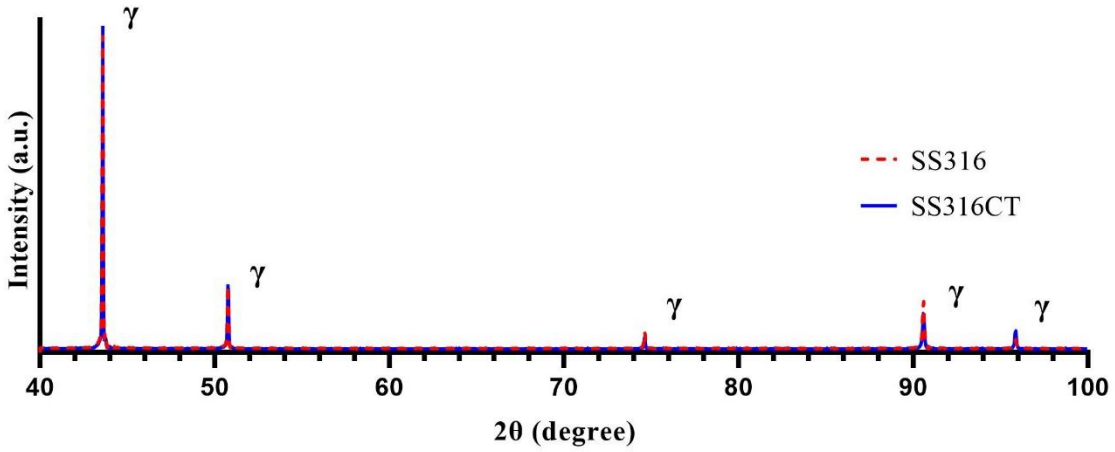

Figure 65 - AISI 316L X-ray diffraction spectra. The deep cryogenic treated curve is presented as a solid blue line and the conventionally heat treated as a red dashed line.

The previous graphs present two curves each, being the red dashed curve for the conventionally heat treated samples and the blue for the cryogenically treated samples. The cryogenically treated curve is the solid blue line and the conventionally heat treated is a red dashed line, as the peaks are on top of each other and using a dashed line facilitates the visualisation.

As shown in the XRD for the AISI 304L samples (Figure 64), the curves for the conventionally heat treated and cryogenically treated groups are very similar and show the same peaks in the same region, being only the austenite (γ) phase peaks seen for both of the treatment conditions. The results presented in Figure 65 for the AISI 316L samples is also similar to the previous one, and only the austenite phase peaks are found in the XRD analyses. For the stainless steels, the XRD analyses only showed peaks related to the austenite phase, meaning that no martensite was found in this test.

For this XRD analysis, the limitations encountered were due to the combination of the very low penetration of the Copper K-α in ferrous alloys and the grain size of this particular alloy being relatively large. This way, only a small number of grains were analysed per test, which can result in suboptimal statistics.

6.1.6. Transmission Electron Microscope

A transmission electron microscope (TEM) analyses was performed on a SS304 and SS304CT samples to verify the presence of any important feature resulting from the influence of the cryogenic treatment in this alloy. This TEM analysis was performed using this material

due to the positive effect of the cryogenic treatment in its wear resistance and the evidence found in the literature that pointed to the possibility of formation nano-martensite in the microstructure of this type of alloy [37,38].

The TEM possesses the capability of acquiring very high magnification images, making possible the use of the selected area diffraction pattern (SAD), which is used to analyse the material's crystal structure. Due to time constraints and availability of the equipment, only one sample of each condition was analysed and the diffraction patterns for each of the conditions are shown in Figure 66.

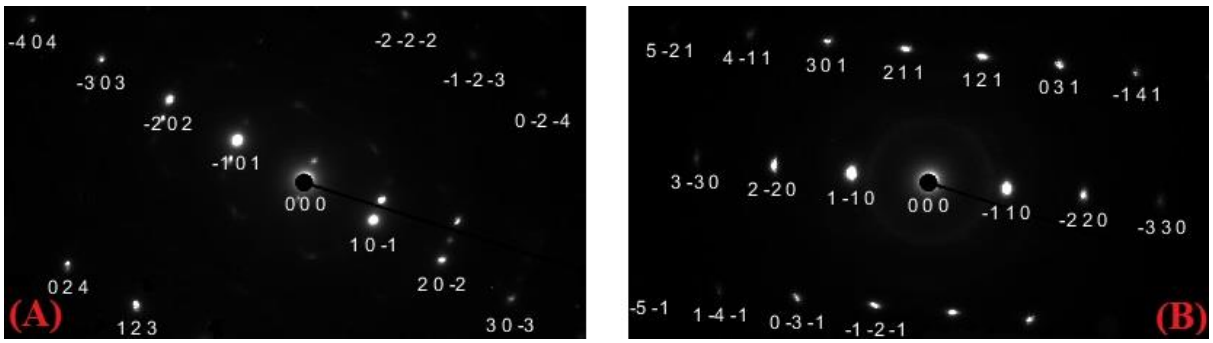

Figure 66 - Diffraction patterns for the AISI 304L samples: (A) SS304; (B) SS304CT.

Using the selected area diffraction pattern (SAD) presented in the previous image, the lattice vectors were quantified and its lengths, ratios and angular distances were calculated. With the previous information, the lattice vector was identified and the zone axis calculated, being D-spacing calculated and compared to the theoretical values for the austenite.

The results from the analyses of these images agreed with the theoretical value for the austenite parameters, being the estimation from the software defined as "very good rating" and presenting a small Standard Deviation for the D-spacing of both conditions. Once the measured parameters agreed with the theoretical parameters for the austenite, it was concluded that the only phase found in this TEM analysis was austenite for this specimen.

The main limitation in this analysis was the quantity of samples and number of analysis performed, since only one sample of each condition was scanned and only a few analyses were performed on each sample. This is mainly due to the fact that this advanced type of analysis presents a high cost, being this brief analysis shown only possible due to the informal help provided by Dr Qi. To better perform this type of advanced investigation, the test needs to be repeated several times and many of the samples (that are complex and take a lot of resource to

be produced) must be scanned and analysed, which would be better performed in a research which focus would be the TEM analysis.

6.2. COMPARISON OF CONVENTIONALLY HEAT TREATED VS CRYOGENICALLY TREATED

In this section, the results presented in Section 6.1 are submitted to a comparative statistical analysis and later presented in the form of graphs to be better presented and discussed. As done in the previous chapters, the premise used for the unpaired two tailed T-test is that the two conditions' results mean value (conventionally heat treated and cryogenically treated) are significantly different from one another, since this premise is true when the P-value presents a confidence higher than 95% combined with the condition that the t-value shows a high number (further from zero). The results for the T-test of the AISI 304L samples is demonstrated in Table 31 and for the AISI 316L samples in Table 32.

Table 31 - Unpaired two tailed t test: AISI 304L tests results comparing the conventionally heat treated to the cryogenically treated samples

Test	t value	Significance (p-value)	Mean Difference	SE Difference	Significantly Different?
Microhardness	1.269	0.214	3.00	2.36	No
Hardness	3.235	0.002	4.80	1.48	Yes
Grain size	1.646	0.117	0.71	0.43	No
Volume Loss	6.848	<0.001	3.99	0.58	Yes

The AISI 304L samples did present a significant difference in some of the parameters when comparing the SS304 and SS304CT groups. The grain size remained as one of the unchanged parameters, being the mean difference between the two groups' measured grain size of approximately 2.7%, which can be considered negligible when taking into account the SE of the difference (which is 60% of the mean difference value) and the results for the t-test, in which the confidence is lower than 88.3% and the premise is considered false. The other parameters will be discussed more in depth during this chapter.

Table 32 - Unpaired two tailed t test: AISI 316L tests results comparing the conventionally heat treated to the cryogenically treated samples

Test	t value	Significance (p-value)	Mean Difference	SE Difference	Significantly Different?
Microhardness	1.242	0.224	2.50	2.01	No
Hardness	0.250	0.803	0.40	1.60	No
Grain size	1.224	0.237	0.45	0.37	No
Volume Loss	2.265	0.053	0.39	0.17	No

The statistical analysis of the AISI 316L results show that there are no differences that are significant enough to validate the premise when comparing the conventionally heat treated and the cryogenically treated samples. Even though the grain size value shows a difference, the standard deviation of the measurements, the small mean difference (~2%) and the low confidence (p-value < 77%) confirm that this difference is inside of the uncertainty interval, meaning that there is no real difference between the two values measured. The difference found in the Volume Loss will be discussed in detail later in this section with the aid of the graphs. Figure 67 illustrates the results and trends found for the Vickers hardness of the stainless steel samples studied in this section.

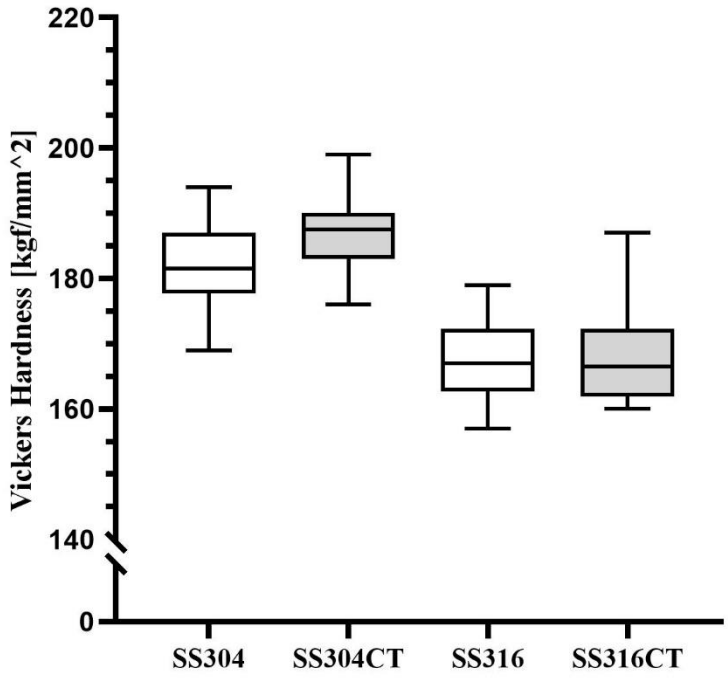

Figure 67 - Austenitic Stainless Steel samples Vickers hardness (HV20).

The previous hardness chart shows that the results for both groups of each alloy are in the same region, having the error bars of the measured values overlapping. For the AISI 304L samples, even though the error bars overlap for almost all of the measured domain, the average hardness value is higher for the cryogenically treated group than it is for the conventionally heat treated group, which implies that there could be a difference in the measured values. To analyse this trend the t-test was performed, which had results that established (confirming the premise with a confidence of 98%) that there is a relevant difference between these two groups, which is presented as an increase of at least 1.82% in the bulk hardness of the tested samples for the SS304CT group.

The AISI 316L groups showed an average hardness value very similar to each other, this way confirming that the cryogenic treatment did not affect the hardness of this alloy in any measurable way. No other differences are verified for this alloy in regards to the hardness measurements, even though the error bars appear to be bigger in the cryogenically treated group, the SS316 and SS6CT presented a very similar Standard Deviation, being this 3.41% and 3.83% respectively. Figure 68 presents the results for the Vickers microhardness for each group of each of the austenitic stainless steels analysed.

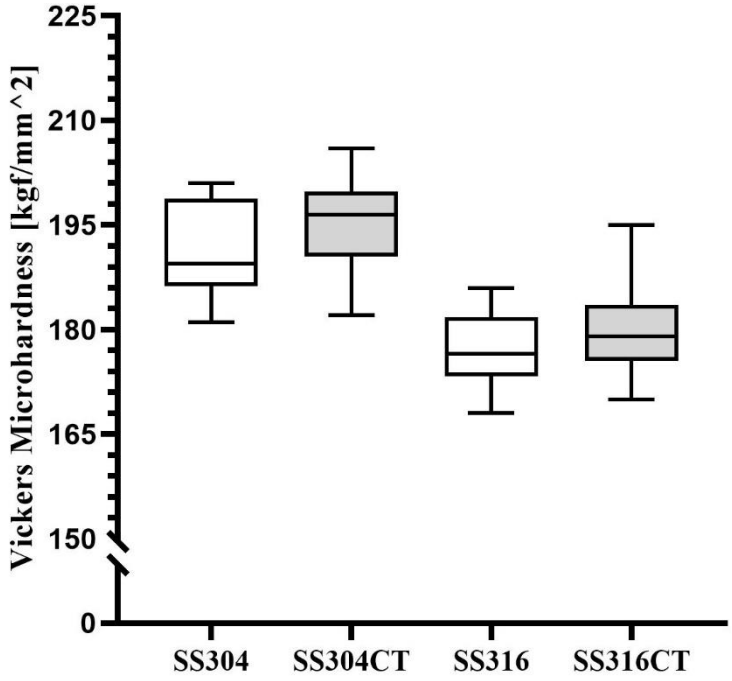

Figure 68 - Austenitic Stainless Steel Vickers microhardness (HV 0.5).

The load applied in the Vickers microhardness test for these alloys was chosen taking into consideration the size of the indentation, being the load used the lowest one that left an indentation that could be precisely measured. As detailed in Section 3.6.3, the measurements were performed automatically in a 4x4 matrix, having 16 different points of indentation. The results presented by this microhardness test have an increased Standard Deviation when compared to the previous shown hardness results, being this due to the fact that the microhardness is more susceptible to smaller differences that may be present in the measured areas, as grain boundaries, imperfections and precipitates, for example. Even so, the measured microhardness always presented a Standard Error smaller than 1%, meaning that the results are accurate and represent well the microhardness of the alloys.

The AISI 316L samples presented similar results for both of the tested groups, not showing any considerable difference in hardness and no other trend in the results, similarly to the hardness for this same alloy. Contrary to the hardness result that had a small increase in value for the cryogenically treated samples, the microhardness test for the AISI 304L did not show this difference. The variance in the mean difference for these samples is present, but due to the Standard Error (SE) of this difference being high (78.7% of the mean difference) and the confidence level lower than 95% (78,6%), the microhardness changes can be considered negligible, this way meaning that there is no difference between the microhardness for the SS304 and SS304CT groups. The austenitic stainless steels volume loss results are shown in Figure 69.

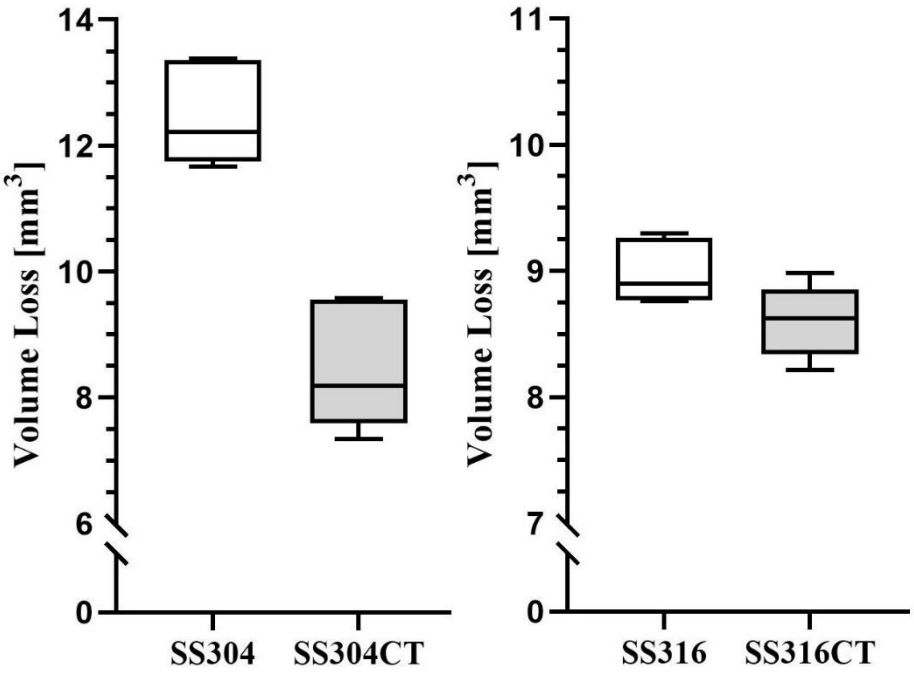

Figure 69 - Austenitic Stainless Steel abrasive wear volume loss [mm^3].

The previous graph shows the results of the AISI 304L sample groups for the ASTM G65 abrasive wear test, in which the cryogenic treated samples had a very significant reduction in the volume loss when compared to the conventionally heat treated sample group. The mean difference in the wear volume was of 31.84%, meaning that the cryogenic treatment had a beneficial effect in the wear resistance of AISI 304L and increase this resistance by this same value. The Standard Deviation is very similar for both sample groups and t-test confirmed with more than 99.99% confidence that this result significant and agrees with the premise.

The AISI 316L results do not present a difference as clear or as large as the one found for the AISI 304L, once the error bars overlap and the averages are not that far apart, as is seen in the graph. There is a decrease in volume loss of 4.34% for the cryogenically treated sample, meaning that there may be a small difference between the two sets of samples. However, the p-value confidence (94.7%) is lower than the one established (95%) in this work for the significance test, this way considering that the real difference in value is not relevant enough to consider the effect of the cryogenic treatment as positive. So, it can be said that there is a trend that is seen, but the decrease of volume cannot be determined as a significant value.

6.3. WEAR SCAR ANALYSIS

In this section, the typical wear scar of each of the austenitic stainless steels studied in this work will be analysed in detail. To do so, a 3D scanned image (obtained using an Alicona) was used for the bulk of the top of the wear scars and Scanning Electron Microscope obtained images will be used to study the cross-section of the central region of these wear scars. The typical wear scar for each type of alloy studied is illustrated in Figure 70.

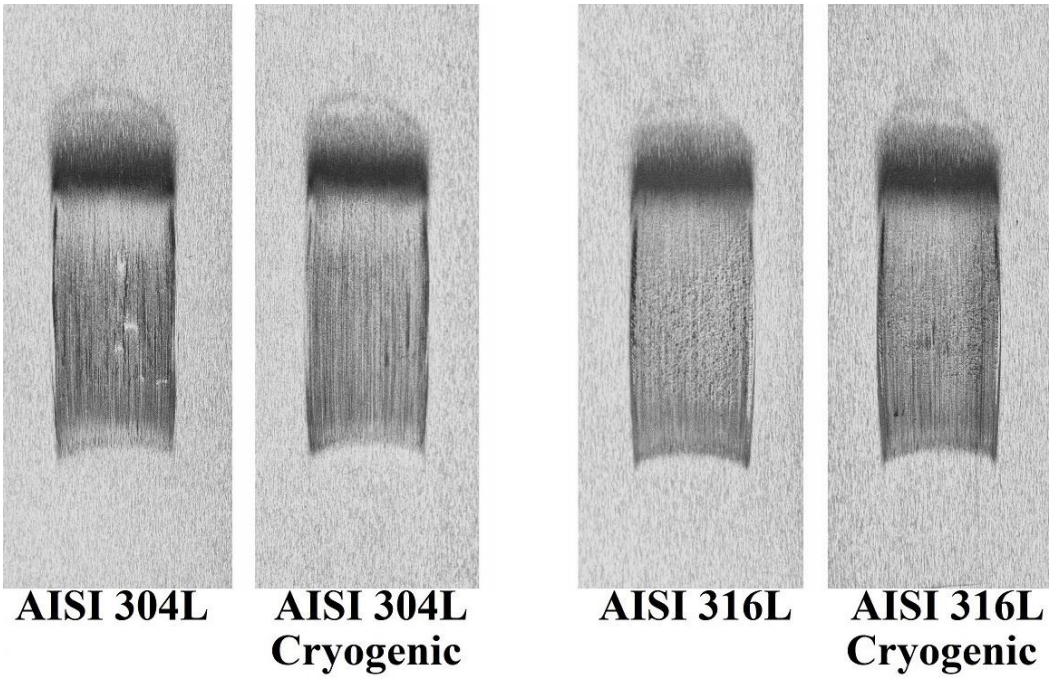

Figure 70 – Typical Austenitic Stainless Steel wear samples.

The samples used for the stainless steel abrasive wear test were the rectangular samples as per the specifications in the ASTM G65 standard, pictured in the previous photograph. To be considered a valid wear test, the samples must present a wear scar that were similar to the ones in Figure 70, which are well aligned in the centre of the sample and have parallel sides.

The pictures presented in Figure 70 were obtained using a regular DSLR camera and due to the way that the light was captured in this photos, the region in the top of the wear scar appeared as a darker region, differently to the images obtained using the Alicona (Sections 6.3.1 & 6.3.2) which are more similar to what would be seen in the real situation (naked eye). This region in the top of the wear scar is a result of an area affected by the flow of the abrasive (dry sand), that hits the top of the sample before entering the region between the rubber-wheel

and the sample itself. The samples showed different features for each of the different conditions and are analysed in more depth in the following sections.

6.3.1. AISI 304L

The typical conventionally heat treated AISI 304L samples' wear scar is pictured below in Figure 71, which presents rolling marks, scratches and a deeper plastically deformed and more aggressive crater-like wear region (detailed in Figure 71C).

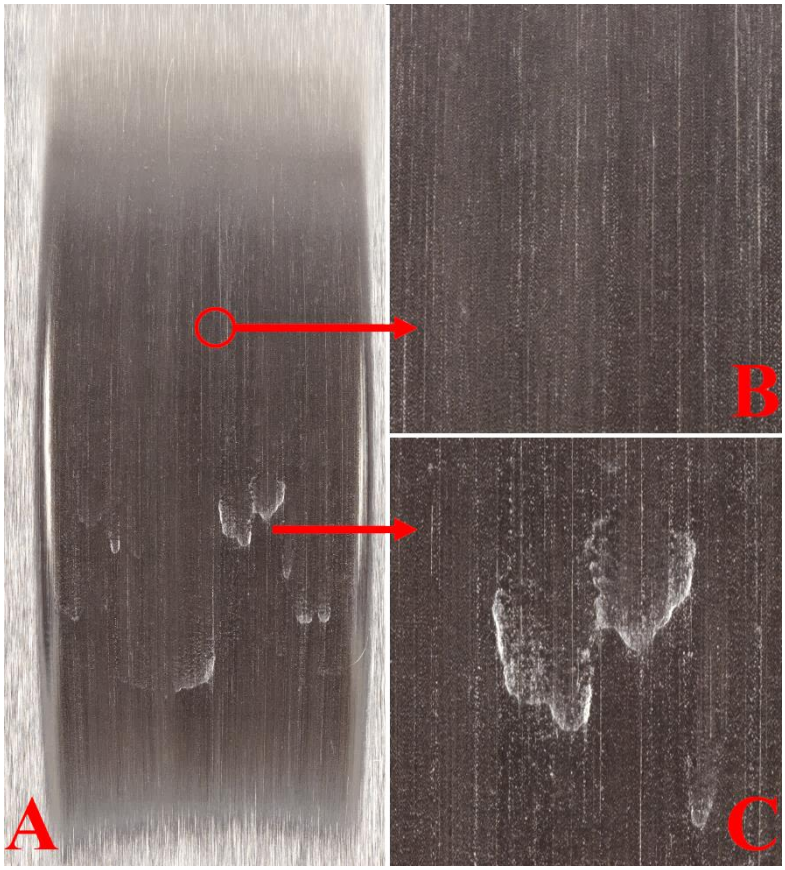

Figure 71 - (A) SS304 typical wear scar; (B) Central region scratches and rolling marks; (C) Severe plastic deformation.

The region in the top section of the wear scar (Figure 71B) presents some similar characteristics to the ones previously seem in the ferrous alloys studied in Section 4.3, with rolling marks that are well distributed and also some long scratches, being both of these features present through the whole length of the wear scar.

The rolling marks present here are a result of the grains of abrasive rolling on the surface of the material while being pressed against it, this way damaging the surface and consequently removing some material. In the case of this alloy, the rolling marks are very faint and small,

being present in the whole wear scar. The scratches are a result of the sand particles being unable to roll in the surface and instead being dragged through its length, hence removing a line of material until the load applied in this grain is released. The scratches in this surface are short and well-spaced, meaning that this feature did not often occur.

One important feature of these wear scars, which was only seen in the SS304 samples, is the presence of deeper worn regions, which are illustrated in Figure 71C. These features occur from the central region of the wear scar, in which the highest load is applied during the abrasive wear test. This feature with excessive material removal starts in a point near the central region and continues until the lower region, meaning that once it starts it is dragged until the end of the wear scar leaving a trail of material removal behind it. This happens due to the U-shaped worn region, which holds the flow of the abrasive particles, increasing the force applied in the direction of the wear and promoting an increase in the removal of alloy material. Figure 72 illustrates the height map of one of the SS304 wear scars, showing the U-shape aggressive wear and the trail of material removed (as explained previously).

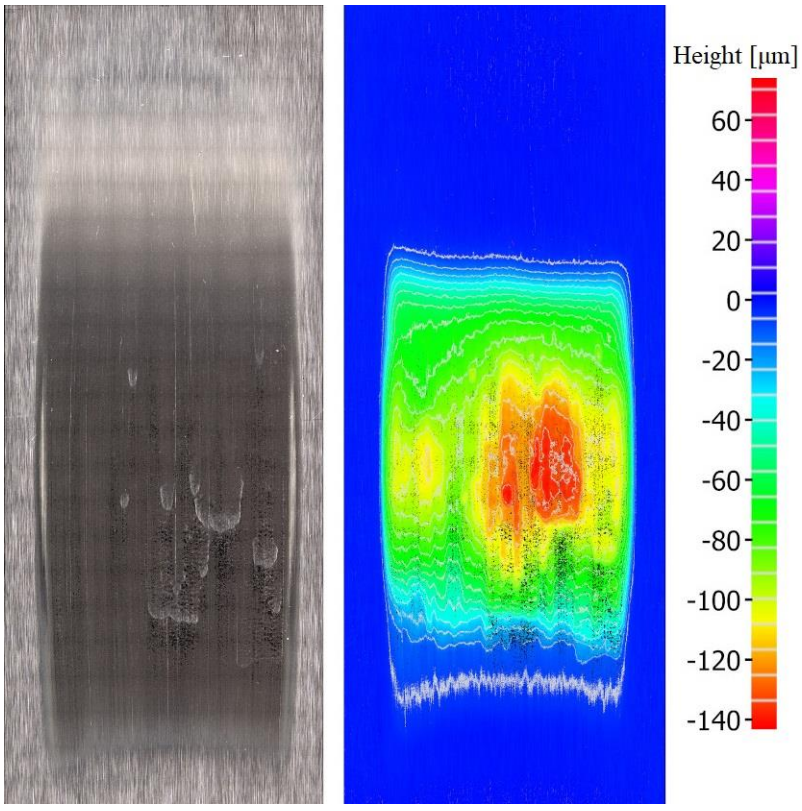

Figure 72 – SS304 wear scar height map.

The cross-section of the conventionally heat treated AISI 304L pictured in Figure 73, also shows these more aggressive wear craters, which presented less prominent waves and the

top of the peaks with more material removed. As seen in the previous samples, there is also a deformed layer just below the surface of the wear scar, which in this case is very small and is followed by the undeformed matrix of the alloy.

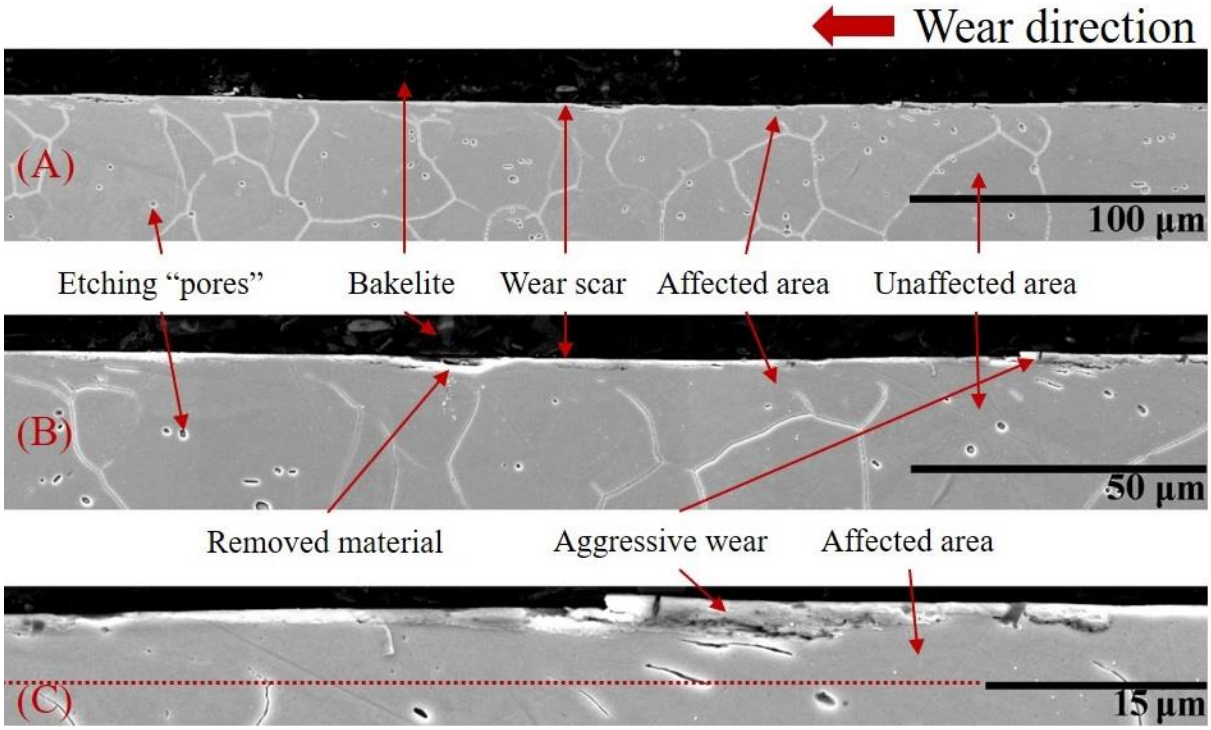

Figure 73 - SS304 wear scar cross-section micrograph detail: (A) 1000x magnification; (B) 2000x magnification; (C) 5000x magnification.

In Figure 73A, the surface of the wear scar is shown, showing three main wear regions and a faint waviness to it. All the wear regions have the same characteristic, having the left side of deformed material and a crack in the left side that leads to the material being later removed. This pattern is similar to the one seen in the SA508 Gr 4N samples, and the mechanism that facilitates the removal of material is also similar. Once the material is heavily deformed in the peak region, a crack forms and grows from the left side of the peak to the right side, once it reaches the other side a whole section of material is removed, instead of having small layers of material being removed (as seen in the AISI 440C samples). Figure 73B shows two stages of the more aggressive wear region, the left side a region in which the material has been removed and the right side a peak that is still suffering plastic deformation and crack growth.

In the detail illustrated in Figure 73C, the peak in which the wear is still happening is seen, having the top of the peak heavily deformed and a crack just below the surface of the wear scar. Once this chunk of material is removed, the crater left increases the wear by restricting the flow of abrasive, which leads to ploughing instead of the rolling movement of

the particles, and leading to the effects seen in Figure 71 and Figure 72. The cryogenically treated AISI 304L samples show a different type of wear scar that does not present the same aggressive wear pattern and the typical example of the wear scars for the SS304CT group is pictured in Figure 74.

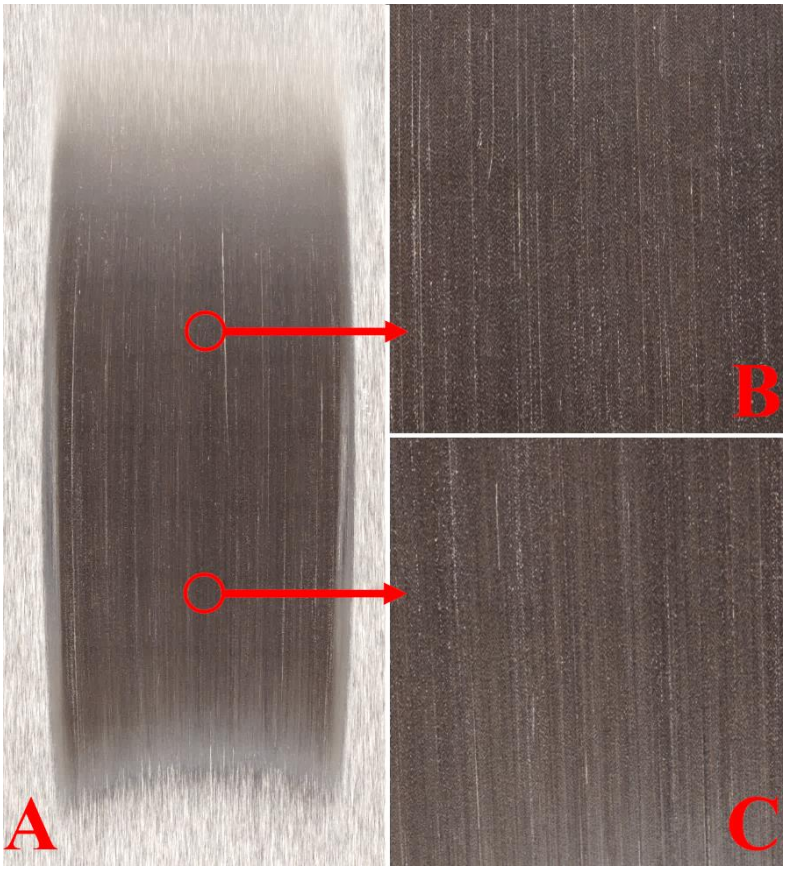

Figure 74 - (A) SS304CT typical wear scar; (B) Central region scratches and rolling marks; (C) Bottom region scratches and rolling marks.

The wear scar in Figure 74A does not have any of the more aggressive wear spots, instead, a pattern of shorter scratches and small wavy lines are present and well dispersed across the whole surface of the wear scar. The entire of the wear region presents the same pattern described, as it is shown in Figure 74 details B and C, only having some more scratches in to bottom of the wear scar due to the abrasive flow.

The difference between the conventionally heat treated and the cryogenically treated samples is very clear in the surface of the wear scar, meaning that the cryogenic treatment had a beneficial effect in the abrasive wear mechanisms in the AISI 304L. The cross-section and details of the central region of this wear scar is presented in Figure 75.

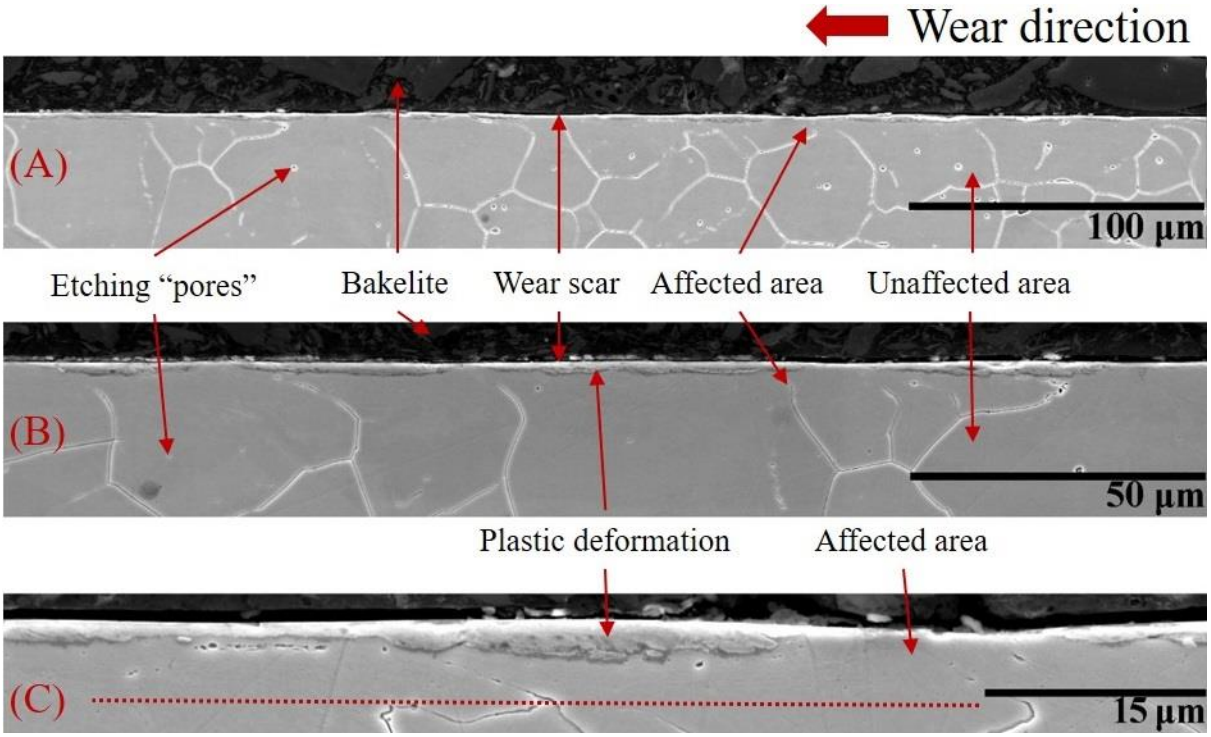

Figure 75 - SS304CT wear scar cross-section micrograph detail: (A) 1000x magnification; (B) 2000x magnification; (C) 5000x magnification.

The Figure 75A pictures a lower magnification image of the wear scar cross-section, presenting the small waves, the plastically deformed material in the top of the peaks and the affected region below it (as it is common). The wave pattern is very regular and no other features are seen in the wear scar itself. In Figure 75B, the details of the plastically deformed region are shown and no cracks are present. The peaks with the higher amount of plastically deformed material are alternated with lower regions with less or no plastically deformed material, in which this material has been removed.

Figure 75C shows how the affected region below the wear scars have the grains deformed in the direction that the wear occurs. The plastically deformed region is thicker on the right side of each peak, getting slimmer as it goes to the left side of the peak due to the alloy removal during the abrasive wear cycle. Comparing the images shown for both groups of samples, it is clear that the cryogenic treatment does present a beneficial effect in the AISI 304L by changing how the alloy responds to the abrasive wear and increasing its wear resistance.

6.3.2. AISI 316L

The AISI 316 samples were submitted to the abrasive wear test and after scanned using an Alicona to generate the 3D scan of the surface and detailed images. The typical wear scar for the SS316 sample group is pictured in Figure 76.

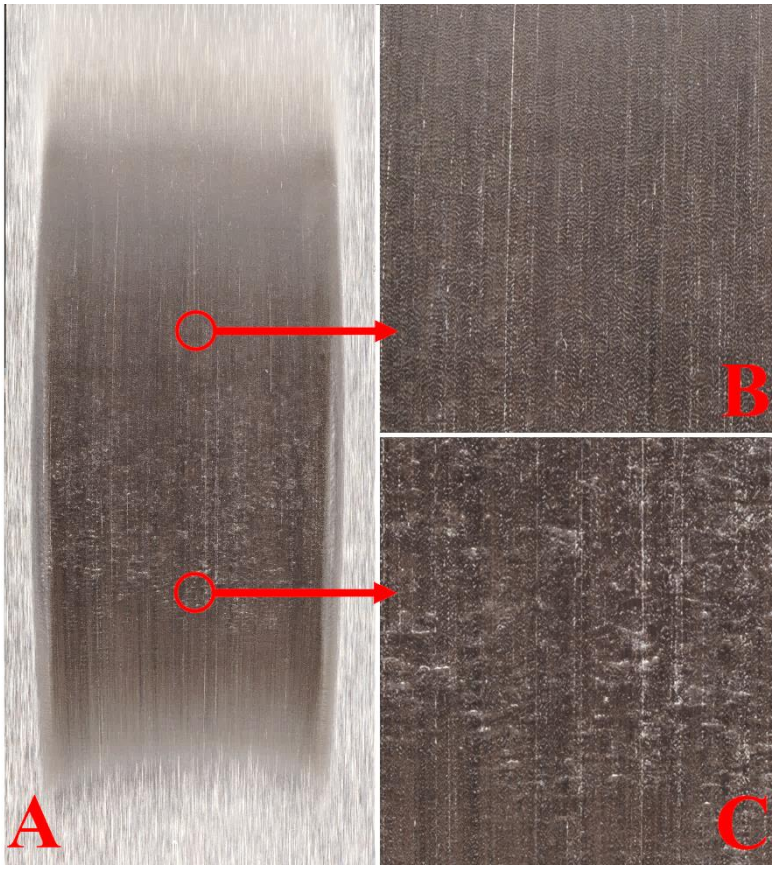

Figure 76 - (A) SS316 typical wear scar; (B) Central region scratches and rolling marks; (C) Bottom region rolling marks and deformation.

The wear scar for this group of samples can be divided in three regions, being the top (Figure 76B) and bottom of the wear scar very similar and the central region (Figure 76C) presenting a feature that was not seen in the previous results of this work. The top and bottom regions showed the most common features seen, being composed of some scratches and average sized rolling marks in the shape of waves, that are very regular and well distributed.

The central region of the wear scar, that is presented in detail in Figure 76C, illustrates a feature resulting from a collection of larger rolling marks that are well spaced between each other, creating a visual effect that assimilates to random pattern of removed material. In fact, these are just bigger wavy marks, having deep valleys and high peaks, which happen due to the high pressure applied in this region, since it is aligned with the diameter of the rubber wheel.

These wave-like structures are better seen in the cross-section image of the presented wear scar, represented in Figure 77. The lower magnification SEM image in Figure 77A shows the two different peaks that occur in the central region, being a regular peak (labelled smaller peak) as seen throughout the whole sample's wear scar and the larger peaks (labelled larger peaks) that give the aforementioned effect.

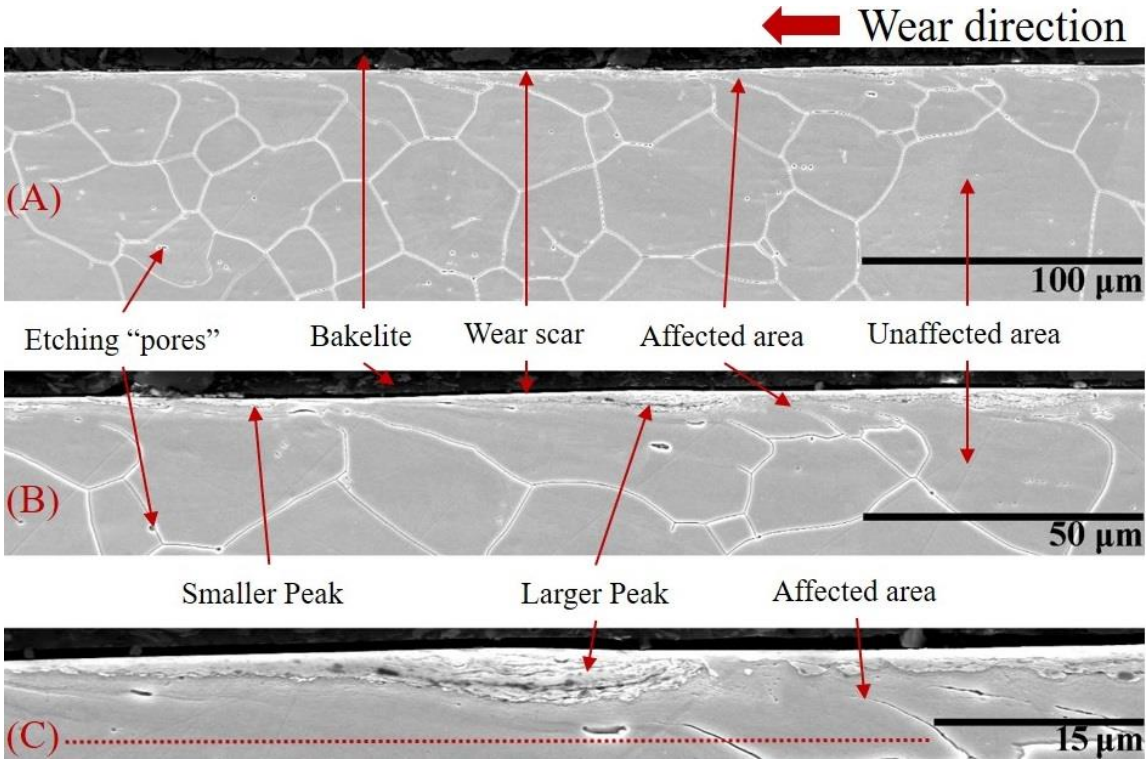

Figure 77 - SS316 wear scar cross-section micrograph detail: (A) 1000x magnification; (B) 2000x magnification; (C) 5000x magnification.

Figure 77B illustrates the details of these two different types of peaks, having on the right side the larger peak and on the left side a regular peak that is situated in the larger peak's valley. Those are very similar and only differ in size, since both presented an amount of plastically deformed material and do not present any crack formation, meaning that the wear occurs gradually. The wear occurs due to the same mechanisms as explained before, being a result of the smaller peaks and larger peaks being removed and creating new valleys and peaks.

Below the surface of the wear scar is situated the deformed region, which is characterised by the matrix being plastically deformed in the direction of the wear and is easily seen due to the grain boundaries also following the same deformation. The detail in Figure 77C shows the inexistence of cracks in the subsurface and the plastic deformation present in the larger peak and the worn region on both sides of it.

Figure 78 presents the typical wear scar for the cryogenically treated AISI 316L samples, which presents features that are similar to the SS316 group of samples. Both of these groups wear scar are shaped much the same, being also similar in size and volume.

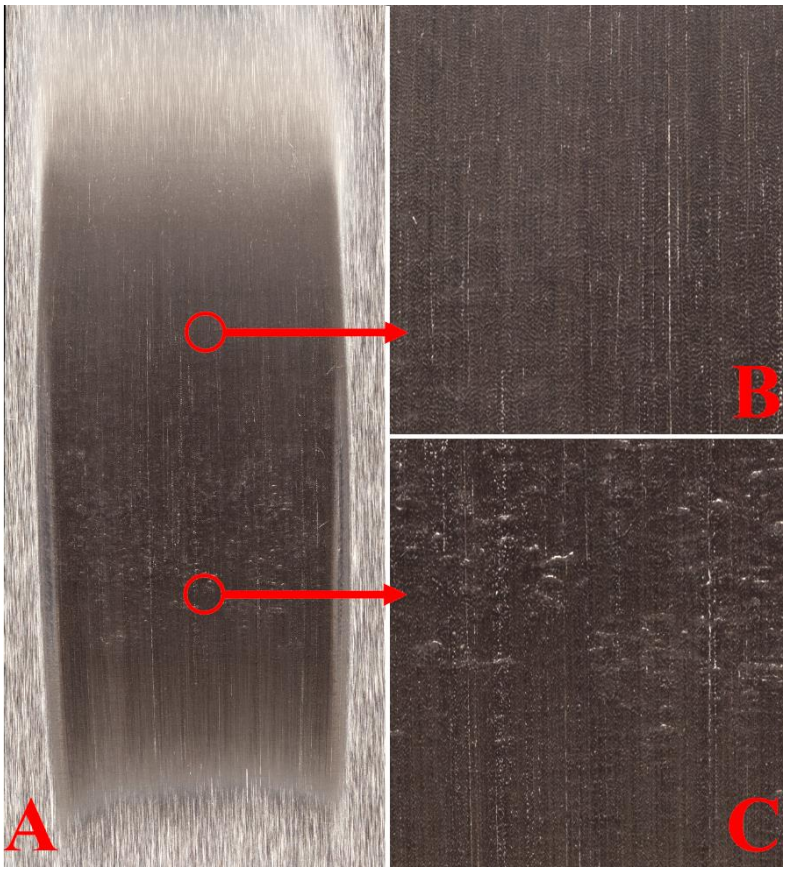

Figure 78 - (A) SS316CT typical wear scar; (B) Central region scratches and rolling marks; (C) Bottom region rolling marks and deformation.

The wear scars shows scratches and rolling marks, as illustrated in Figure 78B, being both of these regular and distributed in the whole area of the scar. The top and bottom region of this wear scar is similar to the one found in Figure 76, not presenting any different features or characteristics, but the central region of the wear presented in Figure 78C showed less of the larger peaks than the conventionally heat treated sample.

The larger peaks in this sample are similar to the ones seem previously, but the quantity and distribution of these peaks are different. It is seen in Figure 78C that there are fewer of the larger peaks and the spacing between these peaks are further apart than the ones for the conventionally heat treated samples, meaning that this feature occurred less in the cryogenically treated sample. These features are still situated in the same central region, this way confirming that these are a result of the larger force applied in this region, that leads to an

increase in plastic deformation in the surface of the material, consequently leading to an increase in volume loss. The trend for this decrease in volume loss is seen in the graph presented in Figure 69, even though the difference did not present the needed confidence (being this one 94.7%) to support the decrease in volume loss. The cross-section of this wear scar is presented in Figure 79.

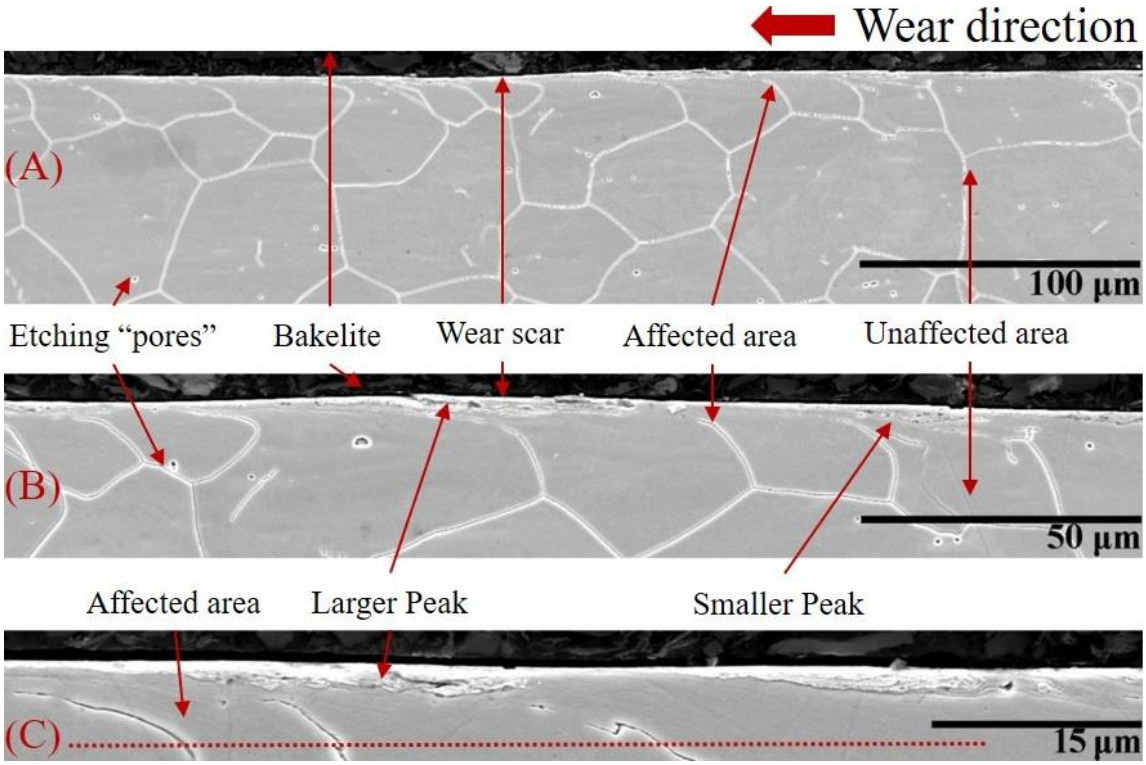

Figure 79 - SS316CT wear scar cross-section micrograph detail: (A) 1000x magnification; (B) 2000x magnification; (C) 5000x magnification.

The cross-section of the wear scar shows similar features to the SS316 group, being composed mainly of larger and smaller peaks, as represented in Figure 79A. The larger peak (Figure 79B) presents an advanced stage of plastic deformation in its the top region, which is leading to the material being detached from the rest of the surface, due to the wear it was submitted to. To the left and right of this larger peak, in the same detail of Figure 79B, smaller peaks with portions of removed material and plastic deformation are seen. In Figure 79C, the lower peaks deformation and the subsurface are shown in more detail.

All the wear scars shown in this research presented the same basic pattern, being composed of a layer of plastically deformed material, a subsurface region in which the matrix was affected by the wear and presented deformation in the direction of the wear particles flow

(mainly characterised by the deformed grain boundaries) and a region below it that presents the unchanged matrix of the material.

6.4. AUSTENITIC STAINLESS STEELS DISCUSSION

The austenitic stainless steel samples were manufactured from two of the most used stainless steel alloys, AISI 304L and the AISI 316L. The raw material for both alloys was supplied in plates that were sectioned by a water jet cutting machine in the dimensions stated by the ASTM G65, being later submitted to a stress relief heat treatment and having half of the samples of each material cryogenically treated.

As with the other samples, these samples were also submitted to the Vickers hardness and microhardness test to verify the homogeneity of each of the samples groups and investigate if the cryogenic treatment had any effect in this mechanical property. The results for the Vickers hardness and microhardness tests for the AISI 316L shows that for both groups of samples tested, the results had a good repeatability with a low Standard Deviation (Table 26 & Table 27), meaning that the samples in each group were very similar to each other. When comparing the conventionally heat treated and the cryogenically treated groups for this alloy, there are no significant measurable differences between them, thus confirming that the cryogenic treatment did not affect its hardness.

The abrasive wear tests for the AISI 316L samples also did not present any measurable difference for wear volume loss (Table 29), or any difference in observable features when comparing the cryogenically treated to the conventionally heat treated samples. The wear scar was characterised by a combination of the rolling wavy marks and a few scratches, having larger well space wavy marks in the central region of the wear, which were presented and analysed in detail in the cross-section images (Figure 77 & Figure 79). Both groups of AISI 316L samples showed very similar wear scars and features (Figure 76 & Figure 78).

The AISI 304L samples were also submitted to the same group of hardness tests for all of its samples, similarly showing a good repeatability of results and a desirable Standard Deviation (Table 26 & Table 27). This time, the SS304CT group had a hardness value 1.82% higher than the SS304 group, which indicates that the cryogenic treatment had an effect on it. For the microhardness, the difference between the value for the cryogenically treated samples and the conventionally heat treated sample was not significant enough, particularly due to this

test results presenting a Standard Deviation higher than the previous one, this way not making possible to confirm this difference.

The results found for the hardness tests in the austenitic stainless steel agree with the found literature, in which the cryogenic treatment did slightly increase the hardness in some cases and did not affect at all the hardness in other cases. From the varied combinations of heat treatments and cryogenic treatments applied to an AISI 302 austenitic stainless steel in the work done by Baldissera [70], the sample submitted to solubilization and to DCT at 88 K for nine hours presented a slightly increase in bulk hardness, being this increase of 1.85%, which is similar to the one found for the SS304CT samples in this work. In the work done by Singh *et al.* [18,36] on AISI 304L weldments, no changes were found for the bulk hardness of the alloy, but a significant increase in microhardness was presented, although the reasons for the difference in the results found for the two type of hardness measurements are not explicit in this work. An important aspect to point out related to this last study is that the microstructure of the alloy used in the present research is different from the welded material used in the aforementioned papers [18,36], since the later was subject to a series of extreme heat cycles during the welding process and the stresses resulting from this process increases the amount of martensite forming, thus the different results related to the microhardness.

The most accepted conclusion about the changes in the microstructure of the austenitic stainless steel that occur due to the cryogenic treatment is the formation of very fine nano-martensite particles (~5 nm) that nucleate in the intersection of dislocations [37,38], this way working as a dislocation-pinning mechanism, which would affect the mechanical properties of the alloy. The formation of the nano-martensite is a result of the strain present in the alloy combined with the low temperatures of the deep cryogenic treatment, being the mechanism behind the formation of strain-induced martensite, that occurs when an austenitic stainless steel is plastically deformed under a certain temperature [71,72].

The results found for the hardness in the AISI 304L also correlate with the results for the abrasive wear tests. When analysing the surface of the wear scar of the conventionally heat treated samples (Figure 71), large patches of plastically deformed regions, in which a higher volume of material removed were found (Figure 72), among the common wavy marks and scratches. On the other hand, the cryogenically treated sample only showed the regular wavy marks with few scratches (Figure 74), being very different to the previous wear scar. The presence of the deeper worn regions in the conventionally heat treated samples affect the

volume of the wear, meaning that the cryogenically treated samples presented a wear volume 31.84% smaller than the wear volume for the conventionally heat treated samples (Table 29). This difference can be attributed to the increased resistance of the cryogenically treated samples (as explained previously) to the plastic deformation resulting from the contact forces of the abrasive with the wear scar surface.

To investigate the presence of the nano-martensite particles in the SS304CT samples, a TEM analysis was performed (6.1.6). The diffraction pattern that resulted from this TEM analysis showed austenite as the only phase present for both groups of samples, meaning that there were no indications that nano-martensite particles were present in the microstructure. Although this result does not agree with the previously mentioned studies (references [37,38]), the limitations of the TEM analysis performed in the present samples should be taken into account, once the tests performed were very simple and only done once (due to the time constraints) and, due to the more complex nature of the TEM analysis, several analysis in a varied quantity of samples are needed to be able to confirm such important findings.

The lack of beneficial results from the cryogenic treatment used in this research to the AISI 316L samples is explained by the difference in chemical composition of both austenitic stainless steels. When analysing the alloy elements present in the austenitic stainless steels studied in this chapter, four main elements are identified, being these: nickel, manganese, chromium and molybdenum (being the later only present in the AISI 316L). Manganese and nickel are well known austenite stabilizers, while chromium and molybdenum ferrite stabilizers [73]. By analysing the chemical composition (Table 5) of the AISI 304L and AISI 316L, it is seen that AISI 316L presents a greater quantity of austenite stabilizers in its composition, meaning that due to this, its martensitic transformation temperature could be lower than the temperature for the AISI 304L.

6.5. AUSTENITIC STAINLESS STEELS SUMMARY

This section presents the summary of the relevant findings for the AISI 304L and AISI 316L.

- The AISI 304L hardness was positively affected by the cryogenic treatment, presenting an increase of 1.82% when compared to the conventionally heat treated samples. The microhardness measurements did not show any difference.
- There were no noticeable changes in the microstructure of the two different groups for each of the alloys when comparing the metallography micrographs, this way confirming that the bulk microstructures of the alloys were not affect by the cryogenic treatment.
- There was a very significant decrease in wear volume loss for the cryogenic treated AISI 304L samples, presenting a decrease of 31.84% when compared to the conventionally heat treated sample groups.
- The surface of the wear scar of the SS304 samples presented more observable wear features when compared to the SS304CT.
- The AISI 316L samples were unaffected by the cryogenic treatment, especially in the Vickers hardness, microhardness and grain size, which all showed very similar results between the two sample groups. The wear volume presented a small decrease (4.3%) for the cryogenically treated samples, but was deemed insignificant due to only presenting a confidence of 94.7%. The wear scar did not show any major differences when comparing the SS316 and SS316CT.

7. GENERAL DISCUSSION

This chapter presents a general discussion about the results found for the alloys and samples groups that were analysed during this work. The focus is to find and analyse the patterns, cross-referencing between the detailed analysis produced in this research and the state of the art literature published. Each of the objectives is answered based on the results found, followed by an evaluation of the analysis methods used. A summary with the important findings is presented at the end.

The selected engineering alloys (Chapter 3.3) were heat treated (Section 3.4.2) and, half of the samples were submitted to the deep cryogenic treatment, which were divided in conventionally treated and cryogenically treated samples. These samples were manufacture according the ASTM G65 standard (Section 3.4.1) and later analysed as described in Section 3.6. The aim of this work was to assess the effect of the deep cryogenic treatment in the abrasive wear resistance of these alloys. The measurable effectiveness of the deep cryogenic treatment for all the tests and samples is shown in Table 33.

Table 33 – Overall results comparison of the effect of the DCT in studied sample groups.

Samples	**Did the deep cryogenic treatment present a measurable effect?**				
	Vickers Hardness	**Vickers Microhardness**	**Grain Size**	**Microstructure**	**Wear Volume**
AISI 440C	**Yes**	**Yes**	No	No	No
SA508 Gr 4N	No	No	No	N/A	No
Ti64	No	No	No	No	No
EBM Ti64	No	No	No	No	No
AISI 304L	**Yes**	No	No	No	**Yes**
AISI 316L	No	No	No	No	No

Table 33 shows that the deep cryogenic treatment had a measurable effect only on a small selection of tests, this being due to the lack of effect from the cryogenic treatment itself and other times the due to the uncertainties and limitations of the available tests. The main known positive effect expected was the increase in hardness of the AISI 440C, due to the effect of the deep cryogenic treatment that transforms retained austenite in martensite [9,13,64,65], which was broadly explored in previous published research (Table 2). The SA508 Gr 4N did not present any change in the measured mechanical properties, being the increase in corrosion resistance the major change due to the deep cryogenic treatment. This positive change is a very desirable characteristic, once in the pressure vessel application the corrosion resistance is a life limiting factor [67,68].

The light alloys used in this research were the cast Ti64 and the EBM obtained Ti64, which were both submitted to the commercial deep cryogenic treatment and directly compared to the untreated (as received) samples of the same alloys. For this material, no changes were found in the mechanical properties, which agrees with recent research [69] published at a similar time to this thesis. For both of these light alloys, no notable differences were found in the analyses of the microstructure, which also indicates that, for this specific condition, the deep cryogenic treatment did affect the cast and EBM Ti64.

The positive result presented for the AISI 304L hardness measurement agrees with the results found in the literature for the austenitic stainless steels [70]. The slightly increase in hardness and the relevant increase in wear resistance for this alloy is explained based in the results found by Myeong et al. [37] and Shimojo et al. [38], which presents in detail the formation of very fine nano-martensite particles (~5 nm) due to the cryogenic treatment and the residual stress present in the samples. These nano-martensite particles work as a dislocation-pinning mechanism, which affects the mechanical properties of the cryogenically treated AISI 304L. The other austenitic stainless steel studied in this research, the AISI 316L, did not present this same effect probably due to a greater quantity of austenite stabilizers (manganese and nickel) [73] in its composition, which can decrease its martensitic transformation temperature and refrain the formation of the nano-martensite particles.

Based on the presented results and the published literature, it is affirmed that the deep cryogenic treatment in general shows the following effects in the engineering alloys studied: transformation of retained austenite in martensite and nucleation of nano-martensite in the intersection of dislocations. Other reported effects like changes in grain size and precipitation and/or redistribution of carbides were not found for the studied samples. Another possible change is the distribution and movement of dislocations, which was not assessed in this work.

Most of the samples were submitted to the same abrasive wear test with the same test parameters, presenting results that can be compared from an engineering and manufacturing point of view, this way showing the best abrasive resistant alloys. The results for all the dry-sand/rubber-wheel abrasive wear test is presented in Figure 80.

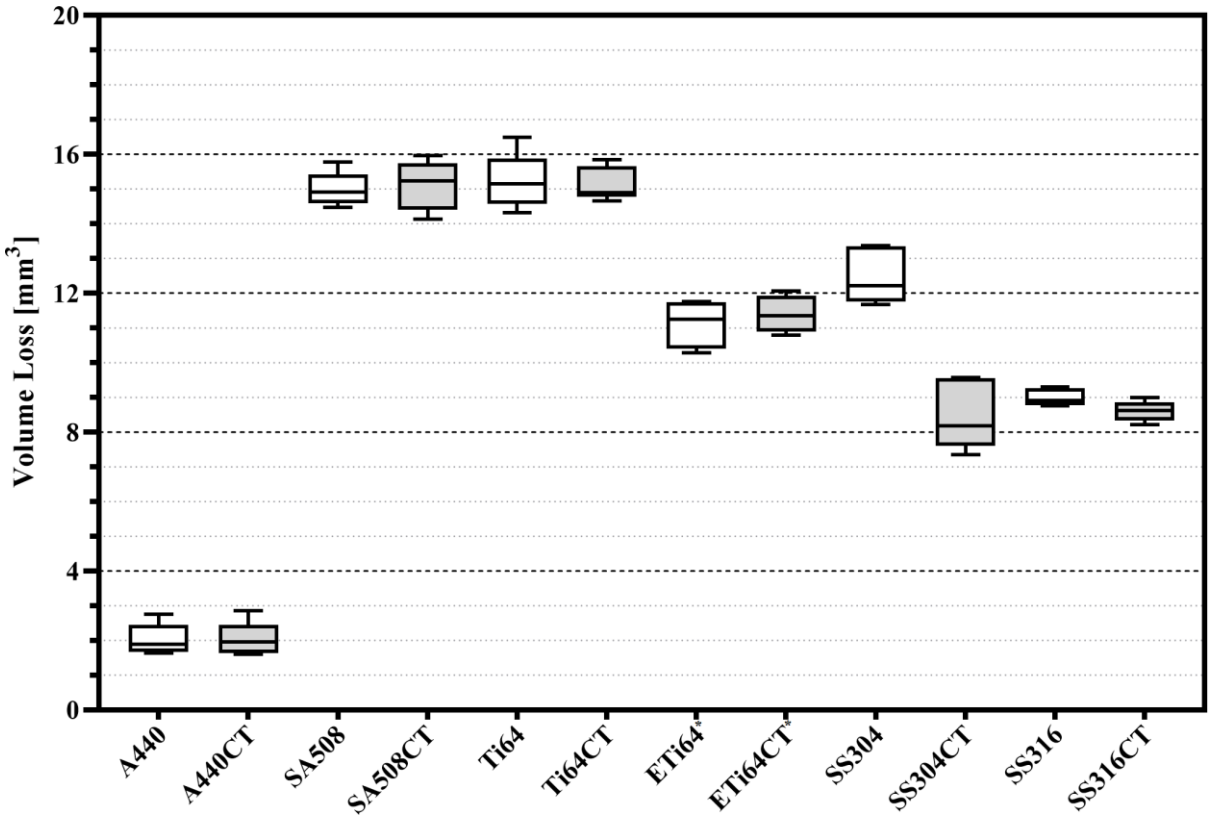

Figure 80 - Summary of the abrasive wear results for all the alloys and samples groups.
*EBM Ti64 samples test method B.

The results comparison shows that the alloy that lost the least material when submitted to the test was the AISI 440C, which is also the highest hardness alloy. The SA508 Gr 4N low alloy did not present a good wear resistance, showing a similar volume loss to the Ti64 samples. As seen in Section 4.3.3, the SA508 Gr 4N presents a great amount of plastic deformation during the abrasion process, which led to a high volume of material being removed. The austenitic stainless steels are in the middle range of the volume loss in the presented graph, having the AISI 316L with the least amount of material removed for both conditions and the AISI 304L presenting a higher wear volume for the conventionally heat treated samples and having the cryogenic treated group with a similar volume loss to the one found for the AISI 316L. This higher volume loss for the SS304 group is also clearly seen in its wear scar (Section 6.3.1), which presents higher volume loss regions with plastic deformation.

The EBM obtained Ti64 samples presented the worst wear resistance of all the studied materials, showing an extreme wear behaviour when submitted to the same test as the other alloys and still showing a high volume when submitted to one third of the test duration of the other samples. This result is mainly due to the known poor abrasive resistance of titanium

alloys [74] in combination with the considerably large number of pores that were present in this EBM sample.

7.1. ACHIEVEMENT AGAINST THE AIM AND OBJECTIVES

Based on the aim defined for this research (verifying the effect of the deep cryogenic treatment in the abrasive wear resistance of engineering alloys), a collection of objectives was determined, which gradually helped to fulfil the needs presented by the aim. This section will present each of the objective's answer.

7.1.1. Objective 1

The selection of the material was achieved using two main parameters; the lack of information in the literature, or being it a novelty material that could be obtained. The first material chosen was the AISI 440C, that served mainly to verify the effectiveness of the cryogenic treatment performed in the alloys used in this research, due to vastly known effect of the DCT in the transformation of retained austenite into martensite. Another desirable characteristic was the shape of the supplied alloy (round bar), once it made possible to design and analyse the use of a non-standard sample holder for the ASTM G65, which proved to be effective. The second alloy was the SA508 Gr 4N, which was selected due to the lack of literature on the effect of the cryogenic treatment in this type of alloy. Its tempered martensite microstructure and the presence of carbides in it also contributed to its selection, since the CT is known to have beneficial effects in alloys which have these characteristics. Both of these alloys showed the effects of the cryogenic treatment, being the AISI 440C a high increase in hardness and in the SA508 Gr 4N an unexpected effect in its corrosion resistance.

The effect of the cryogenic treatment in austenitic stainless steel alloys is a controversial topic, since it has reports that show the beneficial effect in some properties and not others, while some other reports do not show any increase in the mechanical properties. Due to this, the most used commercial austenitic stainless alloys were selected, these being the AISI 304L and AISI 316L. The first presented a slight increase in hardness and a very relevant increase in wear resistance, while the latter did not present any significant measurable difference, only showing some tendency to be beneficial in the wear results, which are not conclusive.

The Ti-6Al-4V alloys were selected due to it being the most common commercial titanium alloy, but also one that does have at least some literature that presented beneficial

effects from the cryogenic treatment. The titanium alloys usually present a bad resistance to abrasive wear and, due to this, the analysis of the effect of the cryogenic treatment was presented as a good parameter. Also, there is a lack of publications about the effects of the cryogenic treatment in the properties of the EBM obtained Ti64. Another important analysis that was done was the comparison of the wear resistance of the cast and the EBM Ti64, due to it being the same alloys produced by two different manufacturing methods.

7.1.2. Objective 2

The test chosen for this work was a low load abrasive wear test done in the Dry-Sand/Rubber-Wheel test rig, which is defined in the ASTM G65 standard [58]. To be able to freely change the parameters and specifications of the samples and the test itself, a custom abrasive wear rig was designed based on the standard dimensions and specifications contained in the ASTM standard. The main characteristics of this rig was to be compliant with the parameters contained in the ASTM standard, present a small form-factor and not present a complex manufacturing process, meaning that the rig should cost less than a commercial version of this same rig. With the design presented in Section 2, all of the desired characteristics previously explained were fulfilled, with the newly designed test rig also having a good repeatability in the results and working for the whole of the research process, proving to be a solid solution to the proposed design.

To test the new rig, sacrificial samples were manufactured from mild steel and the tests were repeated several times. By analysing the formed wear scar in the mild steel samples, the wheel and sample holder were properly aligned, while also calibrating and positioning the sand flow. The first tests were done using AISI 304L samples and due to the high variation, a new test method was developed for the following tests, which did not any major problems relative to the repeatability of the accuracy of the values. The detailed design of the test rig is presented in Section 3.2, being the development of the test methodology shown in Section 3.5.

7.1.3. Objective 3

The abrasive test rig that was designed and built to fulfil the previous objective was used to perform the abrasive wear test in all of the sample studied in this research. The samples of each of the selected alloys were prepared as per ASTM G65, having the defined rectangular dimensions (circular only for the AISI 440C samples) and the needed surface roughness, which was assessed using a profilometer. The samples were submitted to the abrasive wear test in the

designed rig and after were measured using a precision mass scale, after having its scanned using the Alicona, which generated a 3D image of each of the wear scars.

The results obtained for the test were satisfactory in most cases, presenting only an extreme wear and damage to the rubber wheel when the ETi64 samples were first tested, which led to the rubber wheel being changed and the parameters for the ETi64 being modified to test method B.

7.1.4. Objective 4 & 5

After being submitted to the hardness, microhardness and abrasive wear test, the metallography of the alloys was performed. Firstly, the samples were sectioned across the central region of the wear, facilitating the analysis of the surface and subsurface of this wear scar, and at the same time presenting the microstructure of the bulk material. All the samples were mounted, ground and polished to good standard, before being submitted to the etching, which is specific for each of the alloys. These etched samples were analysed in a conventional optical microscope and also in a scanning electron microscope, which facilitates the identification of the smaller features.

The microstructure of all the samples were analysed and none showed a difference between the conventionally heat treated samples and cryogenically treated samples, which means that the cryogenic treatment used in this research did not affect the microstructure of the tested material in any major way. The only sample that did not had its microstructure compared was the SA508 Gr 4N, due the etching not working in the cryogenically treated group. Also, no significant change in grain size was found for the samples.

The analyses of the cross-section of the wear scars made possible the visualization of the mechanisms that were presented in the scan done on the surface by the Alicona. All of the cross-section images agreed with the features found on the top surface, being mostly composed by peaks and valleys and plastically deformed regions. The alloy that showed major differences in the wear scar analysis and in the cross-section images when comparing the conventionally heat treated and the DCT samples was the AISI 304L, that had large areas of plastic deformed and worn material in the conventionally heat treated samples, showing only scratches and wavy marks in the cryogenically treated samples. The detailed analysis of this wear scar is presented in Section 6.3.

From the alloys studied in the present research, the only ones that did not show any difference between the cryogenically treated samples and the untreated samples were the titanium alloys. All of the mechanical tests and analysis performed were not able to show any significant change that could be a result of the DCT treatment, this way the DCT as applied in this research is not effective in the Ti-6Al-4V alloy. This does not necessarily mean that the cryogenic treatment does not work in the aforementioned alloy, but once a combination with other conventional cryogenic treatments may lead to an increase in properties (as found in the literature). Apart from this material, all the other alloys showed some difference, being it more clear as the high increase in hardness for the AISI 440C, unexpected as the corrosion resistance for the SA508 Gr 4N, well defined as the wear scar and hardness for the AISI 304L or even a trend in the wear resistance that can lead to an improvement if paired with a tailored DCT, as showed by the AISI 316L.

7.2. EVALUATION OF METHODOLOGY

This section presents the limitation encountered during the measurements performed in this research, also proposing improvements to overcome the encountered limitations.

7.2.1. Heat Treatments

The heat treatments chosen were based on commonly used heat treatment found in literature and on standards, being the deep cryogenic treatment the standard treatment performed by the company which treated the samples (commercial partner). The limitation is that only a single set of treatment was performed for each of the alloys, which happened due to the quantity of alloys being accessed during this study (six alloys in total) and the time constraints. In a future research, a work loop-cycle should be done, in which the better performing alloy among a few selected alloys should be submitted to a selection deep cryogenic treatments with different parameters (e.g. temperature, duration, cooling rate). This would make possible to better analyse the cryogenic treatment itself.

7.2.2. Hardness and Microhardness

The hardness and microhardness test performed in this work presented satisfactory results when analysing the effect of the deep cryogenic treatment, but did not tell much about the effect of the wear in the subsurface of the material. In a future work, the utilisation of the nano-hardness technique would enable the analysis of the subsurface region, also making possible to analyse more subtle changes that may happened in the hardness of the alloy.

7.2.3. 3D Non-contact Profilometer

The Alicona was used effectively to analyse the samples surface, wear scars and its profile, but was not used to measure the volume of the wear scars itself. The analysis of the volume of the wear scar can be better performed if the samples were fully scanned before and after the abrasive wear test, which was not performed due to the magnification (at the time) of the lens being too high relative to the size of the sample, which incurred in the scanning of the whole samples surface taking more than two and a half hours and generating files that were too large. With both of the scans (before and after), the software can be used to precisely calculate the amount of material that was removed and the quantity that was just deformed, accounting this way for the whole volume displacement of the wear scar.

7.2.4. Transmission Electron Microscope Analysis

The TEM analysis was performed in the AISI 304L to verify the presence of nano-martensite, as presented in the literature. In this work, only one sample of each condition as analysed in a very short session, mainly due to the high cost of the process. This led to not being able to find a similar result to the literature and having this specific test as inconclusive. Due to the nature of the TEM analysis, it would need a whole project entirely focused on this type of analysis.

7.3. GENERAL DISCUSSION SUMMARY

In this present chapter, the results for all the alloys and tests were grouped and the important findings were discussed. Based on the discussion presented, which linked the found results to the research literature previously cited, the following key topics are emphasised:

- The AISI 440C samples submitted to the deep cryogenic treatment presented a considerable increase (18.9%) in hardness and microhardness, when compared to the conventionally heat treated samples.
- The SA508 Gr 4N alloy showed an increased corrosion resistance for the deep cryogenically treated samples. No other changes were found for this alloy.
- The AISI 304L presented an increase in hardness (1.82%) and in wear resistance (31.84%) for the deep cryogenically treated samples.

- The other alloys (AISI 316L, Ti64 and EBM Ti64) did not present any measurable difference between the deep cryogenically treated samples and the non-cryogenically treated samples.
- When directly comparing the cast Ti64 and the EBM Ti64 samples, the cast material presents a higher wear resistance.
- All of the objectives defined to help fulfil the research aim were successfully achieved.
- The assessment of the mechanical properties presented good and reliable results, meaning that the applied methodology was effective.
- The analysis of the topology of the wear scar using the 3D non-contact profilometer was satisfactory, and made possible deep analysis of the wear scar features.

8. CONCLUSIONS

This is the final chapter of this work, which highlights and explains the important discoveries of the present research. A brief summary of the work is presented, followed by the conclusions and the contributions of this research to the field. Finally, ideas for future work that can be developed based on this research are presented.

The effect of the deep cryogenic treatment on the mechanical performance, particularly in abrasive wear resistance, of a collection of engineering alloys was analysed. The selected alloys had different characteristics and a range of applications: two types of austenitic stainless steel (AISI 304L and AISI 316L), a type of martensitic stainless steel (AISI 440C), a low alloy pressure vessel steel (SA508 Gr 4N), a titanium alloy (Ti-6Al-4V) and an additively manufactured titanium alloy (Ti-6Al-4V obtained by electron-beam melting). The studied alloys' samples were submitted to a commonly used conventional heat treatment (apart from the titanium samples, which were not submitted to a conventional heat treatment) and subsequently, half of these samples were submitted to a type of deep cryogenic treatment.

The changes in mechanical performance were assessed through Vickers hardness and microhardness tests, abrasive wear test, microstructural characterisation and the detailed analysis of the wear scar. The aim and the detailed objectives defined in the first chapter of this work have led to the following main conclusions:

- The deep cryogenic treatment had a beneficial effect in the hardness of the AISI 440C, increasing it by at least 16.92%. The increased hardness is due to the effect of the transformation of the retained austenite into martensite that occurs due to the deep cryogenic treatment.
- The AISI 304L presented the biggest changes among the austenitic stainless steel, showing a slightly increase in hardness of 1.82% for the cryogenic treated samples, while showing a decrease in wear volume of 31.84%. The beneficial effects of the cryogenic treatment in this alloy is due the nucleation of nano-martensite particles in the intersection of dislocations.
- The SA508 Gr 4N did not present any mechanical changes due to the cryogenic treatment.
- There were no measurable effects resulting from the deep cryogenic treatment in the studied Ti-6Al-4V alloys (cast and EBM).

- The AISI 316L samples did not show any measurable difference in hardness and wear volume when comparing the conventionally heat treated and the cryogenically treated samples.

The work also supports the following conclusions:

- The cryogenic treatment had a positive effect in the corrosion resistance of SA508 Gr 4N.
- EBM Ti64 presents worse wear resistance compared to Cast Ti64, showing an extreme wear behaviour when submitted to same test as the former.

The novelty of this work is that it has shown that it is viable to perform this treatment in the AISI 304L that will be submitted to abrasive wear, because the increase in wear resistance was considerable. The effects presented in the SA508 Gr 4N were both unexpected and very relevant, since it is related to a life limiting factor on its application, but more research is needed in this aspect.

The thesis has shown that the deep cryogenic treatment is an important heat treatment that has a lot of potential, even in alloys in which initially would not present any of the classic effects (e.g. transformation of retrained austenite, redistribution of carbides), such as austenitic stainless steels.

8.1. FUTURE WORK

Based on the work developed in this research and the conclusions presented, this section illustrates potential future work that can be developed to further contribute to the better understanding and application of the cryogenic treatment and the abrasive wear testing.

8.1.1. Custom ASTM G65 Test Rig

The dry-sand/rubber-wheel test rig used in this research was based on the specifications of the ASTM G65 standard, being the only non-standard parameter the sand that was used for the abrasive tests in this research. Instead of the classic chlorobutyl rubber wheel, the used wheel had the rubber part made of neoprene, which is also specified in the standard.

The alternative sand used in this work was easier to source and had a considerably lower cost, due to it being sourced in the same country in which the tests were performed. The comparison tests between both types of sands would be of importance, once it would make

possible to compare the results obtained using the non-standard sand to the ones using the standard sand. Also, tests using the chlorobutyl rubber could be performed and the results between the two different wheels compared to assess the differences that the rubber used in the wheel could make in the final results of the tests done in this custom test rig.

8.1.2. Martensitic and Low Alloy Steel

The AISI 440C presented a considerable increase in hardness due to the cryogenic treatment effect, which was not showed in the abrasive wear test, once this type of test uses a low load and is focuses in three body abrasion. A more aggressive type of wear test (e.g. pin on disc) in which higher contact stresses can be easily achieved using this same material with the same heat treatment process would make possible to better visualize the beneficial effects of the increased hardness in the wear resistance.

When compared to the conventionally heat treated samples, the SA508 Gr 4N samples submitted to the deep cryogenic treatment did not present any measurable difference in the mechanical properties analysed in this work. One important characteristic that was discovered was the increased corrosion resistance presented by the cryogenically treated samples, which should be tested and deeply analysed in a future work to be developed by Dr Rob Thornton.

8.1.3. Light Alloys

The cryogenic treatment used in this research did not present any measurable effects in the light alloys studied. The literature has examples of both cases in regards to the Ti64 alloy, presenting some cases in which the DCT presented a beneficial effect and other in which no effects were found. The main difference among all these studies is the combination of different types of heat treatments and cryogenic treatments applied to the alloys.

Due to the lack of information on the effect of the DCT in the EBM obtained Ti64 in the literature, it would be beneficial to apply a varied range of heat treatments combined with different cryogenic treatments, this way increasing the chance that the DCT would present an effect. After, a varied range of mechanical tests (e.g. hardness, impact, tensile) can be used to perform the comparison between the DCT samples and the conventionally heat treated samples.

8.1.4. Austenitic Stainless Steels

The AISI 304L did present a beneficial effect from the applied cryogenic treatment, while the AISI 316L only presented a trend that indicates that a beneficial effect may happened, due the results for it not showing a significance high enough. The main next step for these alloys would be changing the parameters of the deep cryogenic treatment, once a lower temperature and a longer holding time increases the effect that this treatment presents [13]. Also, combining the DCT with different types of conventional heat treatments can present different outcomes that should be investigated.

In the analysis methods, including a tensile test would improve the knowledge about the mechanical properties. A corrosion resistance test would also be important, once corrosion resistance is the main characteristic of these alloys. The TEM analysis should be conducted more extensively and combined with a selection of diffraction analysis, being also included a neutron diffraction for a better and more precise result.

9. BIBLIOGRAPHY

[1] ASM Handbook Committee, ASM Handbook. Volume 4: Heat treatment, ASM International, 1991.

[2] J.L. Dossett, H.E. Boyer, Practical Heat Treating, 2nd ed., ASM International, 2006.

[3] M.F. Ashby, D.R.H. Jones, Engineering Materials 2, An Introduction to Microstructures and Processing, 4th ed., Elsevier, 2013.

[4] T. Slatter, R. Thornton, Cryogenic Treatment of Engineering Materials, in: Reference Module in Materials Science and Engineering, Elsevier, 2016.

[5] D. Das, K.K. Ray, A.K. Dutta, Influence of temperature of sub-zero treatments on the wear behaviour of die steel, Wear. 267 (2009) 1361–1370.

[6] E.S. Zhmud, Improved tool life after shock cooling, Metal Science and Heat Treatment. 22 (1980) 701–703.

[7] A.N. Popandopulo, L.T. Zhukova, Transformations in high-speed steels during cold treatment, Metal Science and Heat Treatment. 22 (1980) 708–710.

[8] A.P. Gulyaev, Cold treatment of steel, Vestnik Inzhenerov i Tekhnikov. 4–5 (1946) 140–147.

[9] R.F. Barron, Cryogenic Treatment to Improve Wear Resistance, Cryogenics. 22 (1982) 409–413.

[10] P. Baldissera, C. Delprete, Deep Cryogenic Treatment: A Bibliographic Review, The Open Mechanical Engineering Journal. 2 (2008) 1–11.

[11] A. Bensely, A. Prabhakaran, D. Mohan Lal, G. Nagarajan, Enhancing the wear resistance of case carburized steel (En 353) by cryogenic treatment, Cryogenics. 45 (2005) 747–754.

[12] D.M. Singh G, Gill S, Techno-economic analysis of blanking punch life improvement by environment friendly cryogenic treatment, Journal of Cleaner Production. 143 (2017) 1060-1068.

[13] J.D. Darwin, D. Mohan Lal, G. Nagarajan, Optimization of cryogenic treatment to maximize the wear resistance of 18% Cr martensitic stainless steel by Taguchi method, Journal of Materials Processing Technology. 195 (2008) 241–247.

[14] M. Preciado, P.M. Bravo, J.M. Alegre, Effect of low temperature tempering prior cryogenic treatment on carburized steels, Journal of Materials Processing Technology. 176 (2006) 41–44.

[15] F. Meng, K. Tagashira, R. Azuma, H. Sohma, Role of Eta-carbide Precipitations in the Wear Resistance Improvements of Fe-12Cr-Mo-V-1.4C Tool Steel by Cryogenic Treatment., ISIJ International. 34 (1994) 205–210.

[16] D. Yun, L. Xiaoping, X. Hongshen, Deep Cryogenic Treatment of High-speed Steel and its Mechanism, Heat Treatment of Metals. 3 (1998) 55–59.

[17] A. Molinari, M. Pellizzari, S. Gialanella, G. Straffelini, K.H. Stiasny, Effect of deep cryogenic treatment on the mechanical properties of tool steels, Journal of Materials Processing Technology. 118 (2001) 350–355.

[18] P.J. Singh, S.L. Mannan, T. Jayakumar, D.R.G. Achar, Fatigue life extension of notches in AISI 304L weldments using deep cryogenic treatment, Engineering Failure Analysis. 12 (2005) 263–271.

[19] D. Das, A.K. Dutta, K.K. Ray, Sub-zero treatments of AISI D2 steel: Part I. Microstructure and hardness, Materials Science and Engineering A. 527 (2010) 2194–2206.

[20] D. Das, A.K. Dutta, K.K. Ray, Sub-zero treatments of AISI D2 steel: Part II. Wear behavior, Materials Science and Engineering A. 527 (2010) 2194–2206.

[21] D. Senthilkumar, I. Rajendran, M. Pellizzari, J. Siiriainen, Influence of shallow and deep cryogenic treatment on the residual state of stress of 4140 steel, Journal of Materials Processing Technology. 211 (2011) 396–401.

[22] M. Koneshlou, K. Meshinchi Asl, F. Khomamizadeh, Effect of cryogenic treatment on microstructure, mechanical and wear behaviors of AISI H13 hot work tool steel, Cryogenics. 51 (2011) 55–61.

[23] R. Thornton, T. Slatter, A.H. Jones, R. Lewis, The effects of cryogenic processing on the wear resistance of grey cast iron brake discs, Wear. 271 (2011) 2386–2395.

[24] T. Slatter, R. Lewis, A.H. Jones, The influence of cryogenic processing on wear on the impact wear resistance of low carbon steel and lamellar graphite cast iron, Wear. 271 (2011) 1481–1489.

[25] K. Gu, H. Zhang, B. Zhao, J. Wang, Y. Zhou, Z. Li, Effect of cryogenic treatment and aging treatment on the tensile properties and microstructure of Ti-6Al-4V alloy, Materials Science and Engineering A. 584 (2013) 170–176.

[26] R. Thornton, T. Slatter, H. Ghadbeigi, Effects of deep cryogenic treatment on the dry sliding wear performance of ferrous alloys, Wear. 305 (2013) 177–191.

[27] G. Prieto, J.E.P. Ipiña, W.R. Tuckart, Cryogenic treatments on AISI 420 stainless steel: Microstructure and mechanical properties, Materials Science and Engineering A. 605 (2014) 236–243.

[28] M. Pérez, F.J. Belzunce, The effect of deep cryogenic treatments on the mechanical properties of an AISI H13 steel, Materials Science and Engineering A. 624 (2015) 32–40.

[29] N. YUMAK, K. ASLANTAS, Y. PEKBEY, Effect of cryogenic and aging treatments on low-energy impact behaviour of Ti–6Al–4V alloy, Transactions of Nonferrous Metals Society of China (English Edition). 27 (2017) 514–526.

[30] J. Li, X. Yan, X. Liang, G. Hong, D.Y.Y. Li, H. Guo, D.Y.Y. Li, Influence of different cryogenic treatments on high-temperature wear behavior of M2 steel, Wear. 377 (2017) 1112–1121.

[31] N. Pillai, R. Karthikeyan, S. Kannan, S. Vincent, Effect of Cryogenic treatment on VIKING cold working tool steel and development of wear mechanism maps, Procedia Manufacturing. 26 (2018) 329–342.

[32] K.B. Hariharan, S. Saravanan, N. Parkunam, Life time improvement of D7 tool steel by cryogenic treatment, Materials Today: Proceedings. (2019) 10–12.

[33] Z. Weng, K. Gu, K. Wang, X. Liu, J. Wang, The reinforcement role of deep cryogenic

treatment on the strength and toughness of alloy structural steel, Materials Science and Engineering: A. 772 (2020) 138698.

[34] X. Liu, C. Zhao, K. Zhao, Microstructure evolution and mechanical/physical properties of 25# valve alloys steel subjected to deep cryogenic treatment, Vacuum. 160 (2019) 394–401.

[35] D. Das, A.K. Dutta, K.K. Ray, On the refinement of carbide precipitates by cryotreatment in AISI D2 steel, Philosophical Magazine. 89 (2009) 55–76.

[36] P.J. Singh, B. Guha, D.R.. Achar, Fatigue life improvement of AISI 304L cruciform welded joints by cryogenic treatment, Engineering Failure Analysis. 10 (2003) 1–12.

[37] T. Myeong, Y. Yamabayashi, M. Shimojo, Y. Higo, A new life extension method for high cycle fatigue using micro-martensitic transformation in an austenitic stainless steel 1This work was carried out as a part of the Ph.D. thesis of one of the authors (T.H.M.). 1, International Journal of Fatigue. 19 (1997) 69–73.

[38] M. Shimojo, K. Takashima, Y. Higo, T. Inamura, H. Myeong, Formation of nanosized martensite particles in stainless steels, Metallurgical and Materials Transactions A. 32 (2001) 261–265.

[39] J.Y. Huang, Y.T. Zhu, X.Z. Liao, I.J. Beyerlein, M.A. Bourke, T.E. Mitchell, Microstructure of cryogenic treated M2 tool steel, Materials Science and Engineering A. 339 (2003) 241–244.

[40] K. Gu, J. Wang, Y. Zhou, Effect of cryogenic treatment on wear resistance of Ti-6Al-4V alloy for biomedical applications, Journal of the Mechanical Behavior of Biomedical Materials. 30 (2014) 131–139.

[41] G.W. Stachowiak, A.W.W. Batchelor, Engineering Tribology, 4th ed., Elsevier, 2013.

[42] B. Bhushan, Modern Tribology Handbook, Volume 1, 1st ed., CRC Press, 2000.

[43] J.T. Burwell, Survey of possible wear mechanisms, Wear. 1 (1957) 119–141.

[44] ASM Handbook Committee, ASM Handbook. Volume 18: Lubrication, and Wear Technology, 1992.

[45] B. Podgornik, F. Majdic, V. Leskovsek, J. Vizintin, Improving tribological properties of tool steels through combination of deep-cryogenic treatment and plasma nitriding, Wear. 288 (2012) 88–93.

[46] A. Akhbarizadeh, K. Amini, S. Javadpour, Effects of applying an external magnetic field during the deep cryogenic heat treatment on the corrosion resistance and wear behavior of 1.2080 tool steel, Materials and Design. 41 (2012) 114–123.

[47] Y. Gao, B.-H. Luo, Z. Bai, B. Zhu, S. Ouyang, Effects of deep cryogenic treatment on the microstructure and properties of WCFeNi cemented carbides, International Journal of Refractory Metals and Hard Materials. 58 (2016) 42–50.

[48] A. Bensely, L. Shyamala, S. Harish, D. Mohan Lal, G. Nagarajan, K. Junik, A. Rajadurai, Fatigue behaviour and fracture mechanism of cryogenically treated En 353 steel, Materials and Design. 30 (2009) 2955–2962.

[49] V. Manoj, K. Gopinath, G. Muthuveerappan, Rolling Contact Fatigue Studies on Case Carburized and Cryogenic Treated En 353 Gear Material, International Symposium of Research Students on Material Science and Engineering. (2004).

[50] Z.Z. Hu, Y.Q. Liu, J.H. Liu, M. Ma, Y.Q. Liu, J.H. Liu, The effect of austenite on low cycle fatigue in three-phase steel, International Journal of Fatigue. 19 (1997) 641–646.

[51] T.S. Eyre, Wear characteristics of metals, Tribology International. 9 (1976) 203–212.

[52] A.G. Evans, D.B. Marshall, Wear mechanism in ceramics, in: D.A. Rigney (Ed.), Fundamentals of Friction and Wear of Materials, ASM International, 1981: p. 439.

[53] K. Hokkirigawa, K. Kato, An experimental and theoretical investigation of ploughing, cutting and wedge formation during abrasive wear, Tribology International. 21 (1988) 51–57.

[54] H. Kitsunai Kato, K., The Transition Between Microscopic Wea Modes During Repeated Sliding Friction Observed by a Scanning Electron Microscope Tribosystem, 135 (1990) 237–249.

[55] T. Kayaba, K. Hokkirigawa, K. Kato, Analysis of the abrasive wear mechanism by successive observations of wear processes in a scanning electron microscope, Wear. 110

(1986) 419–430.

[56] Standard Guide for Developing and Selecting Wear Tests - ASTM G190-15, (2015).

[57] A. Misra, I. Finnie, A Review of the Abrasive Wear of Metals, Journal of Engineering Materials and Technology. 104 (1982) 94–101.

[58] Standard Test Method for Measuring Abrasion Using the Dry Sand/Rubber Wheel Apparatus - G65-16, (2016).

[59] J.H. Tylczak, J.A. Hawk, R.D. Wilson, A comparison of laboratory abrasion and field wear results, Wear. 225 (1999) 1059–1069.

[60] J.A. Hawk, R.D. Wilson, J.H. Tylczak, O.N. Dogan, Laboratory abrasive wear tests: investigation of test methods and alloy correlation, Wear. 225229 (1999) 1031–1042.

[61] S. Wirojanupatump, P.H. Shipway, Abrasion of mild steel in wet and dry conditions with the rubber and steel wheel abrasion apparatus, Wear. 239 (2000) 91–101.

[62] ASTM E407-07(2015)e1, Standard Practice for Microetching Metals and Alloys, ASTM International, West Conshohocken, PA, (2015).

[63] F.C. Bell, D.E. Sonon, Improved Metallographic Etching Techniques for Stainless Steel and for Stainless Steel to Carbon Steel Weldments, Metallography. 107 (1976) 91–107.

[64] J.R. Yang, T.H. Yu, C.H. Wang, Martensitic transformations in AISI 440C stainless steel, Materials Science and Engineering A. 438–440 (2006) 276–280.

[65] A. Idayan, A. Gnanavelbabu, K. Rajkumar, Influence of Deep Cryogenic Treatment on the Mechanical Properties of AISI 440C Bearing Steel, Procedia Engineering. 97 (2014) 1683–1691

[66] M.A. Moore, The relationship between the abrasive wear resistance, hardness and microstructure of ferritic materials, Wear. 28 (1974) 59–68.

[67] Y.S. Lim, S.S. Hwang, D.J. Kim, J.Y. Lee, Corrosion behavior of SA508 low alloy steels exposed to aerated boric acid solutions, Nuclear Engineering and Technology. (2019).

[68] D. Xia, C. Zhou, Y. Liu, J. Wang, C. Fu, K. Wang, M. Li, Mechanical Properties and

Corrosion Resistance of SA508-4 Low Carbon Alloy Steel, Electrochemistry. 81 (2013) 262–268.

[69] Y. Meng, M. Villa, K. V. Dahl, T.L. Christiansen, M.A.J. Somers, Synchrotron X-ray diffraction investigation of the effect of cryogenic treatment on the microstructure of Ti-6Al-4V, Applied Surface Science. 502 (2020).

[70] P. Baldissera, Deep cryogenic treatment of AISI 302 stainless steel: Part I – Hardness and tensile properties, Materials & Design. 31 (2010) 4725–4730.

[71] H. Bhadeshia, Martensitic Transformation, in: Encyclopedia of Materials: Science and Technology, Pergamon, 2001: pp. 5203–5206.

[72] Z. Nishiyama, Martensitic Transformation, Elsevier, 1978.

[73] J.R. Davis, Alloying: Understanding the Basics, ASM International, 2001.

[74] K.G. Budinski, Tribological properties of titanium alloys, Wear. 151 (1991) 203–217.